PB 284 207

Progress Report on
Dynamic Characteristics of Major Components
of 1200 MW Fossil Fuel Steam Generating Plant

by

J. L. Bogdanoff

K. W. Kayser

H. Lo

A. J. Schiff

C. T. Sun

H. T. Yang

School of Aeronautics and Astronautics

Purdue University

West Lafayette, Indiana 47907

317-494-8598

REPRODUCED BY
NATIONAL TECHNICAL
INFORMATION SERVICE
U. S. DEPARTMENT OF COMMERCE
SPRINGFIELD, VA. 22161

September 1975

Sponsored in Part by the National Science Foundation

Under Grant Number GI-41897

Any opinions, findings, conclusions or recommendations expressed in this publication are those of the author(s) and do not necessarily reflect the views of the National Science Foundation.

///

50272-101

REPORT DOCUMENTATION PAGE | 1. REPORT NO. NSF-RA-E-75-272 | 2. | PB 248 207

4. Title and Subtitle: Dynamic Characteristics of Major Components of 1200 MW Fossil Fuel Steam Generating Plant

5. Report Date: September 1975

6.

7. Author(s): J.L. Bogdanoff, K.W. Kayser, H. Lo, et al

8. Performing Organization Rept. No.

9. Performing Organization Name and Address: Purdue University, School of Aeronautics and Astronautics, West Lafayette, Indiana 47907

10. Project/Task/Work Unit No.

11. Contract(C) or Grant(G) No. (C) (G) GI41897

12. Sponsoring Organization Name and Address: Applied Science and Research Applications (ASRA), National Science Foundation, 1800 G Street, N.W., Washington, D.C. 20550

13. Type of Report & Period Covered

14.

15. Supplementary Notes

16. Abstract (Limit: 200 words)

The unusual nature of the structure of the major components of a large fossil-fuel steam generating plant and the heavy cost of construction at the present time suggests that a dynamic analysis is in order to determine if current design practice is satisfactory. The plant under study is Unit #3 of the Paradise Kentucky Plant of TVA. This is a 1200 MW coal-fired unit which supplies high pressure steam to the turbine at 3600 psi and 1005°F and reheated steam returns to the turbine at 800 psi and 1000°F. The plant consumes approximately 15,000 tons of coal per day. This study devises detailed models of the major components suitable for dynamic analysis. Results for natural frequencies and corresponding mode shapes are presented. In addition, seismic responses for the steam pipe and chimney are obtained by using the El Centro earthquake record.

17. Document Analysis a. Descriptors

Earthquakes
Coal
Dynamic tests
Fossil fuels
Steam electric power generation

b. Identifiers/Open-Ended Terms

c. COSATI Field/Group

18. Availability Statement: NTIS.

19. Security Class (This Report)

20. Security Class (This Page)

21. No. of Pages: 111

22. Price: PC A06/MF A01

(See ANSI-Z39.18) See Instructions on Reverse

OPTIONAL FORM 272 (4-77) (Formerly NTIS-35) Department of Commerce

TABLE OF CONTENTS

INTRODUCTION

Fossil-fuel steam generating plants provide a substantial fraction of the electric power consumed in the USA. The USA has substantial coal and shale oil reserves, with estimates of upward to 500 years supply at today's recovery and consumption rates. Pollution problems are troublesome when large daily quantities of coal are burned without careful planning of anti-pollution devices, but new developments suggest that in the near future a large fraction of the objectionable discharges from the stacks will be removed at reasonable cost with the aid of new or projected equipment.

Approximately 10% of fossil-fuel steam generating plants are in Zone 3 of the Algermissen Seismic Risk Map (1967) with approximately 27% in Zone 2 Plants in these Zones or future plants placed in these Zones may be subjected to seismic ground motion of undetermined intensities. The possibility of damage to major components thus exists.

It is known that if major components* are put out of service because of damage significant outages of power to consumers will occur as repair and/or replacement of damaged major components is a slow process at best. If several plants are forced out of service at the same time due to a major earthquake, electric power service over a wide area may be disrupted for many months with obvious serious consequences to the public.

At present, plants are designed on a static basis. Seismic loads are taken into account as specified in the Uniform Building Code or in other Codes

*Steam generator and supporting structure, steam piping, coal handling equipment, cooling tower, and chimney.

applicable in the area of the plant site. This practice is followed in other sections of the World. For many types of conventional buildings, the use of seismic equivalent static loads has substantially raised their durability and safety under seismic disturbances.

The unusual nature of the structure of the major components of a large fossil-fuel steam generating plant and the heavy cost of construction at the present time suggests that a dynamic analysis is in order to determine if current design practice is satisfactory.

The unusual nature of the structure of the major components of a large fossil-fuel steam generating plant and the heavy cost of construction at the present time suggests that a dynamic analysis is in order to determine if current design practice is satisfactory.

The specific plant under study is Unit #3 of the Paradise Kentucky Plant of TVA. This is a 1200 MW coal-fired unit which supplies high pressure steam to the turbine at 3600 psi and 1005°F and reheated steam returns to the turbine at 800 psi and 1000°F. The plant consumes approximately 15,000 tons of coal per day.

This report consists in devising detailed models of the major components suitable for dynamic analysis. Results for natural frequencies and corresponding mode shapes are presented. In addition, seismic responses for the steam pipe and chimney are obtained by using the El Centro earthquake record.

CHAPTER 1

THE STEAM GENERATOR AND ITS SUPPORTING STEEL FRAME STRUCTURE

by

HENRY T. YANG

1.1 Introduction

The steam generator and its supporting structure of Unit #3, Paradise, Kentucky consists of approximately 1298 beams and columns and 370 joints; it thus is a complex subsystem. To date, no one has made a study of its nf's and corresponding normal modes and response to seismic disturbances which includes the full structural complexity.

The present paper describes the development of complex models of the steam generator and its supporting structure and the results obtained to date on its calculated nf's and corresponding normal modes. Because of the complexity of the structure and because no prior computations have been made, a number of versions of this subsystem have been developed. The purpose of doing this has been to develop confidence in the computer code and the techniques used to obtain complex models. The first few nf's and modes have been calculated for the various versions of the subsystem and these results are consistent among themselves in a dynamical sense.

Literature on nf's and corresponding normal modes of a large steam generator and its supporting structure is sparse. Typical of what is available is referenced in [1] and [2]. So far, no study such as is described below has been found.

1.2 Description of the System

The steam generator is described by a vertical plane view in Fig. 1.1. It is also described by a rough three dimensional sketch in Fig. 1.2. The steam generator is hung by 220 steel rods at the top to the steel girders. It is also supported horizontally by tie rods connected to the steel columns as shown in Fig. 1.2.

The steam generator weighs approximately 24,000 kips. The distribution of weight for various components is listed in Table 1.1.

The air heater as shown in Fig. 1.1 is connected to the steam generator by an expansion joint which provides little bending or torsional rigidity. The air heater weighs approximately 15% as the steam generator. The supporting columns for the air heater rest on the concrete foundation with no rotational or torsional restraint. The air heater is stabilized from rocking motion by horizontal tie rods connected to the steel columns.

The steel framing structure is described in Fig. 1.3 by a three-dimensional sketch marked with overall dimensions. The structure has a total of 1298 major beam and column members and 370 bracing members. There are 595 joints among which 66 are at the base. The largest girders are at the top of the frame hanging the steam generator. Such plate girders have flanges of $30x\frac{7}{8}$ in.^{2} and are 20 ft. deep. The heaviest columns are at the lower level built with 14 WF 630 wide flanges with two cover plates $30x4\ \frac{3}{4}$ in.^{2} The total weight of the whole steel framing structure is over 13,000 kips which is approximately 50% of the combined weight of the steam generator and the air heater.

Table 1.1 Weight of Structural Components

No.	Structural Component	Weight (Kips)
1	Furnace Front Wall	1,400
2	Furnace Rear Wall	1,130
3	Furnace Side Walls (2)	820
4	Front Wind Box	1,400
5	Rear Wind Box	1,370
6	Pendant Side Walls (2)	164
7	Furnace Floor	1,400
8	Horizontal Convection Pass Side Walls (2)	330
9	Convection Pass Rear Wall	380
10	Convection Pass Front Wall	295
11	Risers	270
12	Economiser Enclosure	470
13	Pendant Floor	376
14	Secondary Super Heater	2,920
15	Furnace Roof	710
16	Pent-House	650
17	Pendant Reheat	1,154
18	Horizontal Reheater	1,400
19	Primary Super Heater	1,430
20	Economiser	3,400
21	Roof Outlet	250
22	Economiser Stringers	515
23	Supply Tubes	12
24	Secondary Super Heater Outlet	258
25	Primary Outlet	380
26	Secondary Super Heater Inlet	880
27	Economizer Inlet	340
		ΣWeight 24,104 (Kips)

Between the levels of 101 and 175 feet above the ground, there are 23 coal silos. When they are filled with coal, the weight could be 6000 tons.

1.3 Finite Elements

(1) Description of the finite elements

Two types of finite element are used. One is the three-dimensional beam finite element which has rigid joints. The other is the three-dimensional truss finite element which has hinged joints. The latter is a special case of the former. Only the former need be described.

A general three-dimensional beam finite element is described in Fig. 1.4.The element is assumed to have six degrees of freedom at each joint: three displacements $\bar{u}$, $\bar{v}$, and $\bar{w}$ in the local $\bar{x}$, $\bar{y}$, and $\bar{z}$ directions, respectively; and three rotations $\theta_{\bar{x}}$, $\theta_{\bar{y}}$, and $\theta_{\bar{z}}$ about $\bar{x}$, $\bar{y}$, and $\bar{z}$, respectively. Corresponding to the six joint degrees of freedom, there are three forces $F_{\bar{x}}$, $F_{\bar{y}}$, $F_{\bar{z}}$, one twisting moment $M_{\bar{x}}$, and two bending moments $M_{\bar{y}}$, $M_{\bar{z}}$, respectively.

The element formulation is derived in the form that the 12 nodal forces are related to the 12 nodal displacements (in Local coordinates) by the stiffness and mass matrices.

$$\underset{12\times1}{\{\bar{F}\}} = \underset{12\times12}{[\bar{k}]}\ \underset{12\times1}{\{\bar{q}\}} - \omega^2\ \underset{12\times12}{[\bar{m}]}\ \underset{12\times1}{\{\bar{q}\}} \tag{1.1}$$

with the stiffness matrix

$$
[\bar{K}] = \begin{bmatrix}
\frac{AE}{L} & & & & & & & & & & & \\
0 & \frac{12EI_{\bar{y}}}{L^3} & & & & & & & & & & \\
0 & 0 & \frac{12EI_{\bar{z}}}{L^3} & & & & & & & & & \\
0 & 0 & 0 & \frac{GJ}{L} & & & & & & & & \\
0 & -\frac{6EI_{\bar{y}}}{L^2} & 0 & 0 & \frac{4EI_{\bar{y}}}{L} & & & & & & & \\
0 & 0 & \frac{6EI_{\bar{z}}}{L^2} & 0 & 0 & \frac{4EI_{\bar{z}}}{L} & & & & & & \\
-\frac{AE}{L} & 0 & 0 & 0 & 0 & 0 & \frac{AE}{L} & & & & & \\
0 & -\frac{12EI_{\bar{y}}}{L^3} & 0 & 0 & \frac{6EI_{\bar{y}}}{L^2} & 0 & 0 & \frac{12EI_{\bar{y}}}{L^3} & & & & \\
0 & 0 & -\frac{12EI_{\bar{z}}}{L^3} & 0 & 0 & -\frac{6EI_{\bar{z}}}{L^2} & 0 & 0 & \frac{12EI_{\bar{z}}}{L^3} & & & \\
0 & 0 & 0 & -\frac{GJ}{L} & 0 & 0 & 0 & 0 & 0 & \frac{GJ}{L} & & \\
0 & -\frac{6EI_{\bar{y}}}{L^2} & 0 & 0 & \frac{2EI_{\bar{y}}}{L} & 0 & 0 & \frac{6EI_{\bar{y}}}{L^2} & 0 & 0 & \frac{4EI_{\bar{y}}}{L} & \\
0 & 0 & \frac{6EI_{\bar{z}}}{L^2} & 0 & 0 & \frac{2EI_{\bar{z}}}{L} & 0 & 0 & -\frac{6EI_{\bar{z}}}{L^2} & 0 & 0 & \frac{4EI_{\bar{z}}}{L}
\end{bmatrix} \qquad (1.1)
$$

Reproduced from best available copy

where EA, EI, and GJ are the axial, bending, and torsional rigidities, respectively; L is the length of the element. The stiffness matrix can be derived either by the stress-strain equilibrium method or by the minimum strain energy method. The mass matrix [m] is formulated on the basis of lump masses. The rotatory inertia is neglected. There are only six nonzero terms on the diagonal which correspond to the $\bar{u}$, $\bar{v}$, $\bar{w}$ displacements at both joints. These terms are all in the same form of $\rho AL/2$ which is half of the mass of the finite element.

Before the assemblage of each individual element, the equations of motion (1) for each element must be transformed from the local coordinates $(\bar{x}, \bar{y}, \bar{z})$ to the global coordinates (x, y, z) by using the nine direction cosines defined as follows.

$$\begin{cases} \lambda_i = \cos \theta_{xi} \\ \mu_i = \cos \theta_{yi} \\ \nu_i = \cos \theta_{zi} \end{cases} \qquad i = \bar{x}, \bar{y}, \text{ and } \bar{z} \tag{1.3}$$

The equations of motion with reference to the global coordinates are in the form

$$\underset{12x1}{\{F\}} = \underset{12x12}{[T]^T} \left[\underset{12x12}{[\bar{k}]} - \omega^2 \underset{12x12}{[\bar{m}]} \right] \underset{12x12}{[T]} \underset{12x1}{\{q\}} \tag{1.4}$$

where the coordinate transformation matrix is defined as

$$[T] = \begin{bmatrix} \Lambda & & & \\ & \Lambda & & \\ & & \Lambda & \\ & & & \Lambda \end{bmatrix} \tag{1.5}$$

with

$$[\Lambda] = \begin{bmatrix} \lambda_{\bar{x}} & \mu_{\bar{x}} & \nu_{\bar{x}} \\ \lambda_{\bar{y}} & \mu_{\bar{y}} & \nu_{\bar{y}} \\ \lambda_{\bar{z}} & \mu_{\bar{z}} & \nu_{\bar{z}} \end{bmatrix} \tag{1.6}$$

The second finite element model is a truss bar element. Such element does not have the three rotational degrees of freedom at each joint as shown in Fig. 1.4. It is the special case of the first model. By the use of such model the compatibility requirement for the three rotational degrees of freedom at each common joint can be relaxed. This element is used to model the members with hinge connections.

The element can also be a mixed model, i.e., an element with six degrees of freedom at one end and only three displacement degrees of freedom at the other end. Such model is used to handle a structure with both hinge and rigid connections.

1.4 Assemblage and Solution

In the formulation of the entire structure, equation (1.4) is first used to formulate each of the members, the individual element equations are then summed up. The zero-displacement boundary conditions are incorporated by removing the rows and columns in the stiffness and mass

matrices that correspond to the zero degrees of freedom.

A boundary spring element is used to handle the joints that are elastically restrained from displacement or rotation. Such element is in the form of either an extensional or rotational spring which can be oriented in any specified direction. If the spring constant is specified as infinite, no displacement or rotation is allowed in the spring direction.

Since the stiffness and mass matrices are in the form of band matrix, only the bands are stored in the computer for the calculation of frequencies and mode shapes. The bands are stored in block and are solved by an iterative procedure. A careful numbering of the joints of the structural model can minimize the bandwidth and result in saving computing time. For the 12 degree of freedom element, the bandwidth is calculated by the formula

$$\text{Bandwidth} = 2(6n+5) + 1 \qquad (1.5)$$

where n is the maximum numerical difference between any two connected joint numbers.

1.5 The Complex Model

i. Model for the steam generator

Based on the distribution of weight given in table 1.1, the steam generator is modeled by 48 lumped masses. This model is described graphically in Fig. 1.5 and numerically in Table 1.2. The magnitued and location of each mass are decided on the basis of the weight distribution and the consideration of the bandwidth in the resulting matrix formulation for the entire steam generator and framing system.

Table 1.2. Lumped mass modeling for the steam generator.

Mass No.	x-ordinate Measured from 23 line	y-ordinate Measured from gv line	z-ordinate Measured from EL0.0	Weight kips
1	106.00'	0.00	422.0	806.0
2	10.34'	0.00	422.0	806.0
3	106.00'	54.00	422.0	806.0
4	10.34'	54.00	422.0	806.0
5	106.00'	0.00	461.5	529.0
6	10.34'	0.00	461.5	529.0
7	106.00'	54.00	461.5	529.0
8	10.34'	54.00	461.5	529.0
9	106.00'	10.45	494.0	106.0
10	10.34'	10.45	494.0	106.0
11	106.00'	43.55	494.0	106.0
12	10.34'	43.55	494.0	106.0
13	106.00'	10.45	512.0	134.0
14	10.34'	10.45	512.0	134.0
15	106.00'	43.55	512.0	134.0
16	10.34'	43.55	512.0	134.0
17	106.00'	10.45	535.0	198.0
18	10.34'	10.45	535.0	198.0
19	106.00'	43.55	535.0	374.8
20	10.34'	43.55	535.0	374.8
21	106.00'	10.45	568.5	122.5
22	10.34'	10.45	568.5	122.5
23	106.00'	43.55	568.5	522.5
24	10.34'	43.55	568.5	522.5
25	106.00'	10.45	582.0	319.3
26	10.34'	10.45	582.0	319.3
27	106.00'	43.55	582.0	1178.1
28	10.34'	43.55	582.0	1178.1
29	106.00'	79.65	582.0	1209.6
30	10.34'	79.65	582.0	1209.6
31	106.00'	79.65	553.0	1127.8
32	10.34'	79.65	553.0	1127.8
33	106.00'	79.65	535.0	413.1
34	10.34'	79.65	535.0	413.1
35	106.00'	79.65	505.0	1042.1
36	10.34'	79.65	505.0	1042.1
37	106.00'	91.96	481.6	46.4
38	10.34'	91.96	481.6	46.4
39	106.00'	121.67	481.6	46.4
40	10.34'	121.67	481.6	46.4
41	106.00'	121.67	505.0	1042.1
42	10.34'	121.67	505.0	1042.1
43	106.00'	111.15	535.0	964.1
44	10.34'	111.15	535.0	964.1
45	106.00'	111.15	568.5	33.55
46	10.34'	111.15	568.5	33.55
47	106.00'	111.15	582.0	315.3
48	10.34'	111.15	582.0	315.3

Σ Weights = 24,211.30 Kips

ii. Model for the steel framing structure

The detail design of the steel framing structure involves numerous engineering drawings. It is difficult to visualize the structure physically on the basis of so many design drawings. It is also difficult to prepare the input data for the finite element computation with so many drawings. To circumvent this difficulty, a small model is built with balsa wood members with a scaling factor of 1/64. The overall dimensions of the model is 5 x 3.27 square feet in base area and 3.94 feet high. A photograph of the model is shown in Fig.1.6. Each member in the model is labeled with its dimensions and mass.

With the help of this model, the preparation and checking of the input data and the interpretation of the results become easier, the physical feeling of the structural behavior becomes within the grasp.

1.6 Assumptions

i. The base of each column is assumed as fixed.
In reality, the concrete footings for the columns and the basement floor-slabs are buried in the excavated limestone rock.

ii. The steam generator is modeled by lumped masses. The frames, walls, and tubes of the steam generator are assumed to be rigid. The lumped masses are thus connected by rigid beam elements.

iii. There are eight masses at the top of the steam generator model. This model is thus hung by eight rods which are hinged to the steel framing structure. The eight rods have the stiffnesses and masses equivalent to the 220 actual rods.

iv. The steel frames have rigid joints. The tie rods have hinged joints.

v. On each floor, only the beams that constitute the major framework are considered.

1.7 Results to Date

Thus far, only free vibration analyses have been performed for the system described in Section (d). In order to evaluate the contribution to the natural frequencies and the mode shapes by different portions of the system, analyses of different subsystems have been made.

i. The central structure without both steam generator and bracing members.

The central portion as shown in Fig. 1.7 was first analyzed. The steam generator and the cross bracing members were neglected. This structure has 434 joints and 865 beam and column members. Among the 434 joints, 36 are at the base. This results in a total of 1968 equations. The way that the joints are numbered results in a matrix bandwidth of 426.

The first mode frequency was found to be 0.4299 Hz. The corresponding mode shape plotted for a few representative members is shown in Fig. 1.8. The mode is seen to be a combination of both side-swaying and slightly torsional motions. The eigenvector output shows that the vertical displacement of all the joints are two-order of magnitude smaller than the side displacements. Such degrees of freedom could have been suppressed in the analysis of the first few modes.

The central processing time for CDC 6500 computer was 50 minutes.

ii. The central structure without the steam generator but with the bracing members.

The bracing members have been recognized as having the stiffening effect for the frame structures. The central structure has a total of

147 cross bracing members. They are all in the vertical planes. The effect of bracing members was included in the analysis.

The first mode natural frequency was found to be 0.5517 Hz. The corresponding mode shape plotted for a few representative members is shown in Fig. 1.9 Because of the nonsysmetrical nature of both the framing and the bracing structures, a mode coupled by side swaying and torsional motion is seen.

The central procession time for the CDC 6500 computer was 52 minutes

iii. The central structure with the steam generator but without the bracing members.

The steam generator has a total weight of 24,000 kips. The central structure without bracing members has a total weight of 7400 kips. When the two systems are combined, the natural frequencies should be considerably less than those for the central structure alone.

The first mode frequency was found to be 0.1556 Hz as compared with the 0.4299 Hz found in Section (i). The corresponding mode shape is shown in Fig. 1.10. The motion is seen to be predominantly side-swaying. The swaying effect of the steam generator apparently over-rides the possible torsional motion.

Since there is no torsional motion, the second mode was also found. The frequency is 0.1987 Hz and the mode is shown in Fig. 1.11.Again, the mode is predominantly side-swaying but the swaying direction is perpendicular to that of the first mode.

The first mode motion of the steam generator is shown for a vertical cross section in Fig.1.12. A horizontal rigid body motion is seen. No rotational or torsional motion is observed. The strong effect of the

translational motion of the steam generator seems to compensate the torsional motion of the framing structure.

The system has a total of 2328 equations with a bandwidth of 474. The CDC 6500 central processing time was 96 minutes for the first mode and 104 minutes for both the first and the second modes.

iv. The central structure with both the steam generator and the bracing members.

After the analysis in Section (iii), the bracing members were included. This system is a complete representation of the central system. The frequencies are expected to be higher than the one without bracing members.

The first mode frequency was found to be 0.2060 Hz. The corresponding mode shape is shown in Fig.1.13. Again, a predominant side-swaying motion is seen. A summary of all the results is shown in Table 1.3.

The CDC 6500 central processing time used was 101 minutes.

v. The whole system

After the above calculations, the final analysis of the whole system as described in Section (c) can be performed. It is expected that the inclusion of the side structure will definitely stiffen the system and increases the natural frequencies. Because of the unsymmetrical nature of the side structure, tortional motion is expected to appear in the second or third mode.

The weights of the air heater and the coal silos will also be included. The increase in 8000 tons of weight is expected to lower the frequencies somewhat.

In this analysis, the system has 595 joints, 1298 beam members, and

Table 1.3. THE FIRST MODE FREQUENCIES FOR THE ANALYSES OF CENTRAL STRUCTURE

ANALYSIS NUMBER	STEAM GENERATOR	147 BRACING MEMBERS	NUMBER OF DEGREES OF FREEDOM	BAND WIDTH	CDC 6500 CP TIME (MINUTES)	FREQUENCY
1	No	No	1968	426	50	0.4299 Hz
2	No	Yes	1968	426	52	0.5517 Hz
3	Yes	No	2328	474	96	0.1556 Hz
4	Yes	Yes	2328	474	101	0.2060 Hz

370 bracing members. Excluding the zero degrees of freedom of 66 joints at the base, the system results in 3170 equations. For the sake of saving computing time, the vertical displacement degrees of freedom will be suppressed in the analysis of first two modes. This assumption has been confirmed by the eigenvector results for all of the calculations in Sections (i) to (iv).

1.8 Results by March 1

The free vibration analysis of the entire complex system up to several modes is expected to be completed by the end of 1975. The number of modes sought will depend on three major factors: (1) the interpretation of the lower modes that have already been found; (2) the smoothness of the computational progress; and (3) the budget for computation.

After a satisfactory number of natural modes have been obtained, a forcing function will be used to find the time-history response of the entire complex system. The model superposition method will be used. Since enormous computational effort is expected, the forcing function will be carefully selected.

The results for the time-history response will include displacements at every joint and forces at every member. This huge set of data will be stored on magnetic tape. The members and the joints will be ranked based on the magnitudes of their stresses or displacements. Only representative and interested portions of the results will be displayed.

References

[1.1] Shiraki, K. and Nakazawa, S., "Study on the Aseismic Design of Boilers and Structural Steels - Considerations on the Vibration Characteristics and Design Criteria for Boilers and Structural Steels," Mitsubishi Technical Review, Sept. 1968, pp. 184-195.

[1.2] Suehiro, T., "Vibration Analysis of a 1000 MW Boiler Frame Structure," Report KBD 19012, Ishikawajima-Harima Heavy Industries Co., Ltd., March 1974.

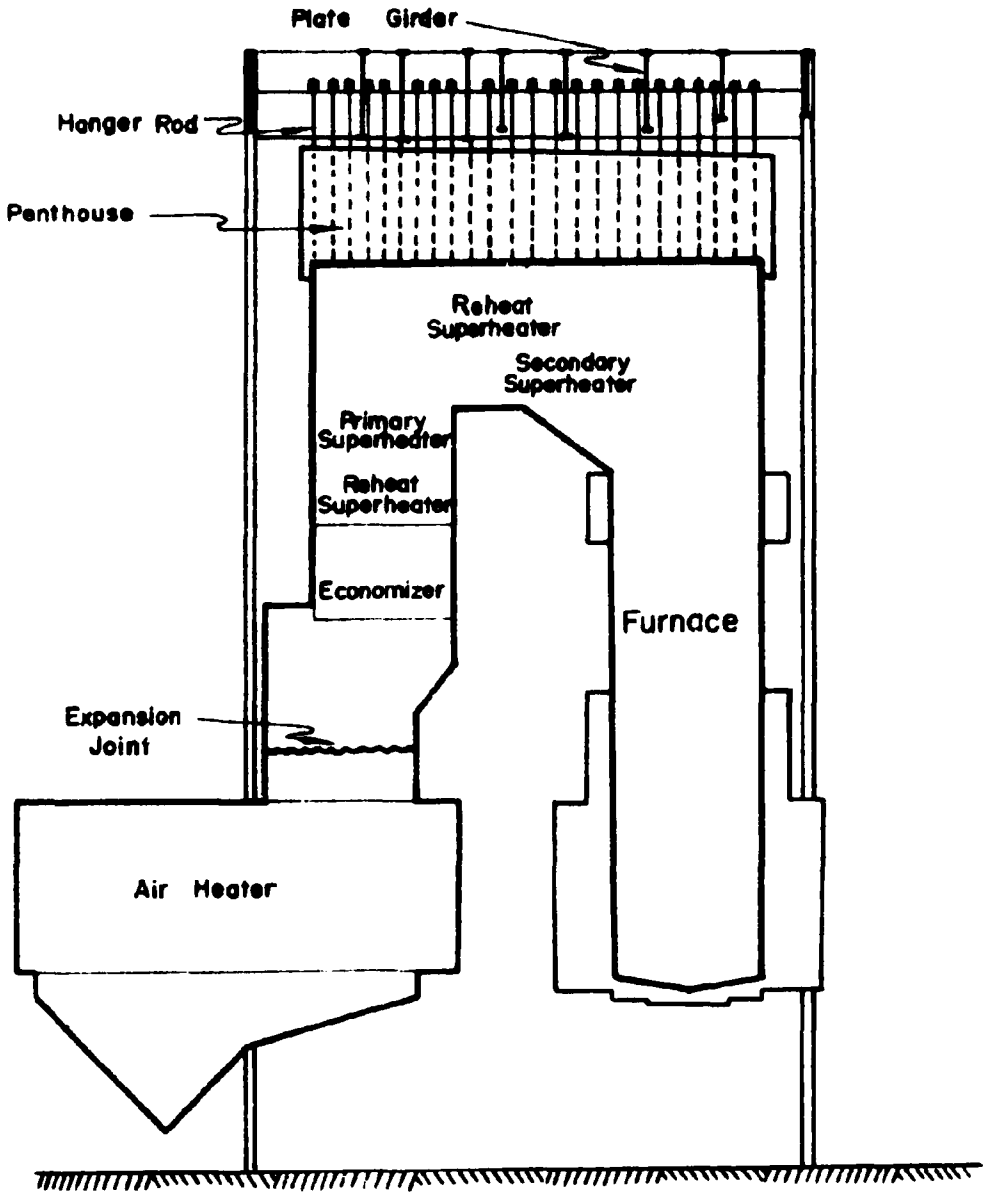

Fig. 1.1. A vertical plane view of the steam generator.

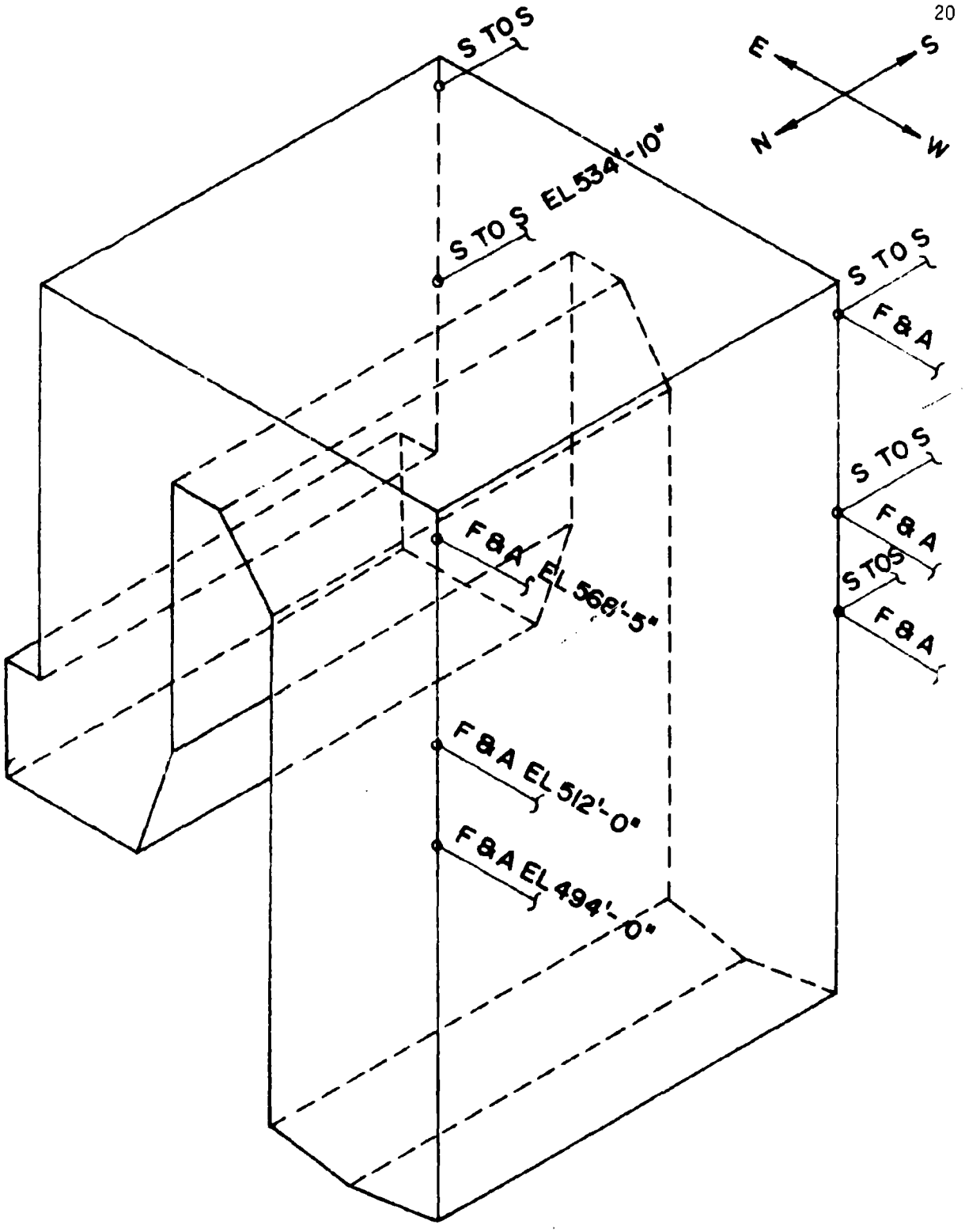

Fig. 1.2. A rough three-dimensional sketch of the steam generator.

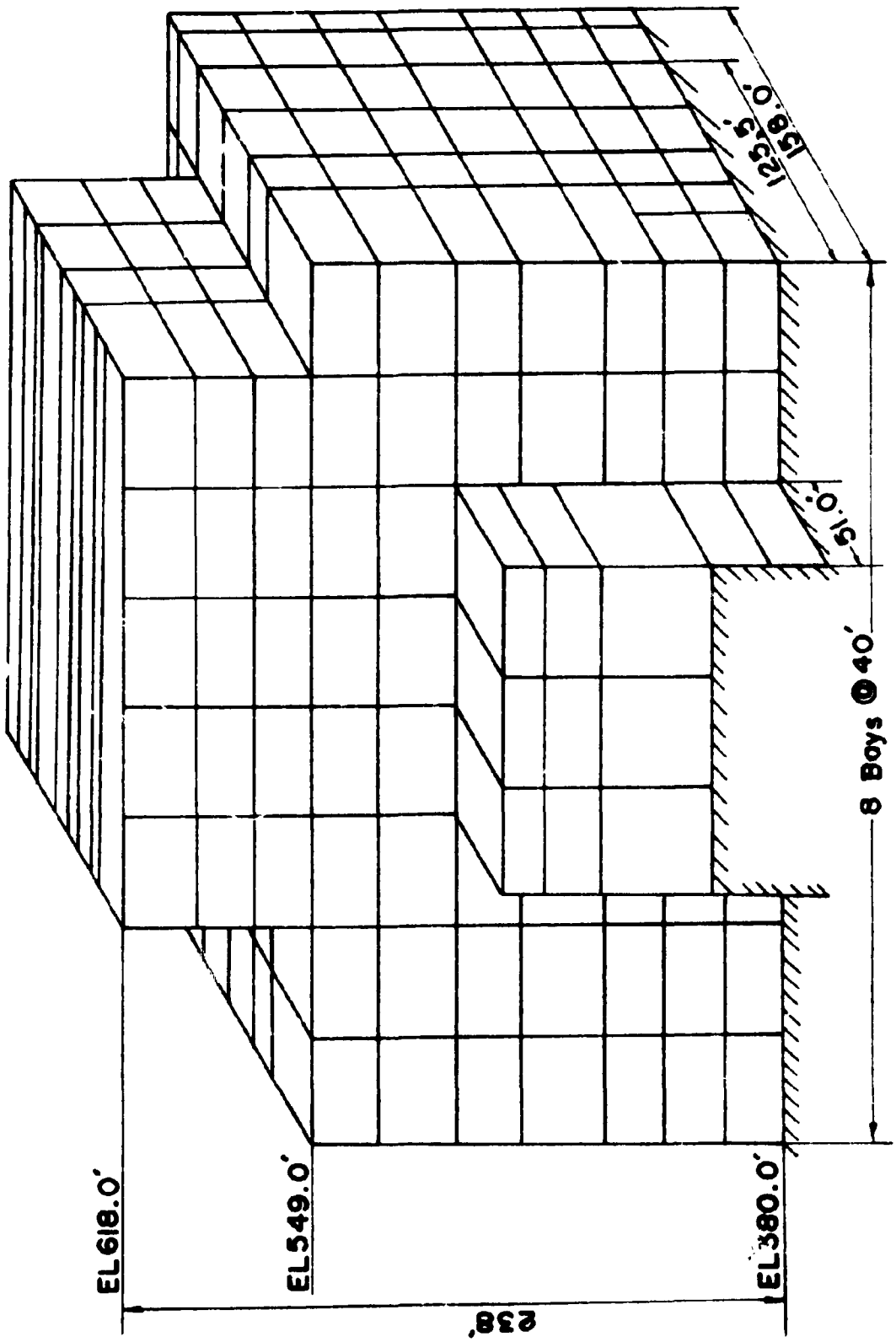

Fig.1.3. The configuration of the steel framing structure.

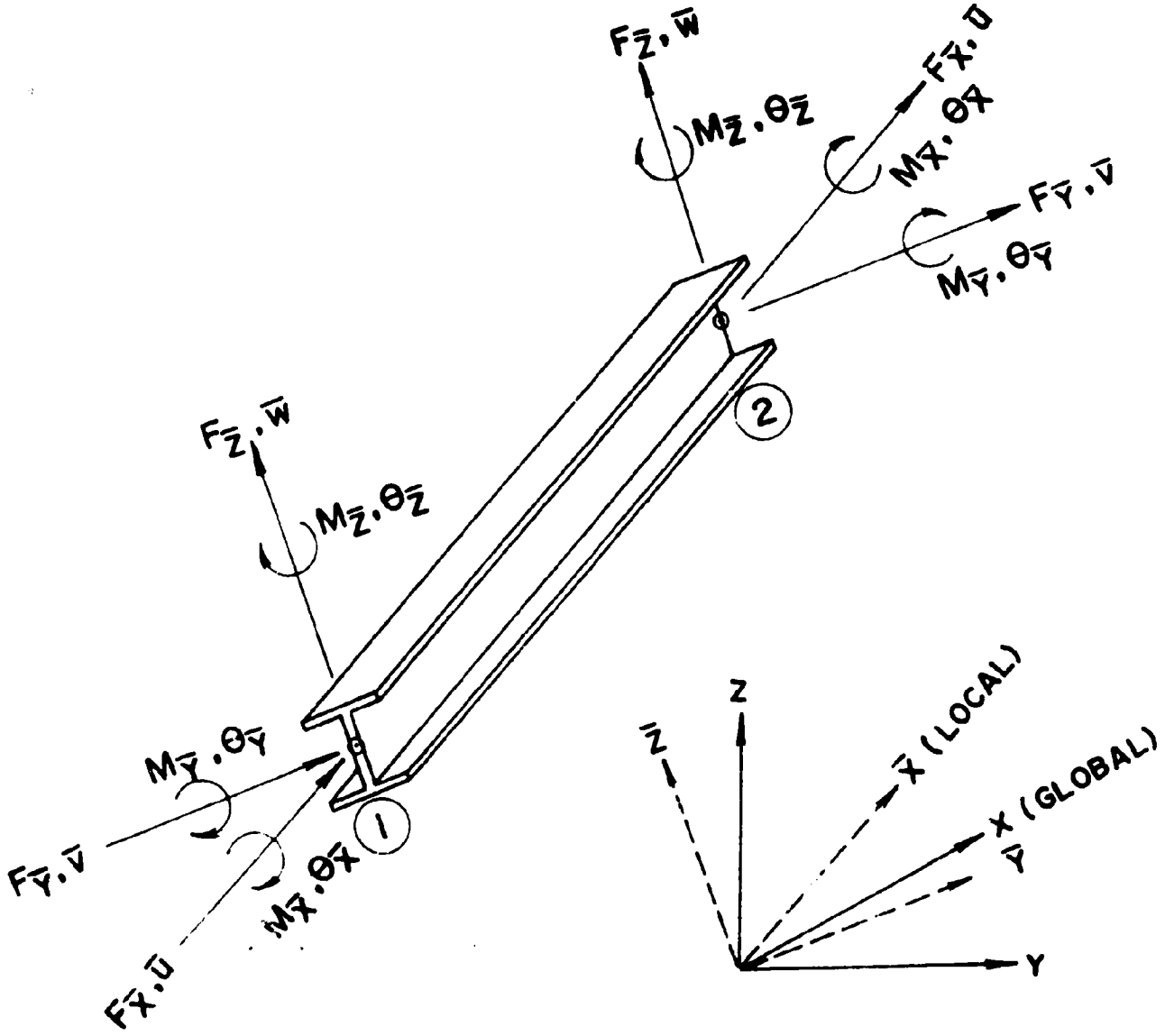

Fig. 1.4. Description of a general three-dimensional beam finite element.

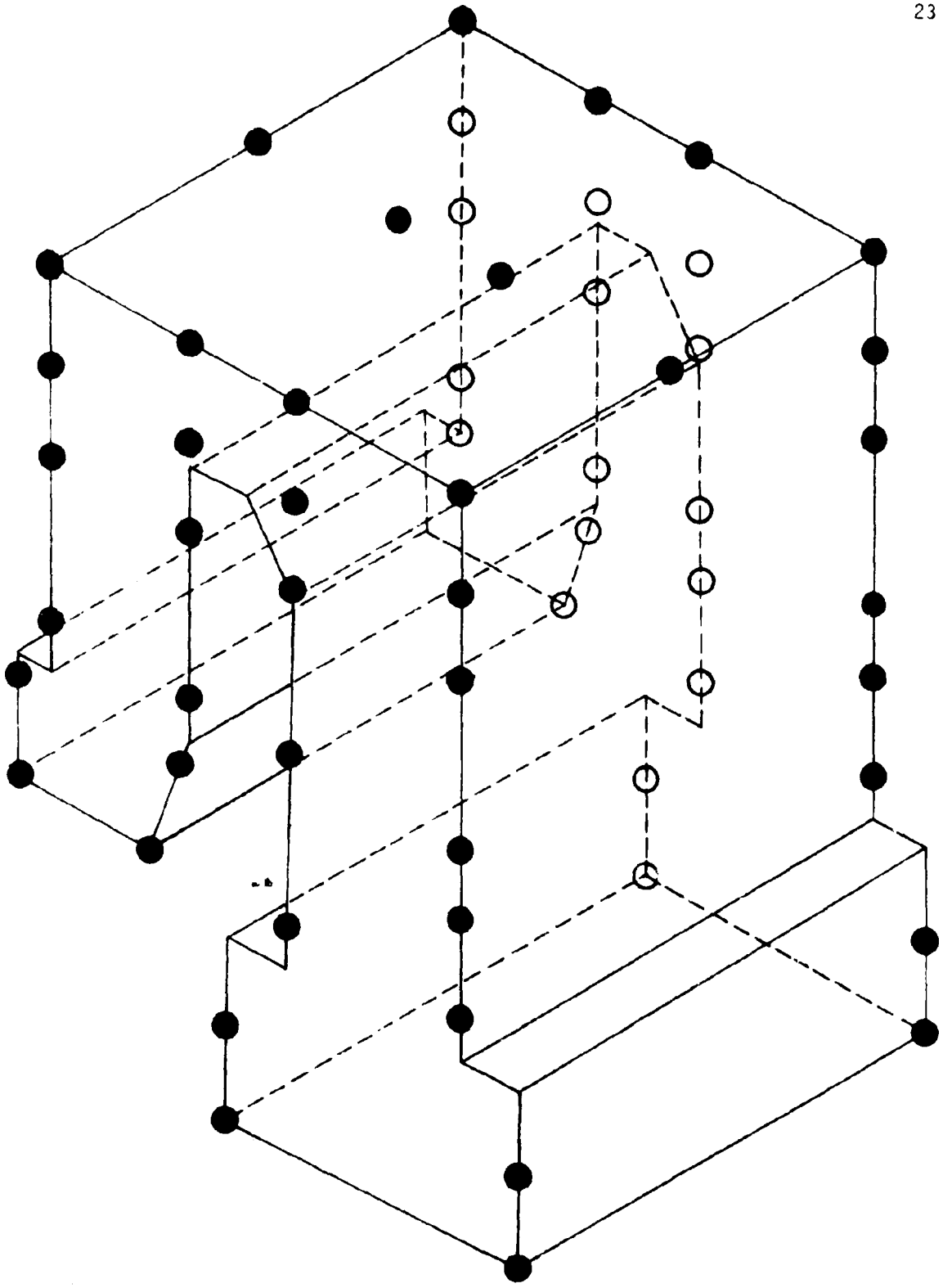

Fig. 1.5. Lumped mass model for the steam generator.

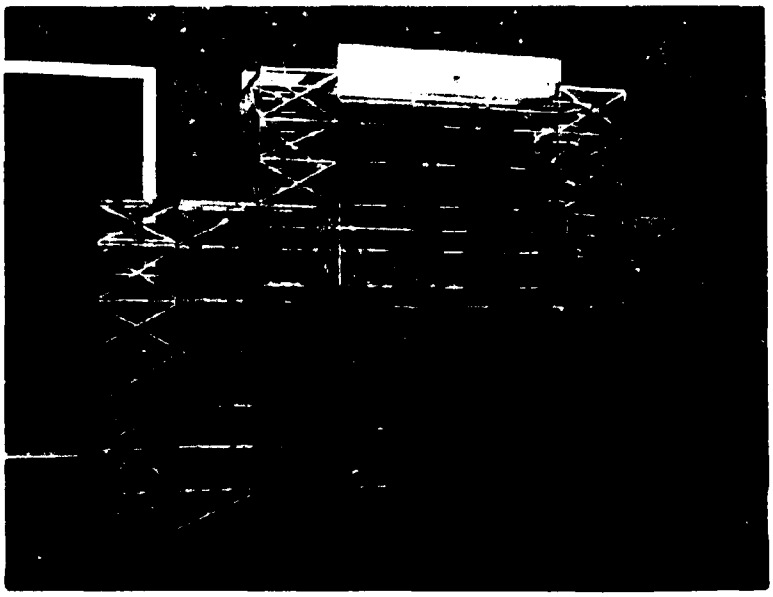

Fig. 1.6 A balsa wood model representing the steel framing structure.

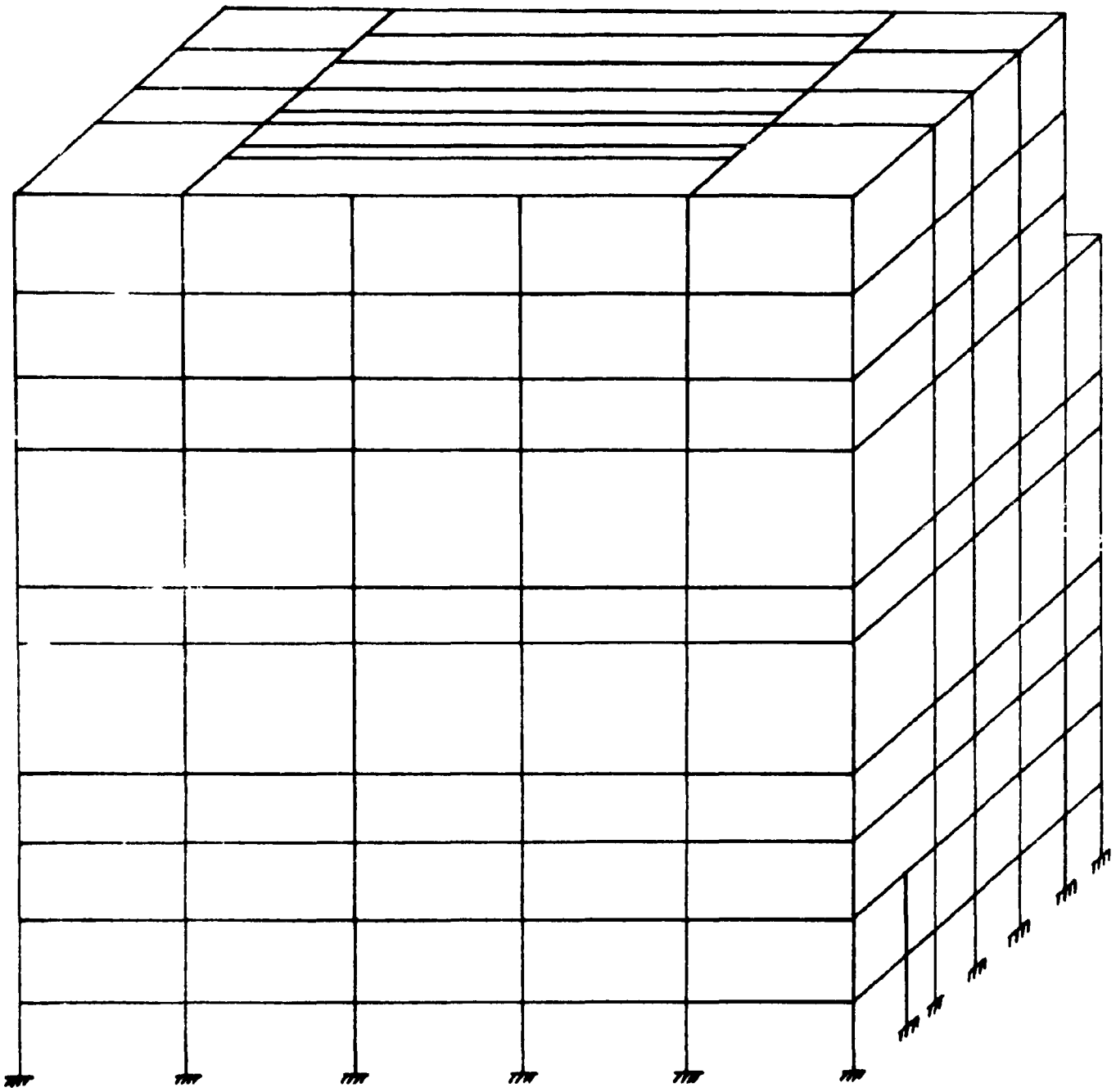

Fig. 1.7. The central portion of the supporting structure for the initial analysis.

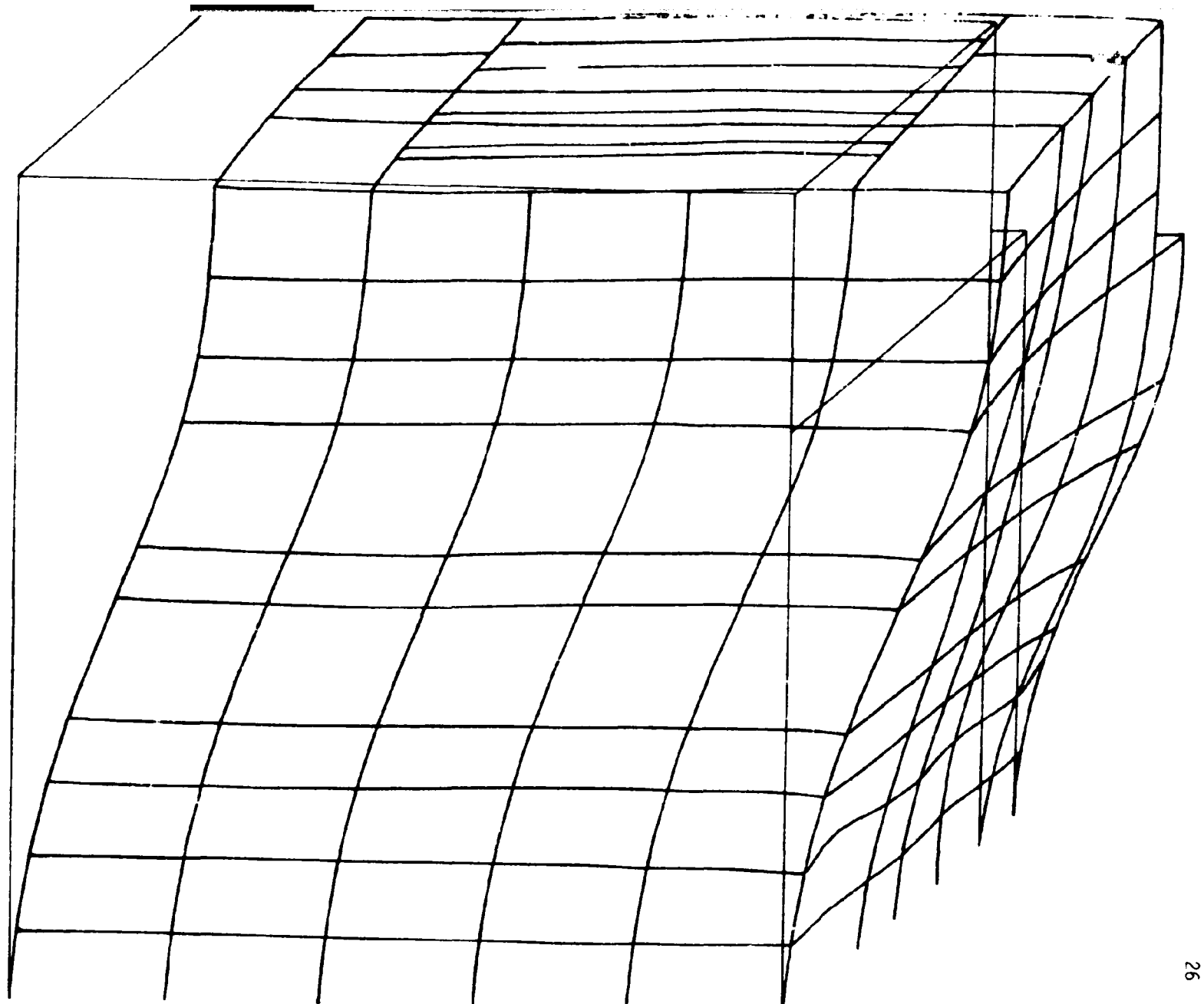

Fig. 1.8. The first mode shape of the central structure without both bracing members and the steam generator (frequency = 0.4299 Hz).

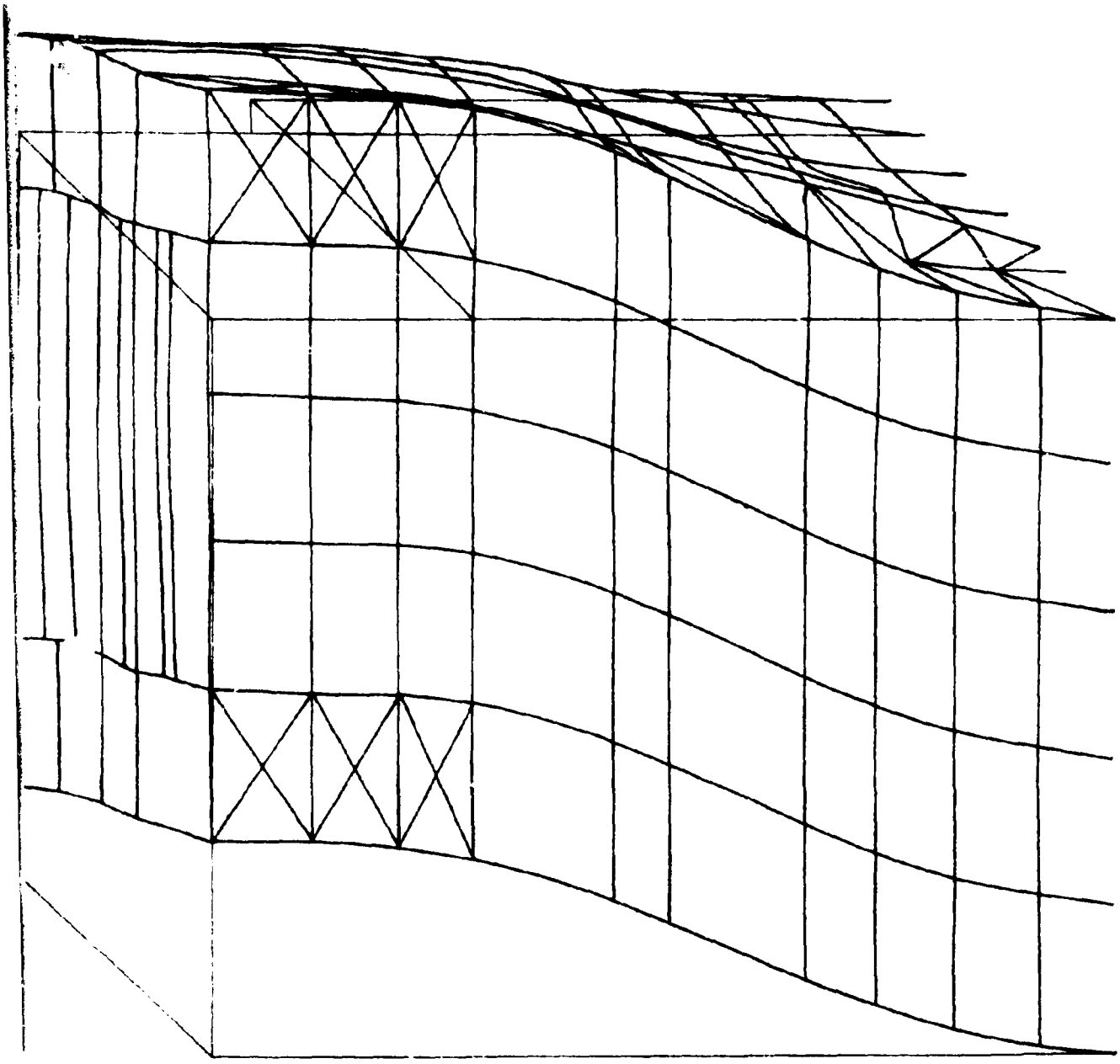

Fig. 7.9. The first mode shape of the central structure without the steam generator but with bracing members (frequency = 0.5517 Hz).

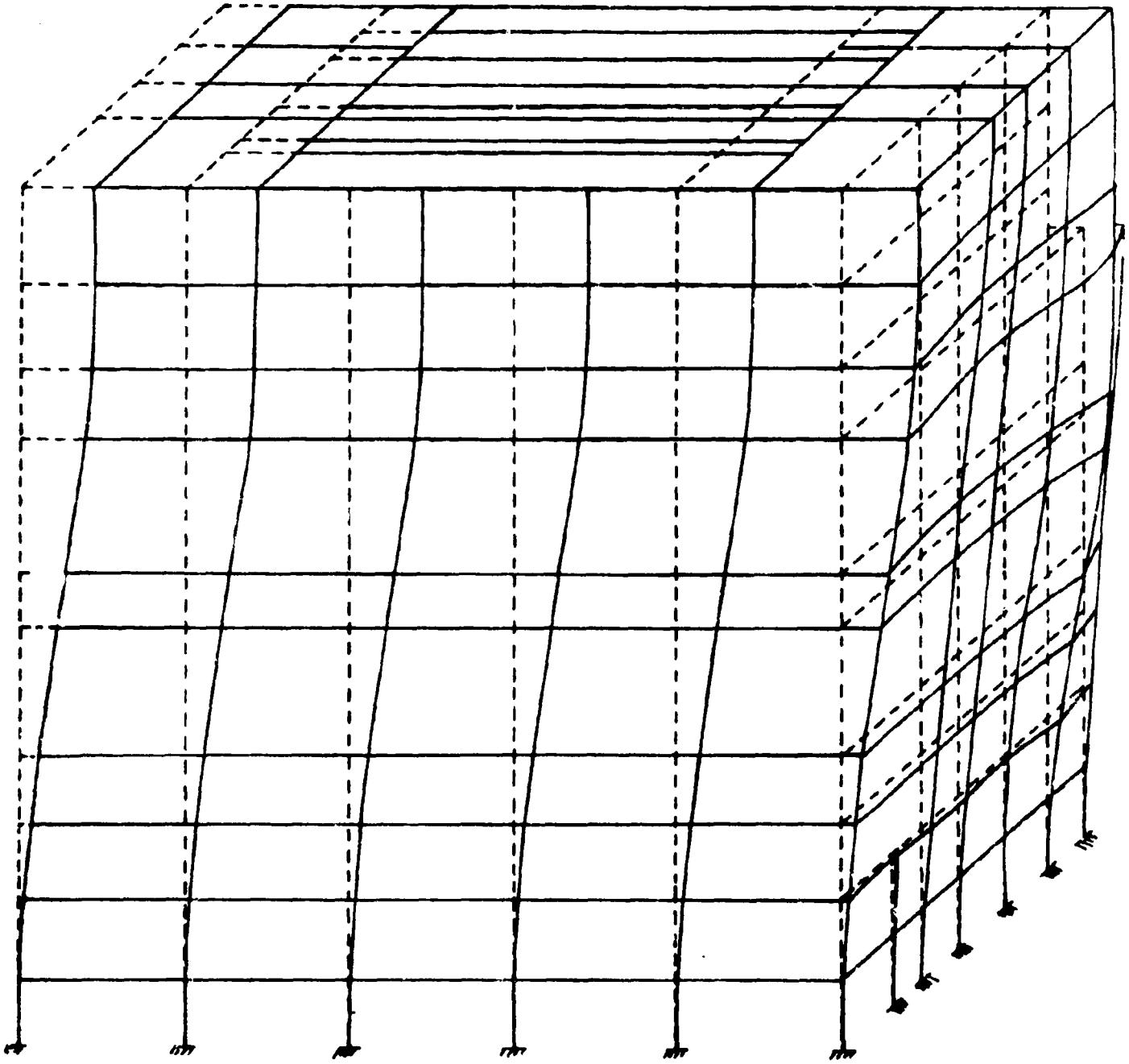

Fig.1.10. The first mode shape of the central structure with the steam generator but without the bracing members (frequency = 0.1556 Hz).

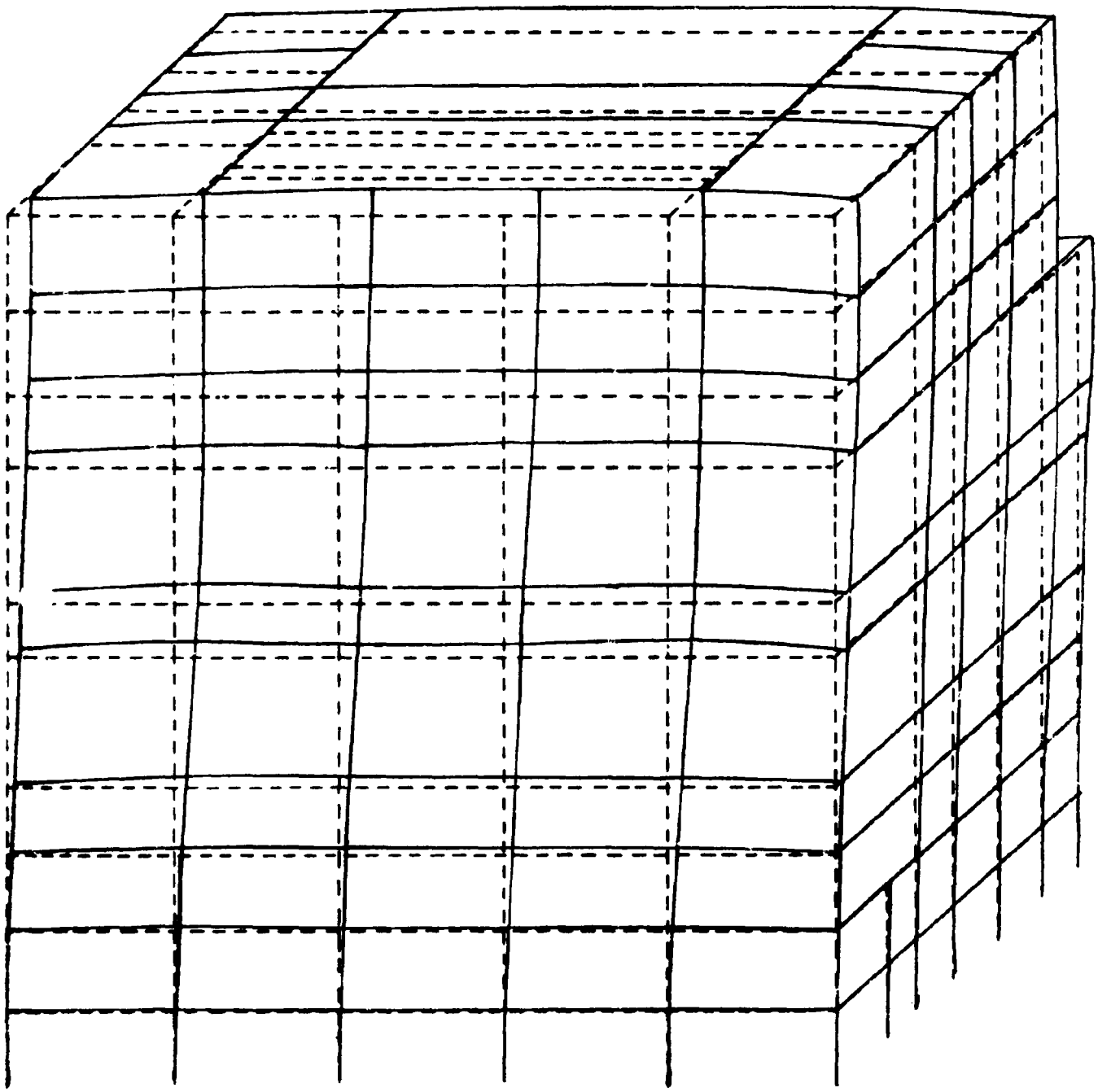

Fig. 1.11. The second mode shape of the central structure with the steam generator but without the bracing members (frequency = 0.1987 Hz).

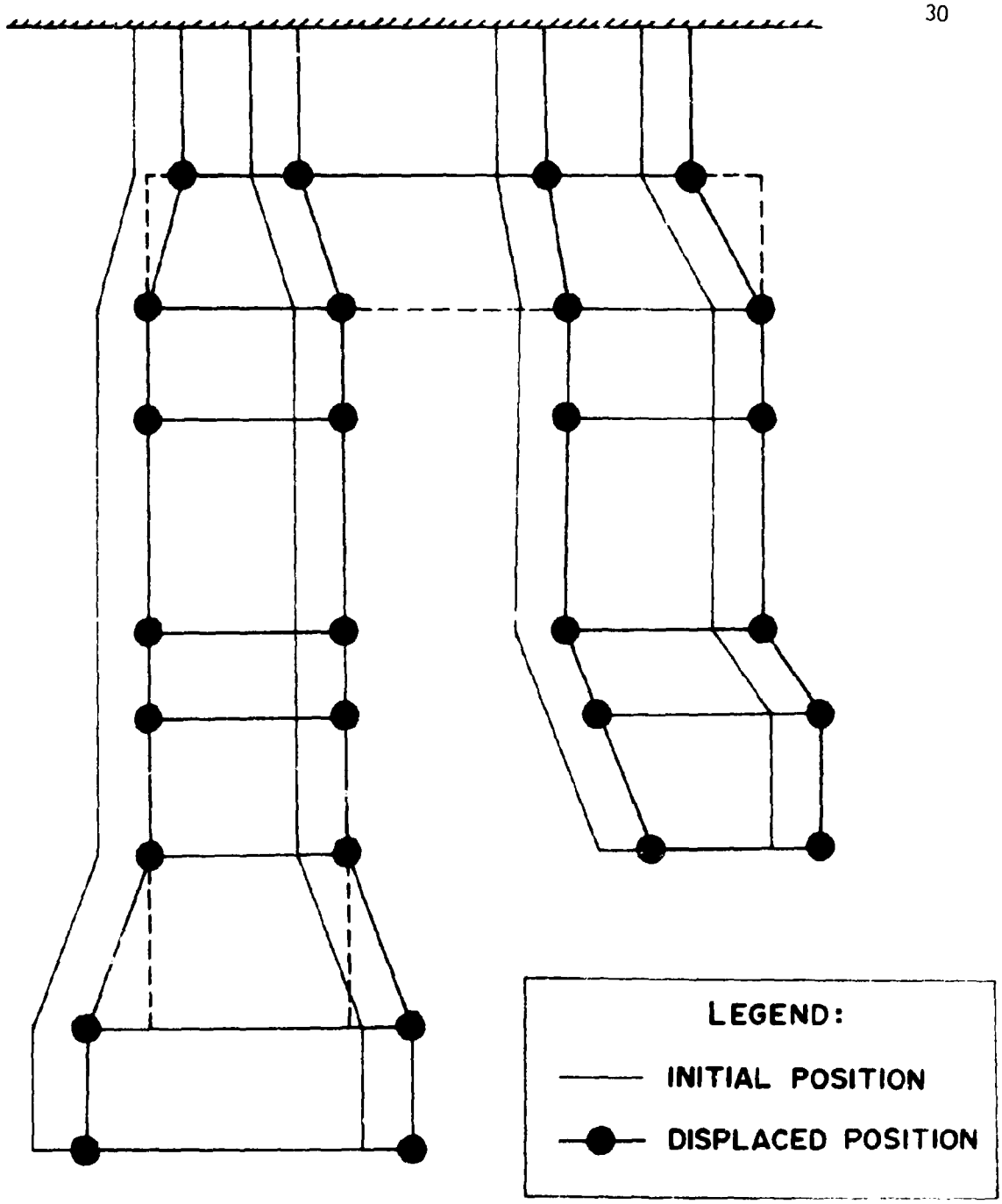

Fig. 1.12. The first mode shape of the steam generator (the displacements are perpendicular to the plane of the paper).

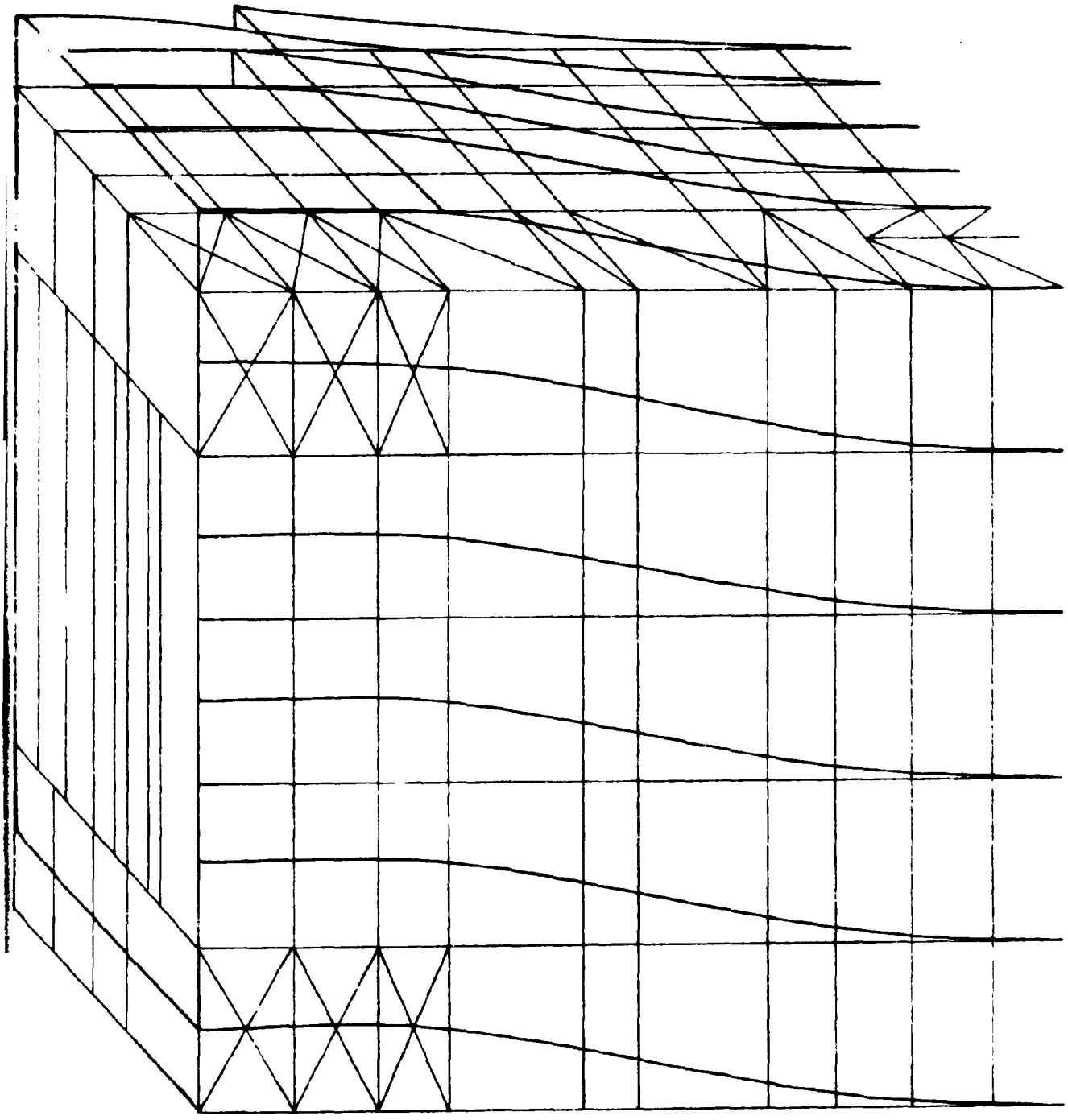

Fig.1.13. The first mode shape of the central structure with both the steam generator and the bracing members (frequency = 0.2060 Hz).

CHAPTER 2

THE HIGH PRESSURE STEAM PIPE

by

C. T. SUN

2.1 Introd ction

The high pressure steam pipe connects the header at the top of the steam generator to the turbine at the ground level. It is a vital part of the electricity generation system in a fossil fuel power plant. A failure of the piping system often means a shutdown of the plant and, as a consequence, a great financial loss.

The current design for the piping system has been based upon static consideration. The supports are designed to take the dead weight and provide flexibility for thermal expansion. Lateral supports are either lacking or very weak. A lateral disturbance such as an earthquake can prove to be hazardous to the pipe.

The purpose of the present study is to determine the natural frequencies as well as the seismic response of a piping system in a power plant. It is hoped that the results of the present work will shed light on the future design criteria for the piping system.

2.2 Geometry and Assumptions

A sketch of the high pressure pipe is shown in Fig. 2.1. Except for the lower end portion, the pipe has 21.25" OD and 4" thickness. The central part runs vertically for about 185'. There are fifteen supports of which

only one provides lateral constraints. A typical design of the supports is shown in Fig. 2.2. It is clear that this type of hanger can only take the dead weight of the pipe but not any lateral loads. As a result, the system is very flexible in the horizontal motions. In view of this, the piping supports will be represented by axial members that take only axial loads.

For this analysis, we neglect damping. Although the internal pressure is high (3,600 psi), the resulting axial stress in the pipe is conceivably small as the pipe is open at both ends. Therefore, the effect of initial stress is negligible.

Two basic types of finite elements are used in this study, namely, the pipe element and the truss element which are provided by the computer program SAP IV. The pipe element can be either straight or curved. Each element has two nodal points with six degrees of freedom at each node. Axial, bending as well as torsional deformations are all accounted for. Lumped mass procedure is used to obtain the mass matrix. The stiffness matrix is the same as given in Chapter 1 for beam finite elements.

The truss element (axial element) consists of two nodal points each having three translational degrees of freedom. The stiffness matrix is given by

$$[K] = \frac{AE}{L} \begin{array}{c} \begin{matrix} u_1 & v_1 & w_1 & u_2 & v_2 & w_2 \end{matrix} \\ \left[\begin{array}{cccccc} \lambda^2 & & & & & \\ \lambda\mu & \mu^2 & & & \text{SYM.} & \\ \lambda\nu & \mu\nu & \nu^2 & & & \\ -\lambda^2 & -\lambda\mu & -\lambda\nu & \lambda^2 & & \\ -\lambda\mu & -\mu^2 & -\mu\nu & \lambda\mu & \mu^2 & \\ -\lambda\nu & -\mu\nu & -\nu^2 & \lambda\nu & \mu\nu & \nu^2 \end{array}\right] \end{array} \qquad (2.1)$$

where A is the cross-sectional area, E the Young's modulus, L the length, and λ,μ,ν are the direction cosines between the local element coordinates and global coordinates.

The equations of motion for the discretized system can be written in matrix form as

$$[K]\,[\delta] + [M]\,[\ddot{\delta}] = [P] \tag{2.2}$$

in which [M] is the mass matrix, δ is the generalized nodal displacement, and the [P] represents the external loads.

2.3 Free Vibration

In the study of free vibrations of the pipe, we assume that the ends are clamped, i.e., all the degrees of freedom at the ends are suppressed. Since the external forces are absent, the equations of motion reduce to

$$[K]\,[\delta] + [M]\,[\ddot{\delta}] = [0] \tag{2.3}$$

The natural frequencies ω of the system are required to satisfy the frequency equation:

$$|\,[K] - \omega^2\,[M]\,| = 0 \tag{2.4}$$

In the numerical calculations, twenty-eight elements (one element between two supports) are used for the pipe and each hanger rod is represented by a truss element. The total number of degrees of freedom is 156. The solutions for the first twenty modes are given in Table 2.1. The CP time for the computation is 44.7 seconds.

As is well known that the accuracy of finite element solutions depends on the number of elements employed, we also use eighty-nine elements (522 dof) to compute the natural frequencies for the first twenty modes. The results are also listed in Table 2-1 for the sake of comparison. It is noted that, in general, the two sets of solutions agree quite well, at least for the first ten modes. The CP time for the 89 element solution, however, runs as high as 336.7 seconds. Thus, if not more than ten modes are required, twenty-eight elements should prove to be sufficient.

The mode shapes of the first three modes are shown in Figs. 2.3, 2.4, and 2.5, respectively. It is found that for the first two modes, the amplitudes in the x-direction are much greater than those in the y-direction, especially in the first mode. The y-direction displacement becomes more pronounced in the third mode. Going through the first twenty modes, we find that the motion in the z-direction is negligible for the first ten modes. It becomes substantial only in the twelfth and thirteenth modes. This clearly indicates that although the supporting hanger rods are slender (1 1/2" in diameter), they do provide substantial rigidity to the pipe in the vertical motion. In view of this fact, we remove the supports but suppress the z-components of displacement at the supported nodes of the pipe. Using 28 elements (130 dof) we compute the natural frequencies for the first ten modes. The solutions agree very well with the solutions with hanger rod supports. The computing time is reduced to 16 seconds.

From the numerical results, we note the fact that the lower vibrational modes with lower frequencies is due to the piping supports that do not possess lateral rigidity to the system. For the sake of comparison, we also

represent the supports by beam elements. With this type of elements lateral constraints to the pipe are given by the beam elements through bending. Using 89 elements, we compute the natural frequencies for the first ten modes which are shown in Table 2.2. By comparing with the previous solutions with truss supports, it is found that the beam type supports increase the values of the first three natural frequencies quite appreciably. The higher modes are less affected by this change.

2.4 Seismic Response

The high pressure steam pipe is supported by the steel frame and connected to the steam generator and the turbine. During an earthquake, the piping system could pick up disturbances from the ground as well as the boiler frame. It seems reasonable to take into account only the interactions between the pipe and the header of the steam generator and the turbine as the supports can not transmit lateral motions. In this report we assume that the upper end is fixed while the lower ends are subjected to a ground acceleration. A more realistic consideration should take the motion of the frame under the same seismic disturbances as a forcing source at the upper end.

To reduce the computing time, we use 28 elements (130 dof) for the analysis of transient response. The El Centro earthquake record is used for the ground motion. Only one component of the acceleration (the north-south motion) is used, see Fig. 2.6. The direction of the acceleration is placed parallel to the x-direction, or the weakest direction of the piping system.

Under the ground acceleration δ_g the equations of motion are

$$[K]\,[\delta_r] + [M][\ddot{\delta}_r] = -\,[M][\ddot{\delta}_g] \qquad (2.5)$$

where δ_r is the relative displacement of the structure with respect to the ground. The solution to equation (2.5) can be carried out either by direct integration or mode superposition. The direct step-by-step integration is more effective for shock problems where many modes are included and fewer time steps are required. In the present study, by judging from the highly oscillatory nature and the long duration of the acceleration history, the method of mode superposition is employed. The ten lowest vibration modes are used in the analysis with the highest frequency being 5.59 Hz.

The ground acceleration history is discretized into 400 time steps for the first 8 seconds. The reasons for stopping at the 8th second are that the acceleration is much more intensive in the first 4 seconds and that use of less time steps would yield more accurate results.

In Fig. 2.7, the maximum displacements and the corresponding times of occurrence are shown. The maximum displacement in the x-direction occurs at 5.8 seconds with the amplitude being 19.3". Such a large translational motion could be hazardous.

The maximum bending moments and the corresponding times of occurrence are shown in Fig. 2.8. It is observed that the bending moments are more severe at the bends near the ends. At 1.48 second the maximum torsional moments on the vertical section reach the maximum value of 3.25×10^6 in-lb. It should be noted that the time at which maximum displacement takes place may not be the time for the maximum bending moment.

From Fig. 2.8, it is seen that on the upper and vertical sections where the outside diameter of the pipe is 21.25" the maximum bending moment is $14. \times 10^6$ in-lb. The corresponding bending stress is 18.45×10^3 psi. This

high bending stress could be critical since the yield stress for steel under high temperature is much lower than that at room temperature. The maximum bending moment on the branched sections is 10.0×10^6 in-lb, as shown in Fig. 2.8. The outside diameter of the pipe is 15.25" and thickness being 2.875". The corresponding bending stress is 25.6×10^3 psi.

Figs. 2.9 and 2.10 show the configurations of the pipe at various times. It is important to note that the deformed configurations resemble that of the first mode in free vibration. This indicates that the system could be undergoing a motion that is dominated by the first natural mode. In order to check the approximate period at which the piping system vibrates under the seismic loading, the displacement at point A (see Fig. 2.7) is plotted versus time in Fig. 2.11. The period is found to be 2.7 seconds. We recall that the period for the first natural mode was 2.85 seconds.

2.5 Future Investigation

Because of the three-dimensional nature of the piping system, the motions in the x-, y- and z-directions are coupled. The dynamic response should be analyzed by taking into account the complete ground motion. By March 1976 such analysis will be completed.

It is known that damping plays an important role in dynamic response of a structure. Since the structural damping is hard to estimate, only the material damping will be considered in the first phase of the project.

Table 2.1 Natural frequencies obtained with different d.o.f.

N. F. (Hertz) / MODE	89 Elements (522 d.o.f.)	28 Elements (156 d.o.f.)	28 Elements (130 d.o.f.)
1	0.351	0.353	0.368
2	0.608	0.596	0.627
3	0.764	0.763	0.810
4	1.162	1.132	1.207
5	2.064	2.066	2.174
6	2.171	2.110	2.247
7	3.692	3.862	3.919
8	3.882	4.084	4.301
9	4.804	4.732	4.834
10	5.521	5.446	5.590
11	6.532	6.168	
12	6.946	7.610	
13	7.828	8.426	
14	9.720	8.911	
15	9.814	10.643	
16	10.763	12.240	
17	12.402	12.273	
18	14.540	14.540	
19	15.038	17.518	
20	16.837	18.692	

Table 2.2 Natural frequencies for different supports.

N. F. (Hertz) / MODE	Truss Supports (89 Elements)	Beam Supports (89 Elements)
1	0.351	0.463
2	0.608	0.694
3	0.764	0.842
4	1.162	1.183
5	2.064	2.107
6	2.171	2.205
7	3.692	3.702
8	3.882	3.888
9	4.804	4.810
10	5.521	5.536

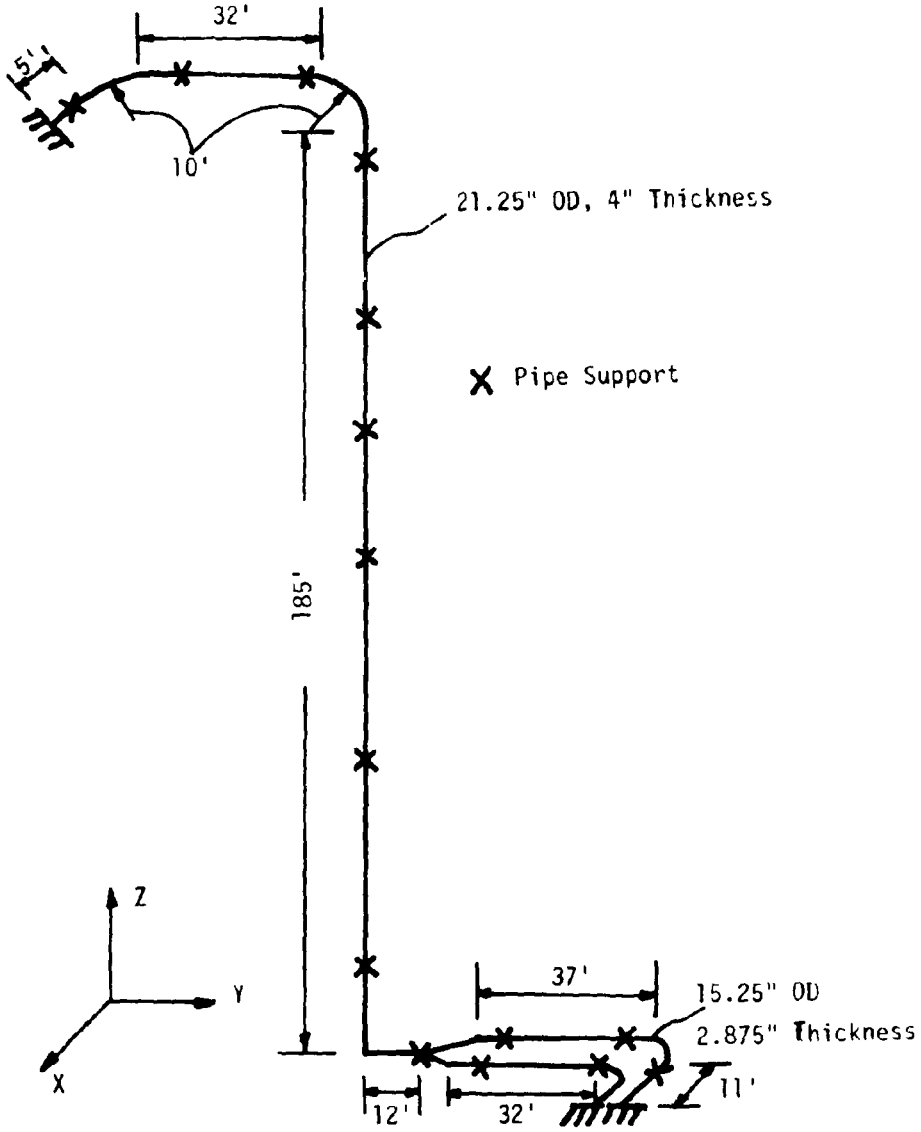

Fig. 2.1 Geometry of the high pressure steam pipe

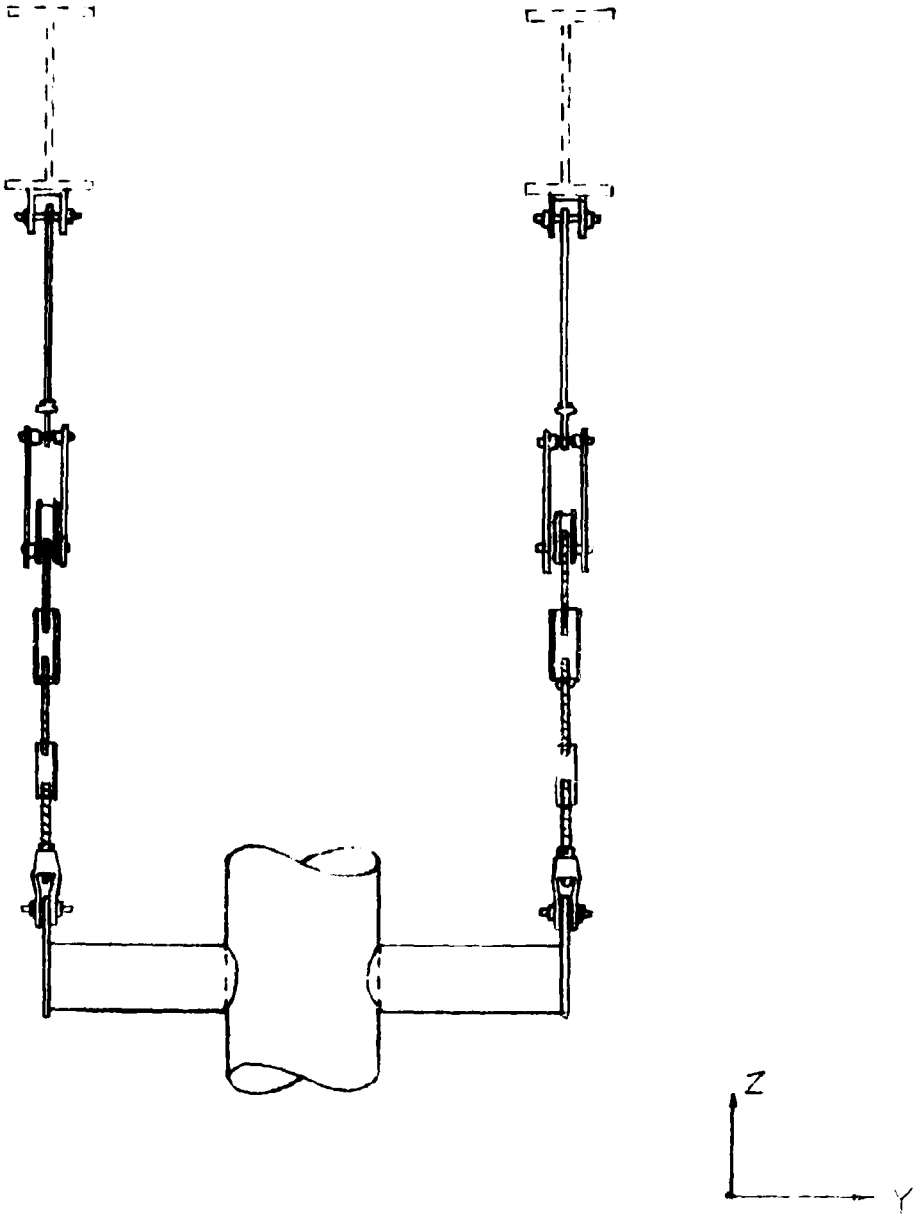

Fig. 2.2 The pipe support

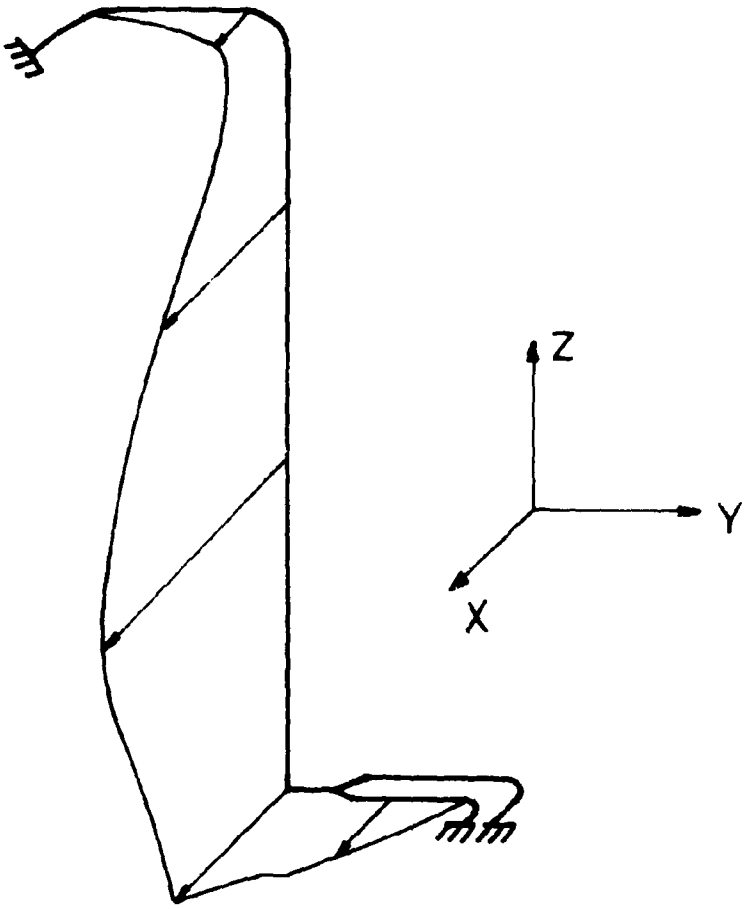

Fig. 2.3 First natural mode

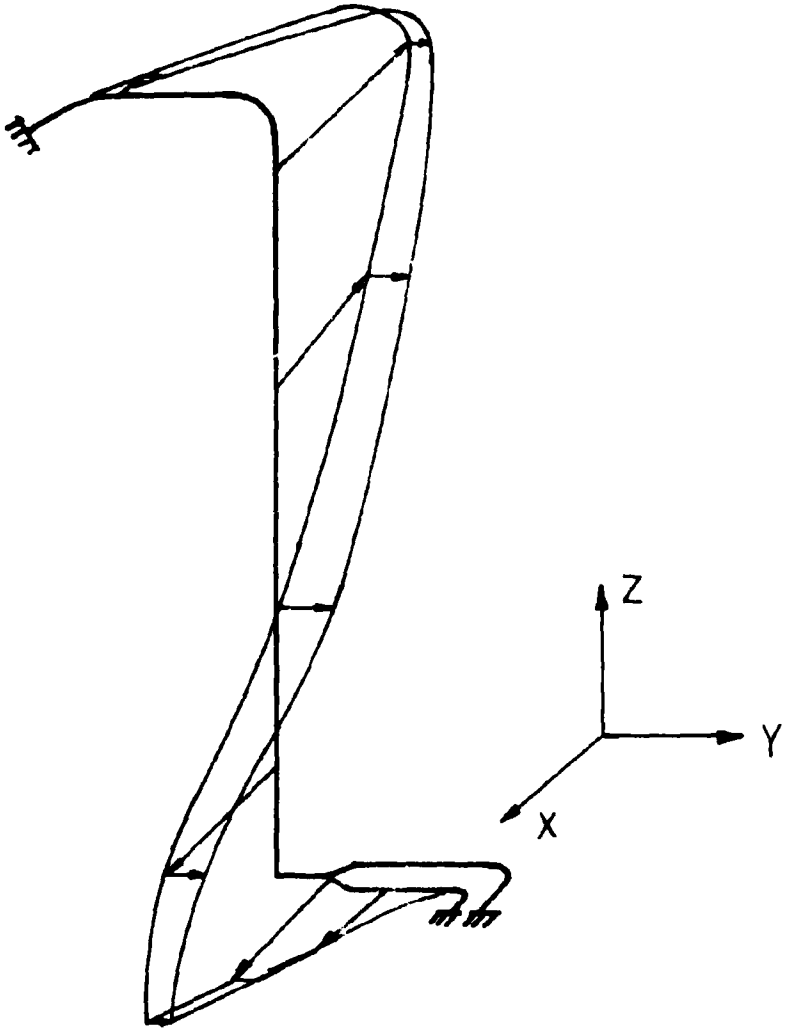

Fig. 2.4 Second natural mode

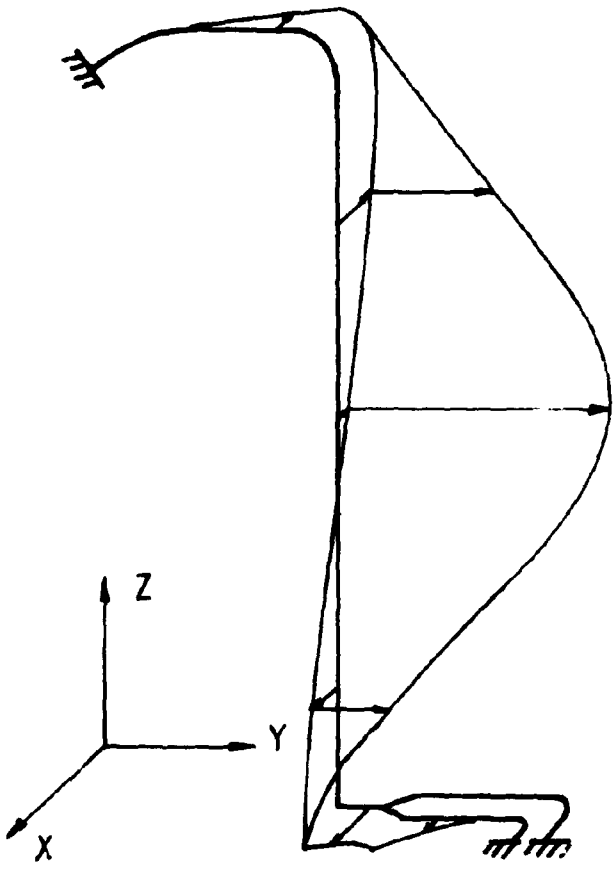

Fig. 2.5 Third natural mode

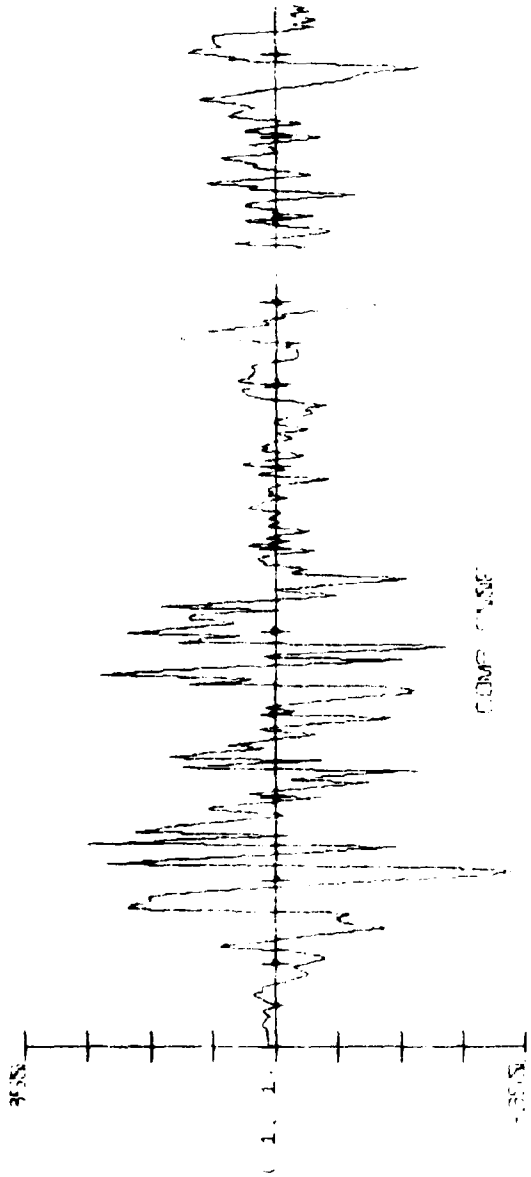

Fig. 2.6 The El Centro earthquake (North-South acceleration)

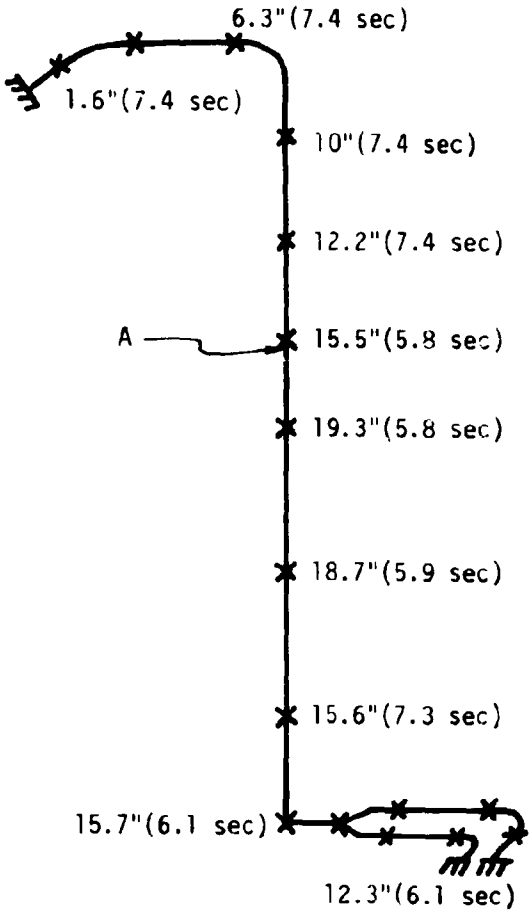

Fig. 2.7 Maximum displacements and the corresponding time of occurrence.

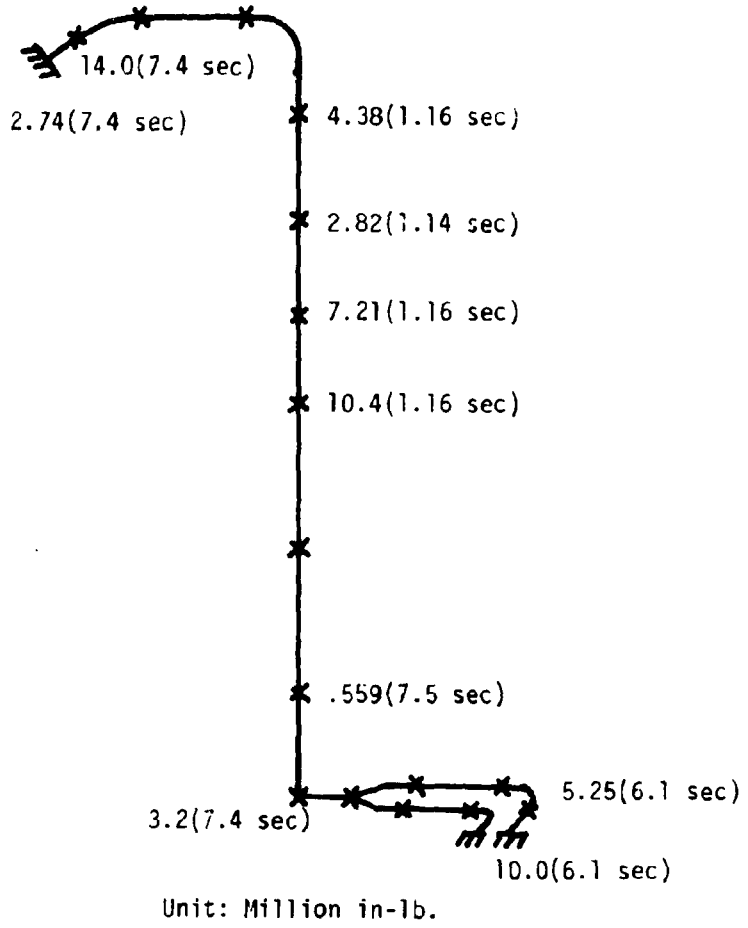

Fig. 2.8 Maximum bending moments and the corresponding time of occurrence.

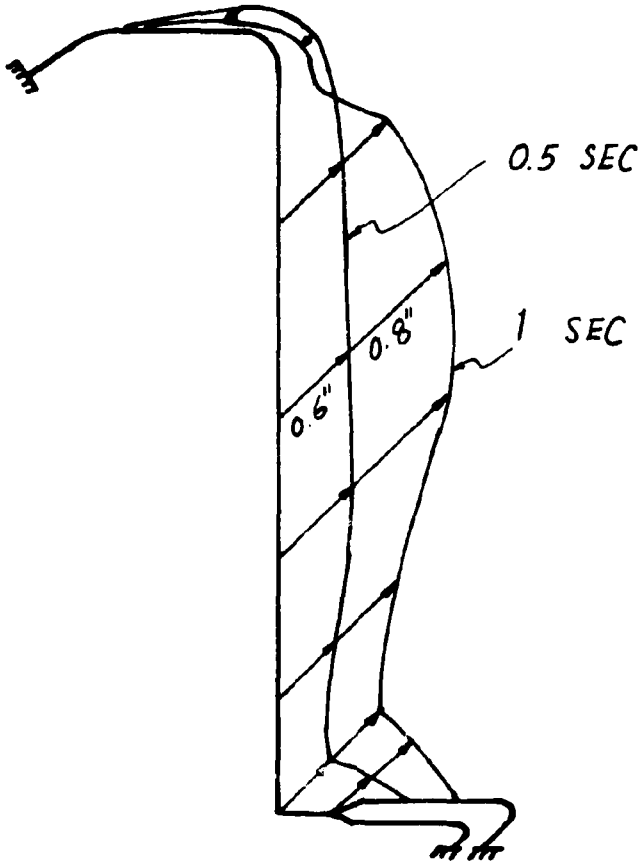

Fig. 2.9 Deformed configurations at t = 0.5 and 1 second.

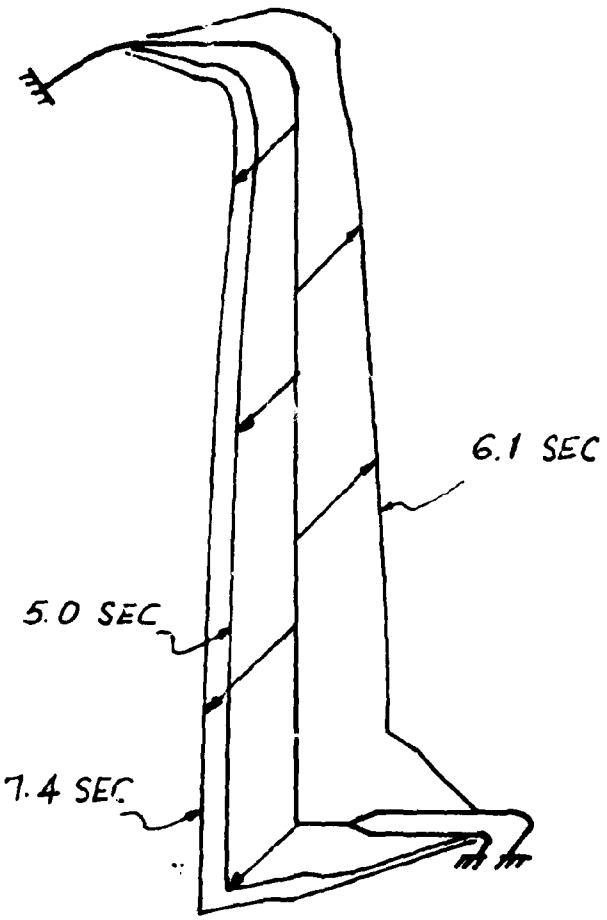

Fig. 2.10 Deformed configurations at t = 5.0, 6.1, and 7.4 seconds.

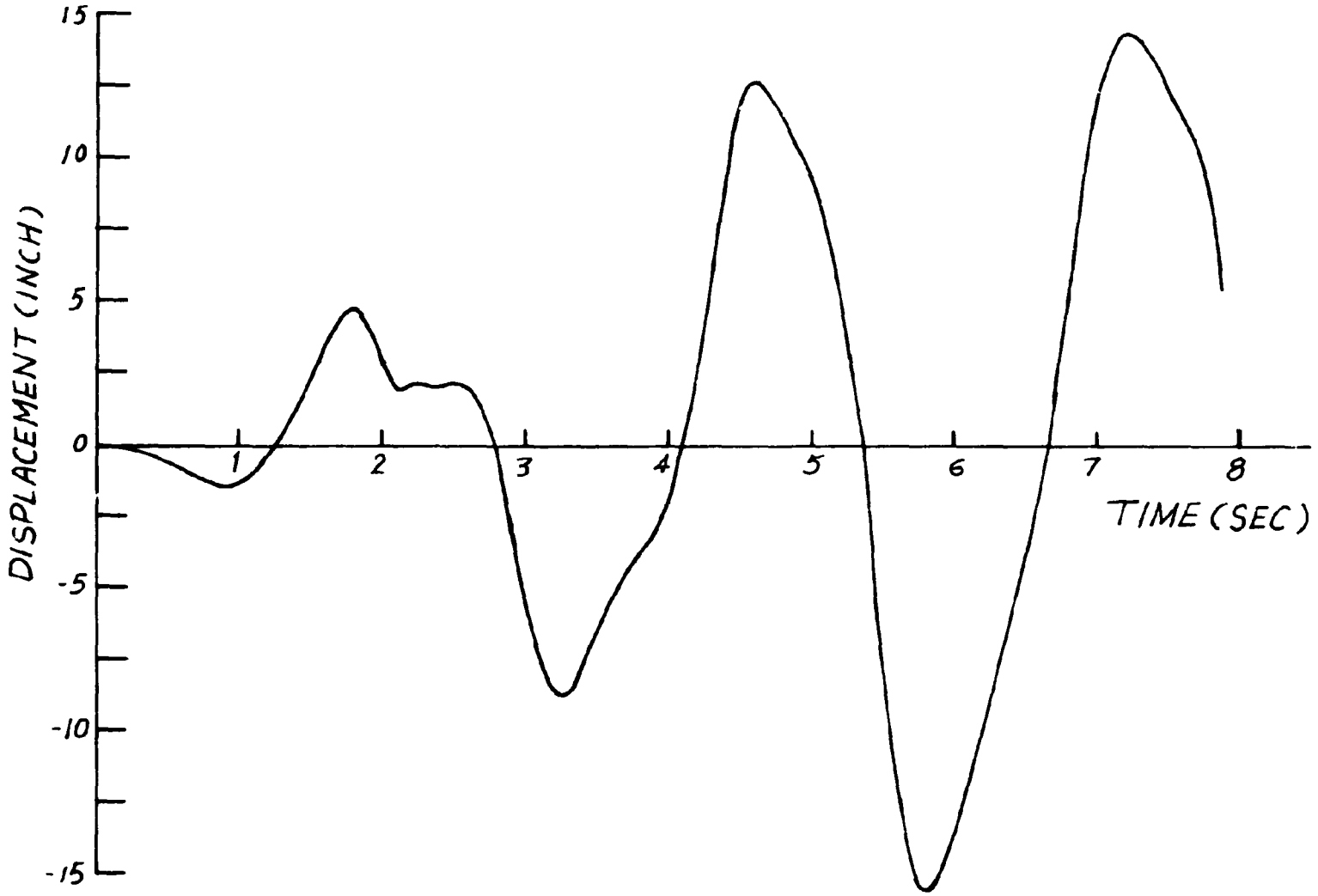

Fig. 2.11 Displacement at Point A (Fig. 2.7) as a function of time.

CHAPTER 3

COAL HANDLING EQUIPMENT

by

K. W. KAYSER

J. A. EULER

3.1 Introduction

In the handling of the coal for a power plant, there are numerous conveyor systems used for the transporting of coal. This section is concerned with the analysis of the structures associated with these conveyor systems. There are essentially two types of coal handling structures of interest. One being the facility which transports the coal to the plant and the other a structure for transporting coal within the yard.

For this analysis, we used conveyors No. 13 and No. 14 of the Paradise plant to represent a facility which transports coal to the plant. A typical transporting facility in the yard is represented by conveyors 28 and 29 of the Paradise plant which is a facility associated with Unit 3 of the plant. In what follows, the facility for transporting coal to the plant will be designated by Coal Handling Structure No. 1 (CHS 1), and the yard facility will be designated by Coal Handling Structure No. 2 (CHS 2).

The general approach to the analysis was to replace the multi-elemented structures by equivalent beams having the same static properties, and then using the finite element method to calculate the natural frequencies and mode shapes.

To date, the first 15 natural frequencies and mode shapes have been obtained.

3.2 Description of the System

Coal handling structure No. 1 is described by the two-dimensional view of Figure 3.1. The inclined conveyor section consists of approximately 700 truss elements and is supported by the bents. It is attached at one end to the earth and at the other to the plant.

Coal handling structure No. 2 is shown in the two-dimensional view of Figure 3.2. For this structure the two conveyor sections consist of approximately 1000 truss elements and have three supporting bents plus a supporting tower structure.

Simple models for these structures have been obtained by constructing equivalent beam elements of suitable length that have the physical properties of the actual structure for that length.

3.3 Modeling of the Structures

To obtain an equivalent beam for a bent the assumption was made that the bent is composed of beam elements. The bent was then assumed to be fixed at one end and the loads shown in Figure 3-3 were applied at the other end. The displacements δ_x, δ_y, and δ_z at the free end of the bent due to these applied loads were

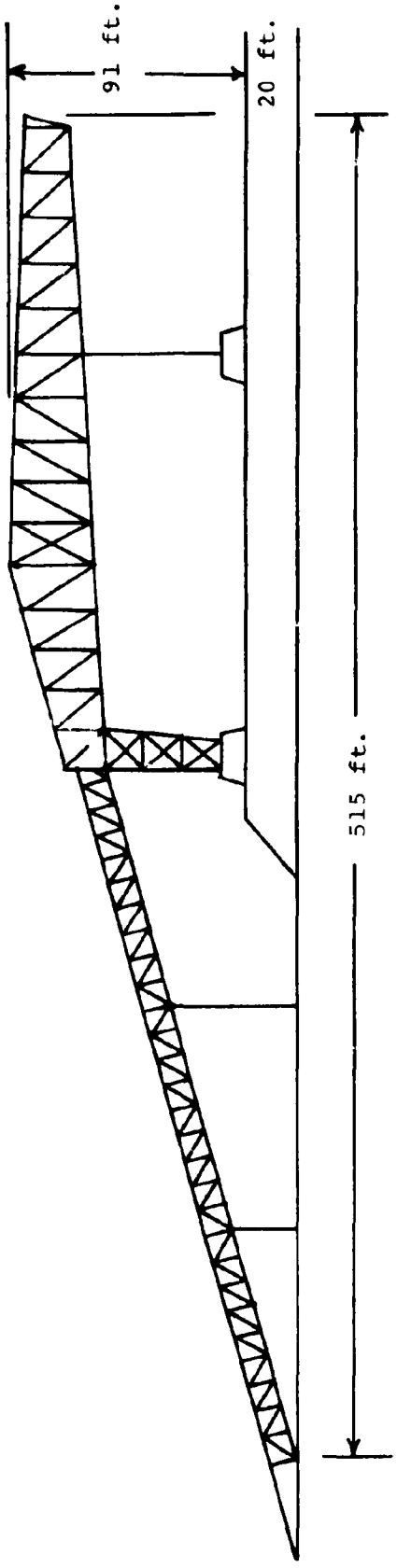

Fig. 3-2 Coal Handling Equipment for Coal Yard

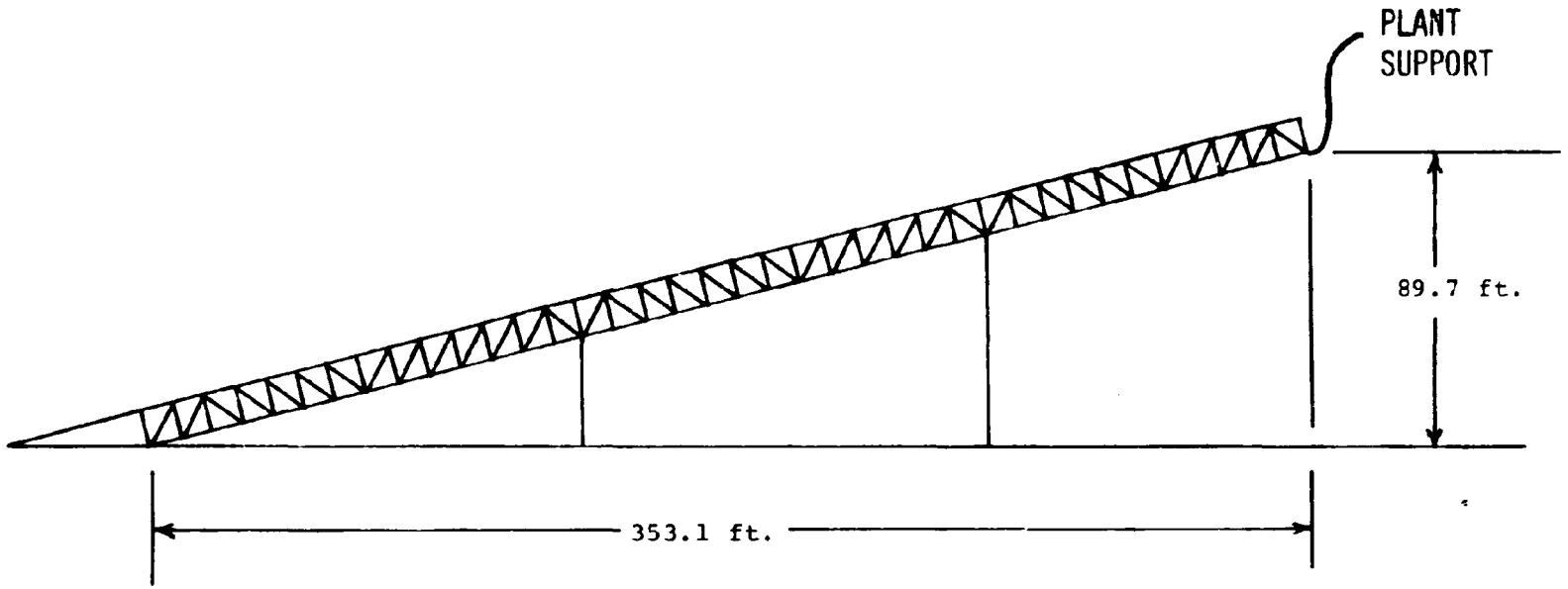

Fig. 3-1 Coal Handling Equipment for Central Power Station

then obtained by modeling the bent with finite beam elements and using the static analysis section of the SAP IV program.

The equivalent beam for the bent must have the same displacements as the bent. From analytical considerations the displacements of the equivalent beam are given by

$$\delta_x = \frac{2F_x \ell^3}{3EI_z} \quad ; \quad \delta_y = \frac{2F_y \ell}{EA} \quad ; \quad \delta_z = \frac{2F_z \ell^3}{3EI_x}$$

Thus the physical characteristics of the equivalent beam are given by:

$$EI_x = \frac{2F_z \ell^3}{3\delta_z} \quad ; \quad EI_z = \frac{2F_x \ell^3}{3\delta_x} \quad ; \quad EA = \frac{2F_y \ell}{\delta_y}$$

A similar approach was used for finding the equivalent beam for the conveyor sections. A section of the conveyor structure was fixed at one end and the force configurations of Figure 3.4 were applied at the other end. It was assumed that the conveyor section was composed of truss elements. The displacements δ_x, δ_y and δ_z for the section due to the applied loads were then obtained by modeling the section with truss elements and using the static analysis section of the SAP IV program.

From analytical considerations it follows that the force configurations of Figure 3.4 must yield displacements for the equivalent beam given by

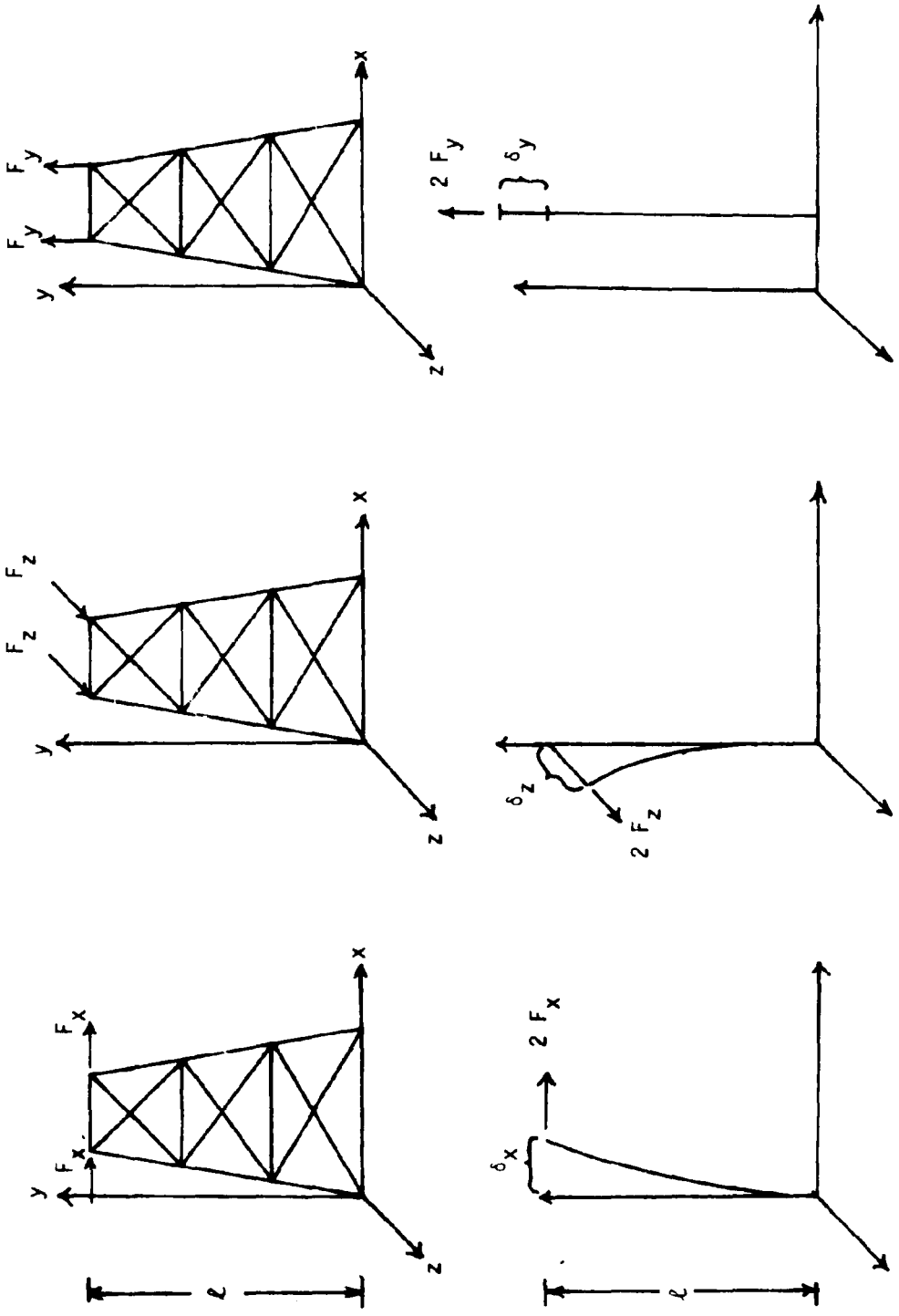

Figure 3-3 Beam Equivalency for Bents

$$EI_z = \frac{F_y b\ell^2}{\delta_x} \quad ; \quad EA = \frac{4F_y \ell}{\delta_y} \quad ; \quad EI_x = \frac{F_y a\ell^2}{\delta_z}$$

Therefore the physical characteristics at the conveyor section are given by

$$EI_z = \frac{F_y b\ell^2}{\delta_x} \quad ; \quad EA = \frac{4F_y \ell}{\delta_y} \quad ; \quad EI_x = \frac{F_y a\ell^2}{\delta_z}$$

For determining the equivalent beam for the conveyor part of the structure, various lengths of the section were used. It was found that this did not alter the values obtained for the physical characteristics of the equivalent beam.

For determining the equivalent beam for the tower of coal handling structure No. 2, the tower was considered to be composed of truss elements and later of beam elements. Both results gave close results so that either method can be used.

3.4 Natural Frequencies and Mode Shapes

In replacing the coal handling structures with their equivalent beams, it is seen from Figure 3.5 that CHS 1 was replaced by three equivalent beams and CHS 2 by 6 equivalent beams. These beams were then broken down into finite beam elements to be described earlier so as to facilitate the use of the SPA IV program for determining the natural frequencies and mode shapes. From Figure 3.5 we see that CHS 1 has 21 elements and 22 nodal points while CHS 2 has 32 elements and 33 nodal points.

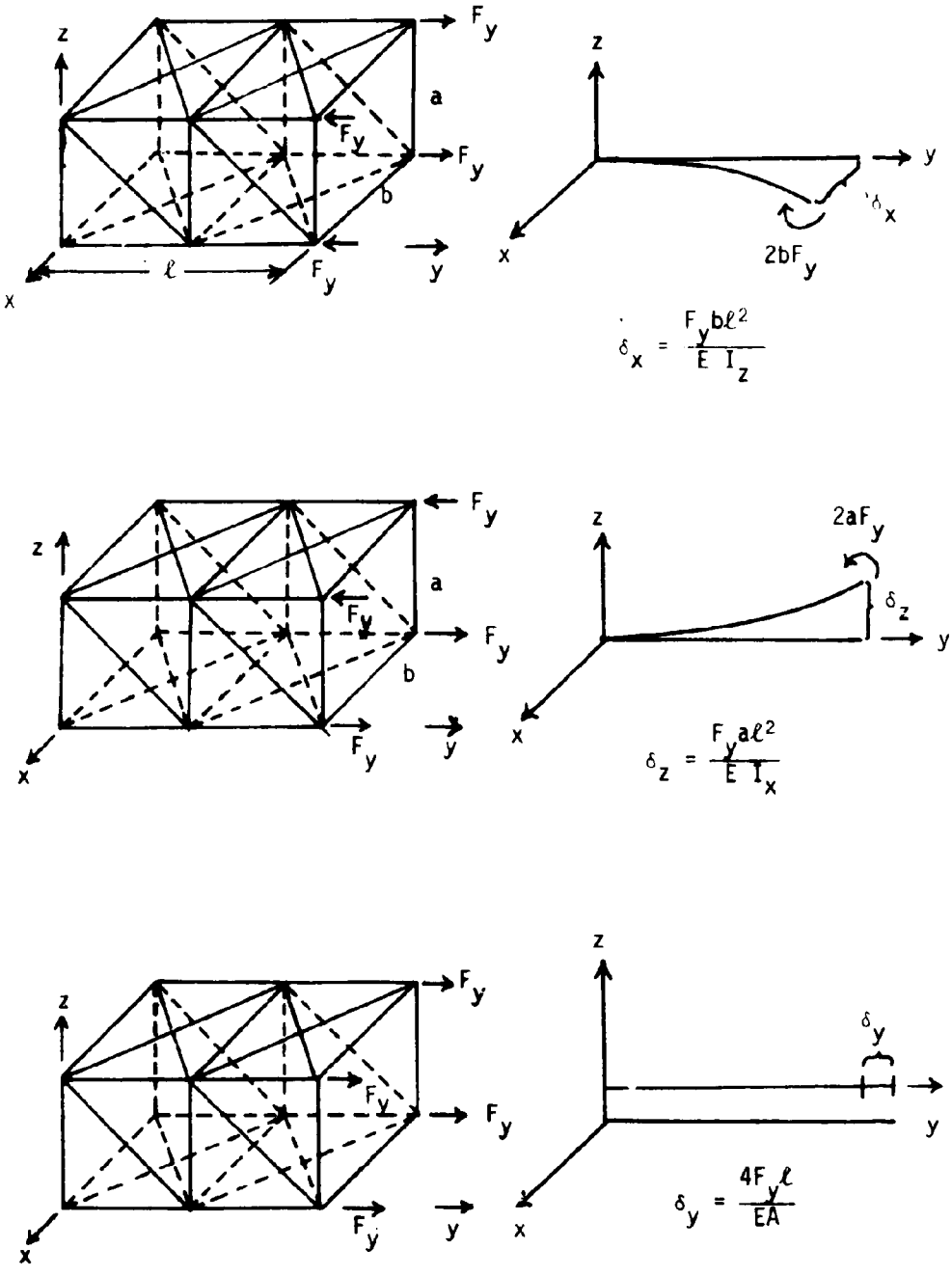

Figure 3-4 Beam Equivalency for Conveyor Section

The boundary for both structures assume that all of the bents are fixed to the ground, i.e., no displacement or rotation allowed. Both inclined conveyors are assumed fixed at the ground except that in-plane rotation is allowed. At the connection of the conveyor to the plant it was assumed that no relative displacements occurred but that rotation is allowed about any axis. In addition, the tower of CHS 2 was assumed fixed to the ground.

With the constraints imposed by the boundary conditions, we obtain a 126 dof model representing CHS 1, while CHS 2 is a 169 dof system. The way that the nodes were numbered resulted in a matrix bandwidth of 18 for CHS 1 and 24 for CHS 2. The first fifteen natural frequencies and mode shapes were obtained for both structures. The frequencies are given in Table 3.1 and the first four mode shapes are shown in Figures 3.6 through 3.13.

Modes 1 and 4 of CHS 1 are essentially lateral modes while modes 2 and 3 are mixed between transverse and longitudinal modes.

For CHS 2, modes 1 and 2 are lateral while 3 and 4 are mixed.

The central processing time for the CDC 6500 computer for the first 15 natural frequencies was 29 seconds for CHS 1 and 39 seconds for CHS 2.

3.5 Results by March 1, 1976

Since the coal yard equipment (CHS 2) is physically unconnected to the rest of the plant, the seismic response for this structure can be investigated independently. This analysis will be completed by March 1, 1976. For investigation of the seismic response of the conveyor to the plant, the plant seismic response is needed. Therefore, this portion of

the study may not be completed by 1 March 1976.

3.6 Future Work

Since it is difficult to determine the torsional properties of the actual structures, an investigation should be made of the sensitivity of the frequency response of the models to changes in the torsional properties. Also, to increase the feasibility of using these methods as a design tool an investigation should be made of ways to reduce the difficulty of obtaining the equivalent beam model. One step in this reduction was finding that only one section of the conveyor need be analyzed to determine the physical properties of the total equivalent beam.

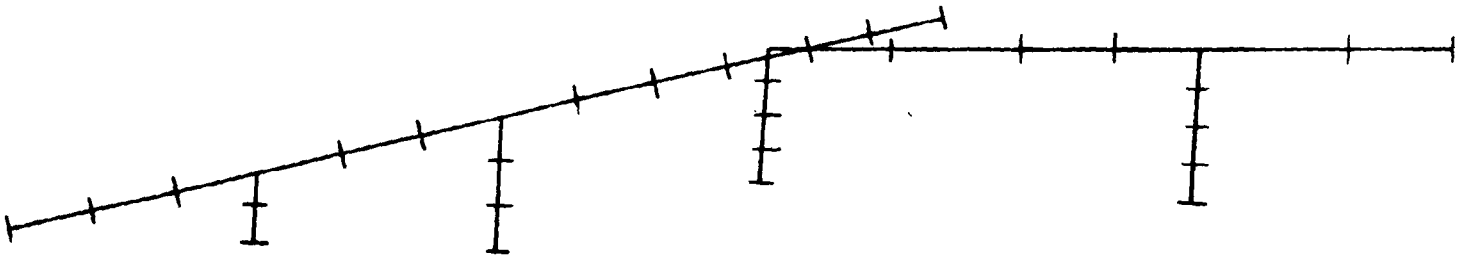

Model of Coal Handling Equipment for Central Power Station

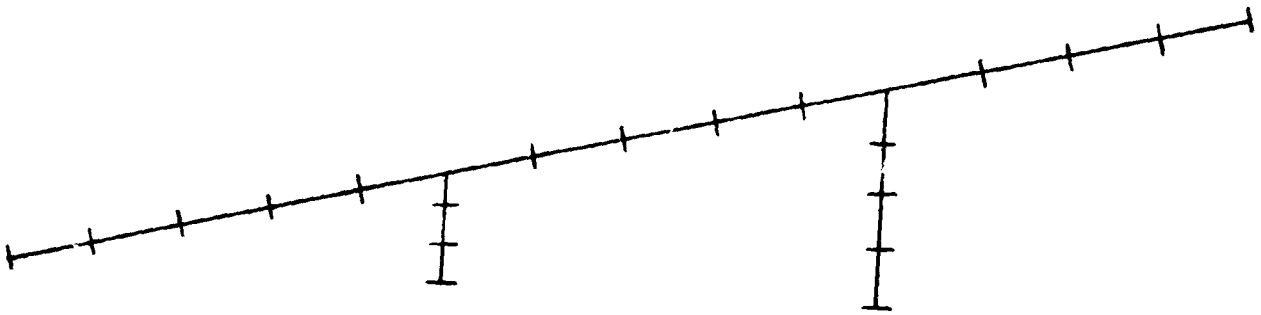

Figure 3-5 Model of Coal Handling Equipment for Coal Yard

Table 3-1

The Natural Frequencies in Hz for the Coal Handling Structures

Mode	CHS 1	CHS 2
1	.597	.516
2	.603	.927
3	1.285	.938
4	1.529	1.089
5	1.763	1.240
6	2.054	1.794
7	2.529	1.847
8	2.776	2.102
9	3.058	2.154
10	3.496	2.314
11	3.890	2.401
12	4.841	2.660
13	4.930	2.675
14	5.830	2.991
15	6.086	3.040

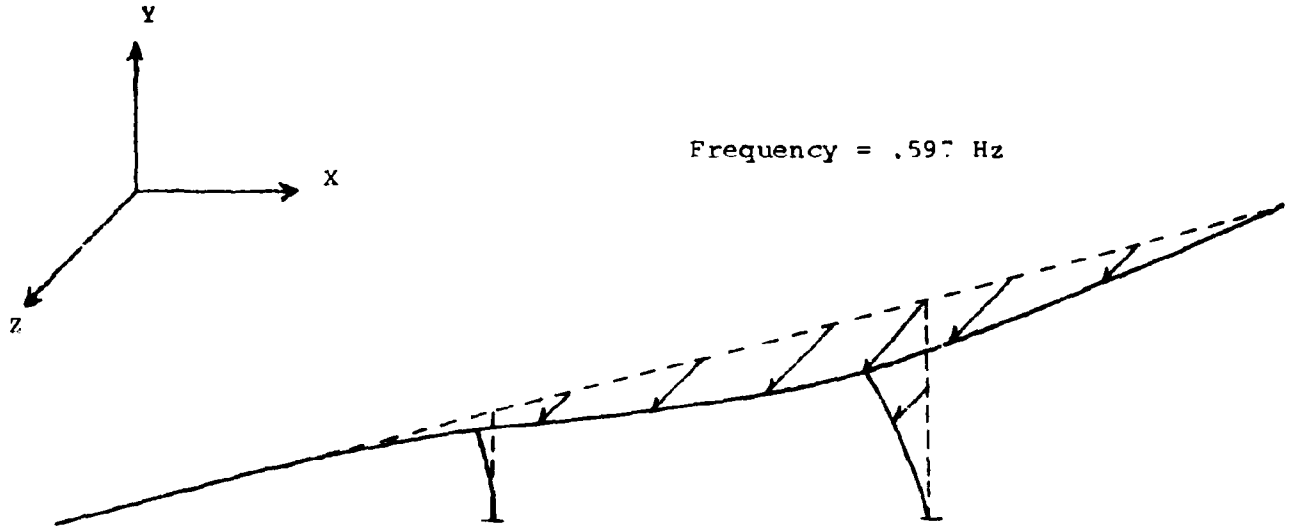

Figure 3-6 1st Mode of Coal Handling Equipment for Central Power Station

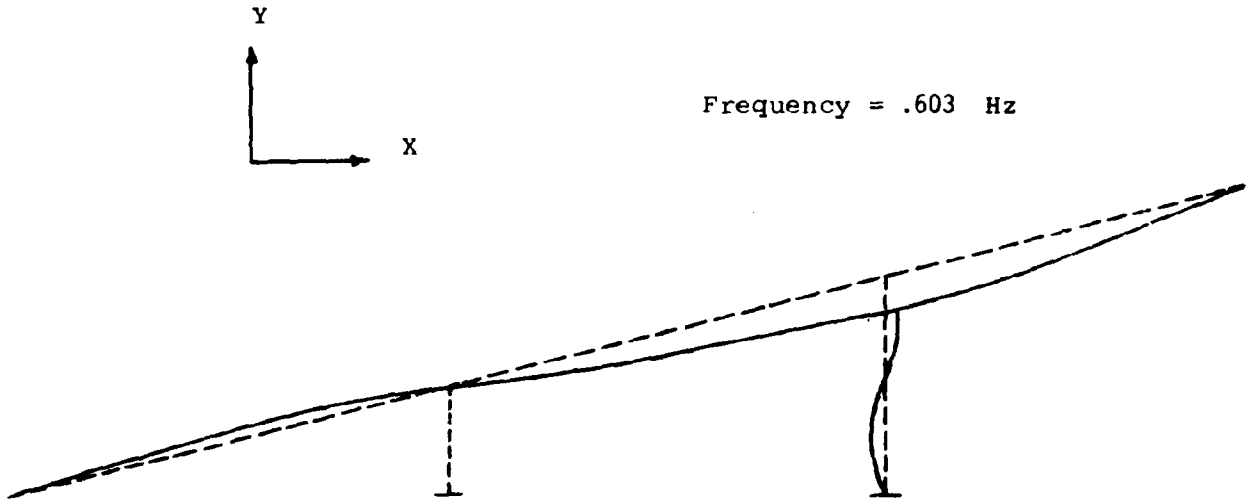

Figure 3-7 2nd Mode of Coal Handling Equipment for Central Power Station

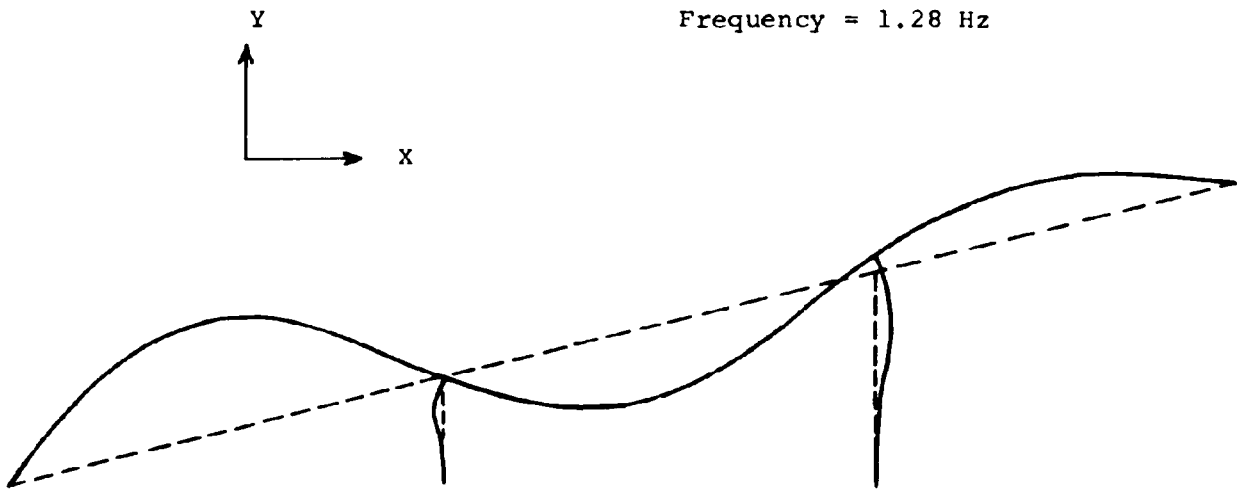

Figure 3-8 3rd Mode of Coal Handling Equipment for Central Power Station

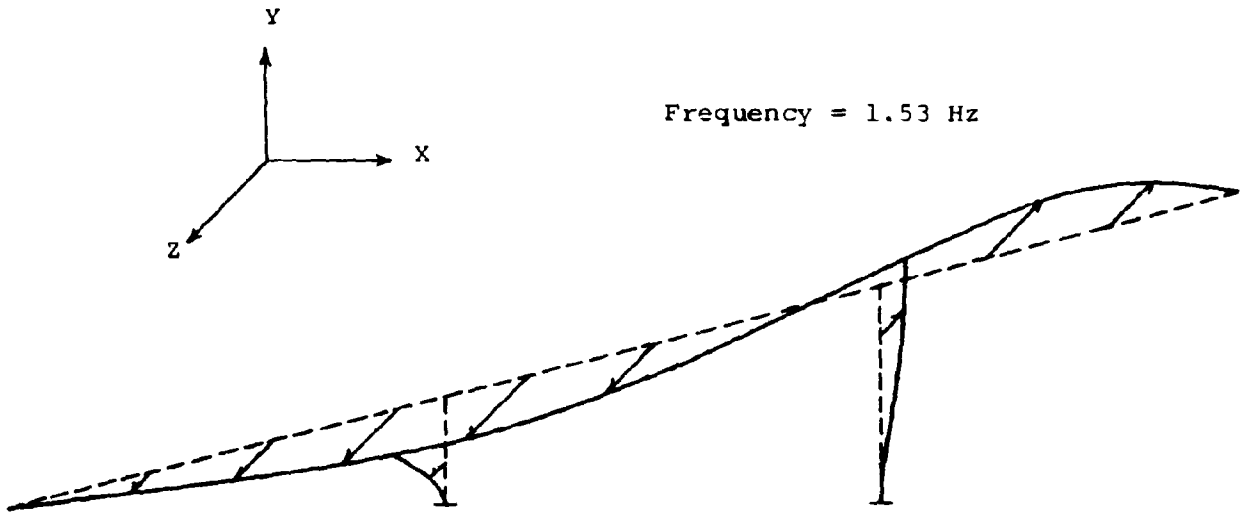

Figure 3-9 4^{th} Mode of Coal Handling Equipment for Central Power Station

Figure 3-9

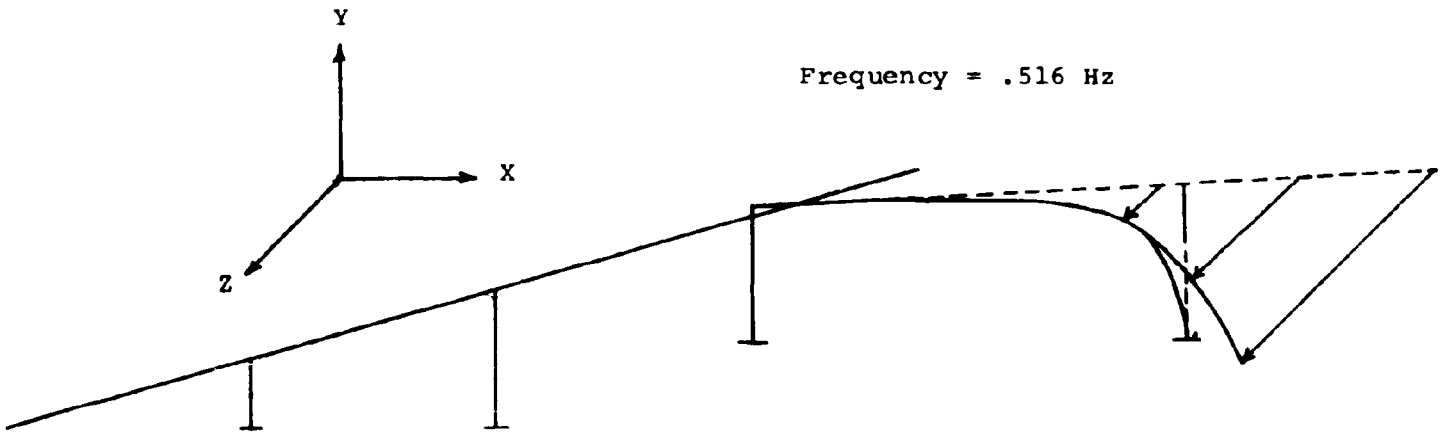

Figure 3-10 1st Mode of Coal Handling Equipment for Coal Yard

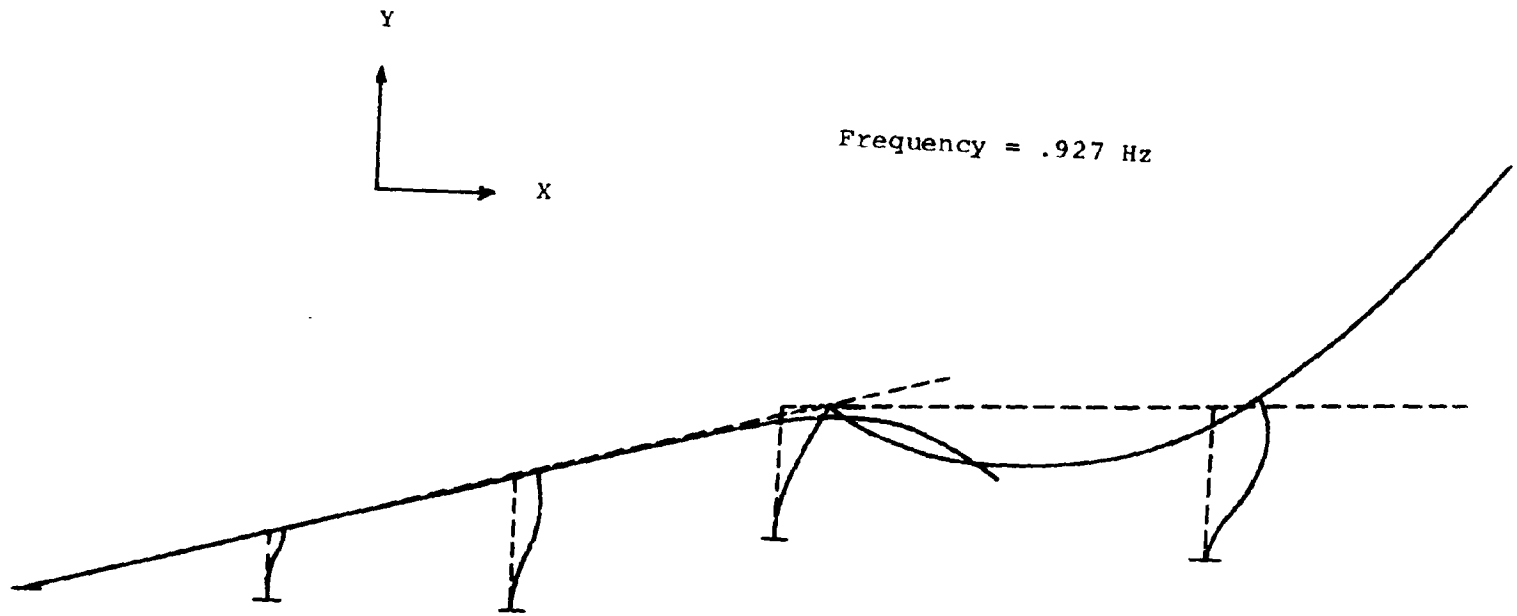

Figure 3-11 2nd Mode of Coal Handling Equipment for Coal Yard

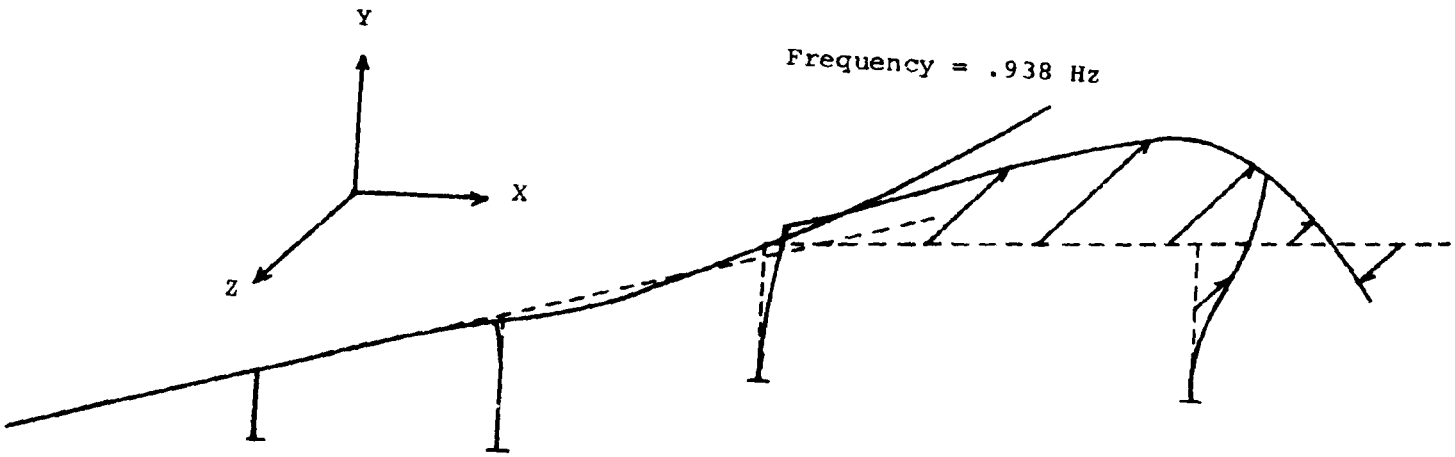

Figure 3-12 3rd Mode of Coal Handling Equipment for Coal Yard

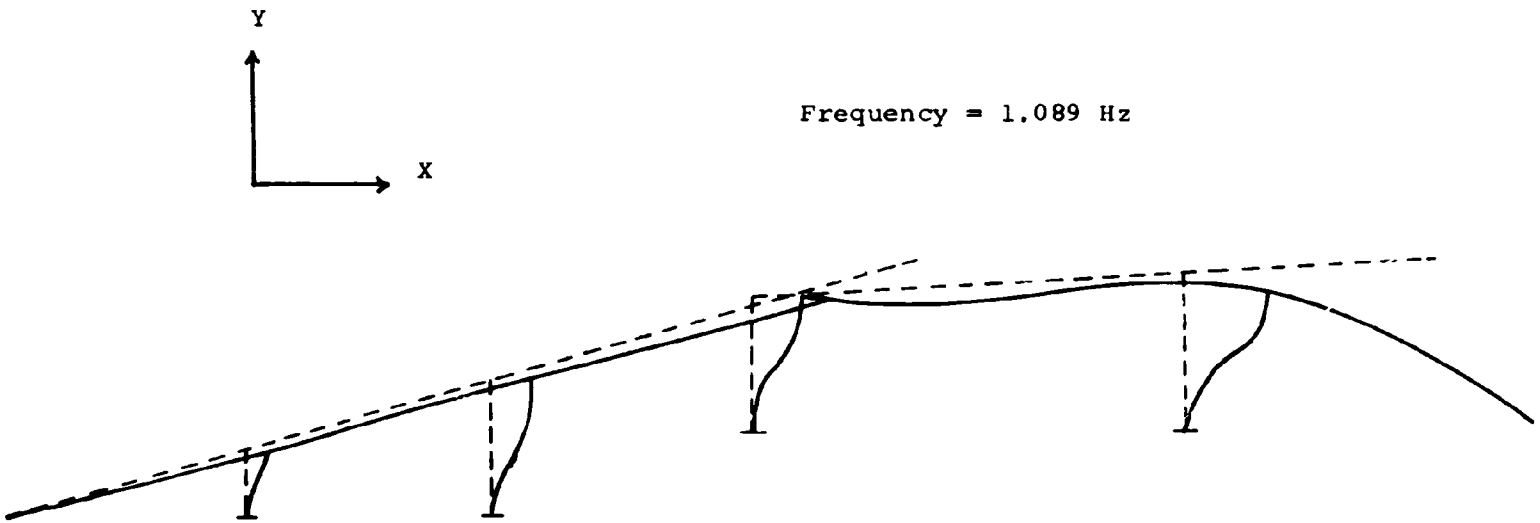

Figure 3-13 4th Mode of Coal Handling Equipment for Coal Yard

CHAPTER 4

COOLING TOWER

by

HENRY T. YANG

4.1 Introduction

Cooling towers are hyperbolic probaloids of revolution in form and are usually made of reinforced concrete of variable thickness. They respond to wind loads and seismic disturbance. Because they are vital to the operation of a large power plant, their dynamical behavior is of considerable interest.

Two complex models are developed for the cooling tower of Unit #3, Paradise, Kentucky (TVA) using quadralateral finite elements for the shell and beam elements for the support system. Natural frequencies and corresponding normal modes are calculated and the results compared. Also complex models are developed for cooling towers previously reported in the literature and nf's and modes calculated. Results obtained compare well amongst themselves and with previously reported results.

4.2 Description of the System

There are three cooling towers in the Paradise steam generating plant. The reinforced concrete cooling tower is in the form of a hyperbolic paraboloidal shell of revolution as shown in Fig.4.1. The shell thickness varies from 24 inches at the base to 7 inches at the throat and then to 9 inches at the top. The tower is supported by 40 pairs of reinforced concrete columns of circular cross sections. Each pair has a concrete footing buried in the excavated limestone rock. The top of the tower is stiffened by a reinforced concrete ring of rectangular cross section. The top of the ring provides a walk way.

4.3 Finite Elements

Two types of finite element are used in modeling the cooling tower: a quadrilateral flat plate element and a beam element. The former is used to model the shell portion. The latter is used to model the top stiffened ring and the 80 supporting columns. The detail of the beam element can be found in the description for Fig.1.4. The plate element is described in this section.

A general three dimensional quadrilateral plate element is shown in Fig. 4.2. The plate has constant thickness and is of quadrilateral shape. The element has four nodal points and each of which has five degrees of freedom: three displacements $\bar{u}$, $\bar{v}$, and $\bar{w}$ in the $\bar{x}$, $\bar{y}$ and $\bar{z}$ local coordinate directions, respectively, and two rotations about the $\bar{x}$ and $\bar{y}$ axes, respectively. Corresponding to the five displacement degrees of freedom are the three direct forces $F_{\bar{x}}$, $F_{\bar{y}}$, and $F_{\bar{z}}$ and two bending

moments $M_{\bar{x}}$ and $M_{\bar{y}}$, respectively.

The plate is assumed to displace linearly in the $\bar{x}$ and $\bar{y}$ directions and bi-cubically in the $\bar{z}$ direction. The three displacement functions are in the following polynomial forms.

$$\begin{aligned}
\bar{u}\ (\bar{x}, \bar{y}) &= a_1 + a_2\bar{x} + a_3\bar{y} + a_4\ \bar{x}\bar{y} \\
\bar{v}\ (\bar{x}, \bar{y}) &= b_1 + b_2\bar{x} + b_3\bar{y} + b_4\ \bar{x}\bar{y} \\
\bar{w}\ (\bar{x}, \bar{y}) &= c_1 + c_2\bar{x} + c_3\bar{y} + c_4\bar{x}^2 \\
&\quad + c_5\bar{x}\bar{y} + c_6\bar{y}^2 + c_7\bar{x}^3 + c_8\bar{x}^2\bar{y} \\
&\quad + c_9\bar{x}\bar{y}^2 + c_{10}\bar{y}^3 + c_{11}\bar{x}^3\bar{y} + c_{12}\bar{x}\bar{y}^3
\end{aligned} \tag{4.1}$$

The 20 constants in equation (4.1) are determined by the 20 nodal degrees of freedom as assumed in Fig. 4.2.

The strain energy expression in terms of the displacements and their derivatives are well-known,

$$\begin{aligned}
U_m &= \frac{1}{2} \int_V [\bar{D}_{\bar{x}} \left(\frac{\partial u}{\partial \bar{x}}\right)^2 + \bar{D}_1 \left(\frac{\partial u}{\partial \bar{x}}\right)\left(\frac{\partial v}{\partial \bar{y}}\right) + \bar{D}_{\bar{y}} \left(\frac{\partial v}{\partial \bar{y}}\right)^2 \\
&\quad + 4\ \bar{D}_{\bar{x}\bar{y}} \left(\frac{\partial u}{\partial \bar{y}} + \frac{\partial v}{\partial \bar{x}}\right)^2]\ d\bar{x}d\bar{y}\ d\bar{z} \\
U_f &= \frac{1}{2} \int_V [D_{\bar{x}} \left(\frac{\partial^2 w}{\partial \bar{x}^2}\right)^2 + 2\ D_1 \left(\frac{\partial^2 w}{\partial \bar{x}^2}\right)\left(\frac{\partial^2 w}{\partial \bar{y}^2}\right) + D_y \left(\frac{\partial^2 w}{\partial \bar{y}^2}\right)^2 \\
&\quad + 4\ D_{\bar{x}\bar{y}} \left(\frac{\partial^2 w}{\bar{x}\ \bar{y}}\right)^2]\ d\bar{x}d\bar{y}\ d\bar{z}
\end{aligned} \tag{4.2}$$

with

$$D_1 = \nu \sqrt{D_x D_y} \quad ; \quad \bar{D}_1 = \nu \sqrt{\bar{D}_x \bar{D}_y}$$

$$D_{xy} = (1-\nu)/2 \sqrt{D_x D_y} \quad ; \quad \bar{D}_{xy} = (1-\nu)/2 \sqrt{\bar{D}_x \bar{D}_y} \tag{4.3}$$

where the subscripts m and f designate the membrane and flexural energies, respectively; D_x and D_y are the orthogonal bending rigidities; and $\bar{D}_x$ and $\bar{D}_y$ are the orthogonal membrane rigidities.

In principle, the stiffness matrix formulation for this element can be obtained by substituting the displacement functions of equation (4.1) into the strain energy expressions of equations (4.2) and then following the Castigliano's theorem by performing differentiations of the resulting energy expressions with respect to each of the 20 degrees of freedom. Such derivation is tedious. The volumn integration is very complex because of the quadrilateral nature of the area. For easy integration, the area coordinates are used as the local coordinates. As regard to the mass formulation, the lumped mass matrix is used.

The formulation is in the following symbolic form

$$\underset{20x1}{\{\bar{F}\}} = \left[\underset{20x20}{[\bar{k}]} - \omega^2 \underset{20x20}{[\bar{m}]} \right] \underset{20x1}{\{\bar{q}\}} \tag{4.4}$$

Through a congruent coordinate transformation technique, the element equation 4.4 in local coordinates is transformed into the formulation in global coordinates.

$$\underset{24x1}{\{\bar{F}\}} = \underset{24x20}{[T]^T} \left[\underset{20x20}{[k]} - \omega^2 \underset{20x20}{[m]} \right] \underset{20x24}{[T]} \underset{24x1}{\{q\}} \tag{4.5}$$

There are six degrees of freedom at each nodal point in the global coordinates: three displacements u, v, and w in the global x, y, and z directions, respectively; and three rotations θ_x, θ_y, and θ_z about the three axes, respectively.

Equation (4.5) for each individual element can be assembled readily to obtain the system formulation.

If two of the nodal points of the quadrilateral element are specified at the same location, a triangular element is obtained.

One of the major advantages of using the quadrilateral and triangular plate elements is, as can be seen later, that they can account for the discrete-type column supports in a manner more exact than those have been done previously by using ring-type axisymmetric shell elements.

4.4 Assumptions

1. The base of the supporting columns are fixed.
2. The shell material is orthotropic. Modulus of elasticities are different in the circumferential and meridional directions due to different arrangements of reinforcing bars.

4.5 Results up to Date

The flat quadrilateral plate element used in the modeling of hyperbolic paraboloidal shell cooling tower was first evaluated through its performance in two examples.

The first example is a cooling tower described in Fig. 4.3. The isotropic modulus of elasticity of the reinforced concrete cooling tower is 3×10^6 psi; the Poisson's ratio is 0.15; and the mass density is 0.225×10^{-3} lbs-sec^2/in^4. The base of the tower is assumed as fixed. This

example was analyzed several times by different people. Carter et al. (Ref. 4.1) used a numerical integration technique, Abu-Sitta et al. (Ref. 4.2) used a finite difference technique, and Gould et al. (Ref. 4.3) used the ring-type axisymmetric shell finite elements. Their results for the natural frequencies are shown in Table 4.1.

In this study, three different finite element meshes were used: 4x16, 6x20, and 8x20, respectively. The three meshes correspond to 288, 600, and 840 degrees of freedom, respectively. The results are also shown in Table 4.1 for comparison. It is seen that for the 4x16 mesh, the frequencies are, in general, slightly over 10% higher than the recognized "correct" solutions. The results are improved as the mesh is refined. For the 8x20 mesh, the frequencies are almost no different than the recognized solutions. It is convinced through this example that the quadrilateral elements are accurate for the dynamic analysis of cooling towers. The CDC 6500 central processing time for computing all the frequencies are given in Table 4.1 for the three different meshes.

It is noted that in obtaining the results in Table 4.1, Gould used 13 axisymmetric shell elements which corresponds to 78 degrees of freedom. It is also noted that the axisymmetric shell elements cannot directly include the discrete column supports.

The cooling tower with discrete column supports has been treated by Gould et al. (Ref. 4.4). In Ref. 4.4, the cooling tower was modeled by ring-type axisymmetric shell elements. The supporting columns were modeled by a special ring type elastic element whose stiffness and mass properties are equivalent to those of the discrete columns. The example performed in Ref. 4.4 is shown in Fig. 4.4. This cooling tower has 44 pairs of

Table 4.1.The natural frequencies (in Hz.) for a cooling tower with base fixed.

Circumferential Mode	Longitudinal Mode	Carter et al. (numerical integration)	Abu-Sitta et al. (finite difference)	Gould et al. (ring-shell elements)	This Study		
					4x16 Mesh	6x20 Mesh	8x20 Mesh
0	1	7.7494	8.1500	7.7583			
	2	11.4166	11.3799	11.4187			
	3	11.9022	11.8257	12.0747			
1	1	3.2884	3.3345	3.2910	3.2653		
	2	6.7405	6.8816	6.8176			
	3	10.5207	10.5316	10.6666			
2	1	1.7654	1.7848	1.7662	1.8681	1.8153	
	2	3.6931	3.7234	3.6960			
	3	6.9562	6.9553	7.0058			
3	1	1.3749	1.3929		1.5356	1.4528	1.3627
	2	1.9904	2.0150		2.0969		
	3	4.3254	4.3353				
4	1	1.1808	1.2003	1.1820	1.3830	1.3248	1.2039
	2	1.4475	1.4597	1.4491	1.6136	1.5648	1.4468
	3	2.7777	2.7762	2.7866	2.8882		
5	1	1.0348	1.0441	1.0354	1.2447	1.1808	1.0556
	2	1.4293	1.4417	1.4345	1.5855	1.5806	
	3	2.0559	2.0555	2.0640	2.3176		
	4				3.4110		
6	1	1.1467	1.1544		1.3120	1.2672	1.1382
	2	1.3231	1.3335		1.5492	1.5461	
	3	2.0141	2.0152		2.1702		
	4				2.9107		
7	1	1.3014	1.3055		1.4460	1.4556	1.3230
	2	1.5133	1.5189		1.6040	1.6220	
	3	1.9217	1.9200		2.1470	2.0705	
	4				2.8062		
8	1				1.5059	1.6418	
	2				1.6636	1.8460	
	3				2.1579	2.0647	
	4				2.8110		
Total Time (Minutes)					29.0	67.9	38.0

supporting columns. The modulus of elasticity for both the concrete shell and columns are $4x10^6$ psi; the Poisson's ratio is 1/6; and the mass density is $0.225x10^{-3}$ lbs-sec^2/in^4.

In Ref. 4.4, the cooling tower was first analyzed with the base fixed and then with the base supported by 88 discrete columns. The results for natural frequencies are shown in Table 4.2.

For the case of fixed base, the present results obtained by the use of 8x20 mesh (840 degrees of freedom) agree reasonably well with those given by Gould et al. For the case with discrete column supports, the present results obtained by the use of 8x22 mesh (1188 degrees of freedom) are, in general, lower than those obtained by Gould et al.

In the 8x22 mesh, the lowest row was modeled by 66 triangular elements instead of 22 quadrilateral elements. Each original quadrilateral element was divided into three triangular elements with two nodes at the top and three nodes at the base. By doing so, the 44 pairs of column finite elements were able to be connected to the 44 nodes at the base of the shell.

The CDC 6500 central processing time used in obtaining all the frequencies are listed in Table 4.2.

With the successful completion of the first two examples, it is convinced that correct results can be obtained for the cooling tower in the Paradise Steam Generating Plant. This cooling tower has been described in detail in Section (4.1).

Three different meshes were used to compute the natural frequencies for the Paradise cooling tower: 4x16 mesh (480 degrees of freedom); 6x20 mesh (840 degrees of freedom); and 8x20 mesh (1080 degrees of freedom). The top ring beam was modeled by 10, 20, and 20 beam elements respectively.

Table 4.2. The natural frequencies (in Hz) for a cooling tower with discrete column supports.

Circumferential Mode	Longitudinal Mode	Fixed Base		Discrete Base	
		Gould et al.	This Study 8x20 Mesh	Gould et al.	This Study 8x22 Mesh
0	1	6.558		5.780	
	2	10.117		9.557	
1	1	2.709		2.296	
	2	5.752		3.893	
2	1	1.475		1.311	
	2	3.095		2.172	
3	1	1.194	1.1854	1.086	1.0921
	2	1.672		1.314	
4	1	1.104	1.1255	0.945	0.9510
	2	1.302	1.3041	1.204	1.1686
5	1	1.131	1.1457	1.032	1.0245
	2	1.453	1.4634	1.256	1.2195
6	1	1.400	1.4055	1.235	1.1893
	2	1.568		1.455	
Total Time (Minutes)			37.6		54.2

In these three meshes, each quadrilateral element in the base row was divided into three triangular elements so that it has three nodes at the se line. Thus for the 6x20 and 8x20 meshes, the base circle of the er has 40 nodes which were able to be connected to the 40 pairs of discrete column elements. For the 4x16 mesh, the 40 pairs of columns were replaced by 36 pairs of equivalent columns.

Since the arrangements of the reinforcing bars in the circumferential direction are different than those in the longitudinal direction, each quadrilateral finite element is orthotropic. The distributions of the longitudinal and circumferential stiffnesses due to the arrangements of reinforcements given in the detailed design drawings are computed and shown in Figs. 4.5 and 4.6. The present analysis was based on such information.

The results are shown in Table 4.3. The mode shapes for the first and second meridional modes and various circumferential modes are shown in Figs. 4.7 and 4.8.

4.5 Results by March 1 of 1976.

The first few natural frequencies for the cooling tower will be used to obtain a time-history response due to a prescribed earthquake. Modal superposition method will be used. The results will include the responses of the six displacement and rotation components at each nodal point and the membrane and flexural stresses at each finite element at different time steps. The displacement and stress components in each column will also be obtained.

Table 4.3.The natural frequencies in Hz. for the cooling tower of Paradise Steam Generating Plant.

Circumferential Mode	Longitudinal Mode	4×16 Mesh	6×20 Mesh	8x20 Mesh
0	1			
	2			
	3			
1	1			
	2			
	3			
2	1	1.2538	1.2391	1.2148
	2	1.9882		
	3			
3	1	0.8875	0.8777	0.8857
	2	1.6263	1.5321	1.4504
	3			
4	1	0.9851	0.9306	0.9057
	2	1.3965	1.3592	1.3353
	3			
5	1	0.8446	0.8255	0.8491
	2	2.0430		
	3			
	4			
6	1	1.0235	1.0763	1.0351
	2	1.9160	1.6691	
	3			
	4			
7	1	1.2708	1.4156	1.2997
	2	1.9363	1.7525	
	3	2.1250		
	4			
8	1	1.3795	1.6789	
	2	2.0641		
	3			
	4			
Total Time (Minutes)		35.4	43.5	[illegible]

REFERENCES

[4.1] Carter, R. L., Robinson, A. R., and Schnobrick, W. C., "Free Vibration of Hyperboloidal Shells of Revolution," Journal of the Engineering Mechanics Division, ASCE, Vol. 95, No. EM5, Oct. 1969, pp. 1033-1052.

[4.2] Hashish, M. G. and Abu-Sitta, "Free Vibration of Hyperbolic Cooling Towers," Journal of the Engineering Mechanics Division, ASCE, Vol. 97, No. EM2, April 1971, pp. 253-269.

[4.3] Sen, S. K. and Gould, P. L., "Free Vibration of Shells of Revolution," Journal of the Engineering Mechanics Division, ASCE, Vol. 100, No. EM2, April 1974, pp. 283-303.

[4.4] Gould, P. L., Sen, S. K., and Suryoutomo, H., "Dynamic Analysis of Column Supported Hyperboloidal Shells," Earthquake Engineering and Structural Dynamics, Vol. 2, 1974, pp. 269-279.

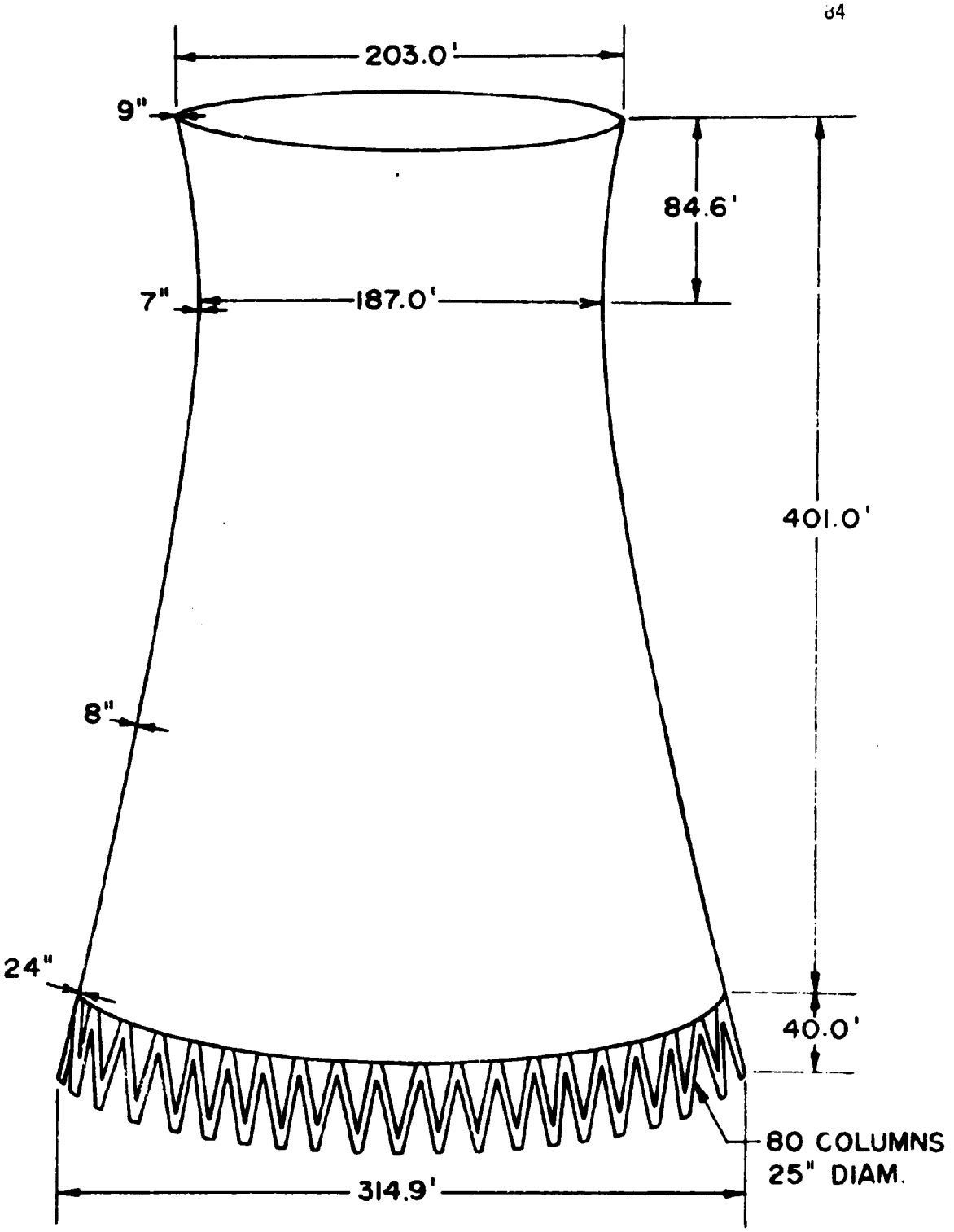

Fig. 4.1. The sketch of a hyperbolic paraboloidal cooling tower in the Paradise Plant.

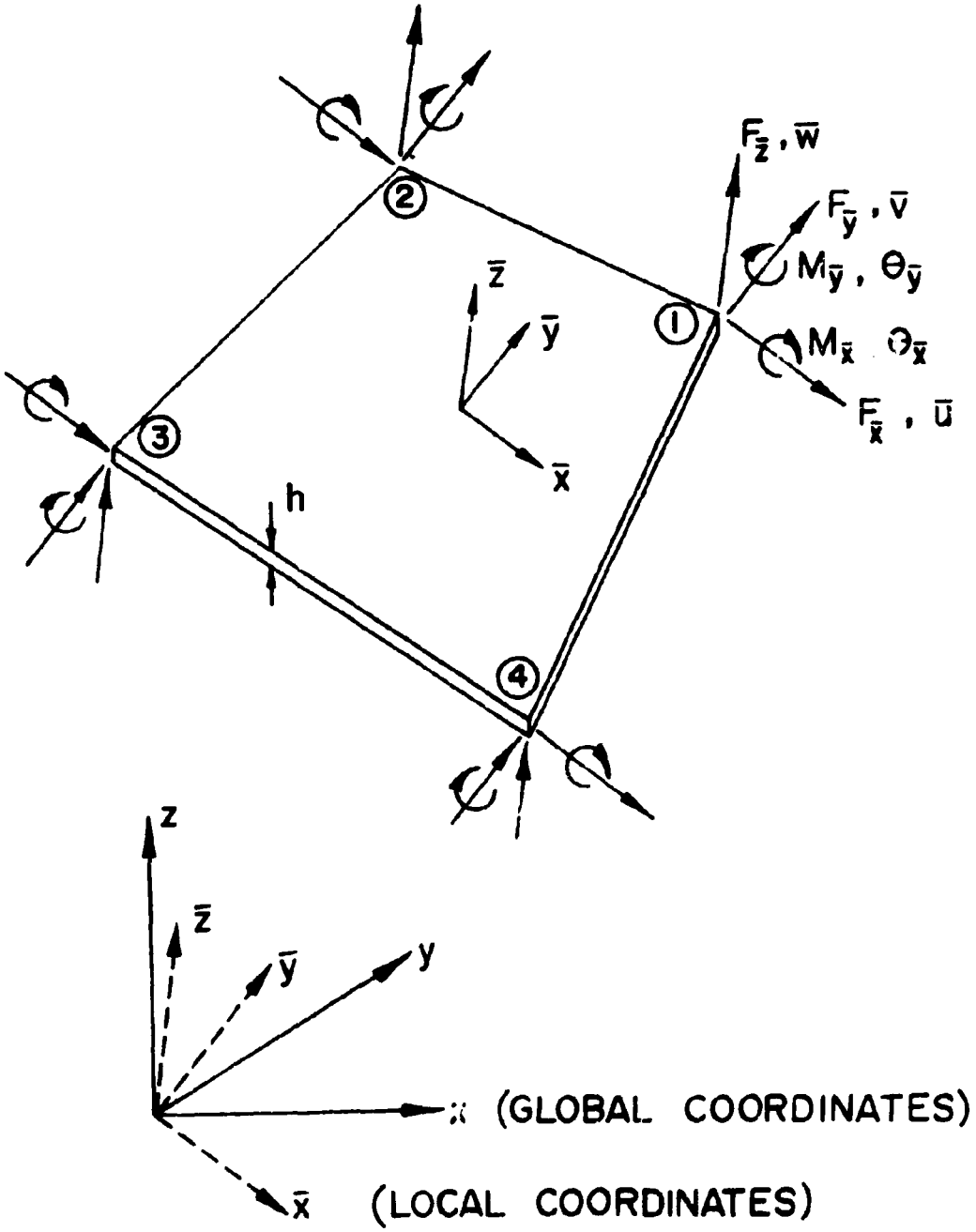

Fig. 4.2. A general quadrilateral plate finite element in the three dimensional space.

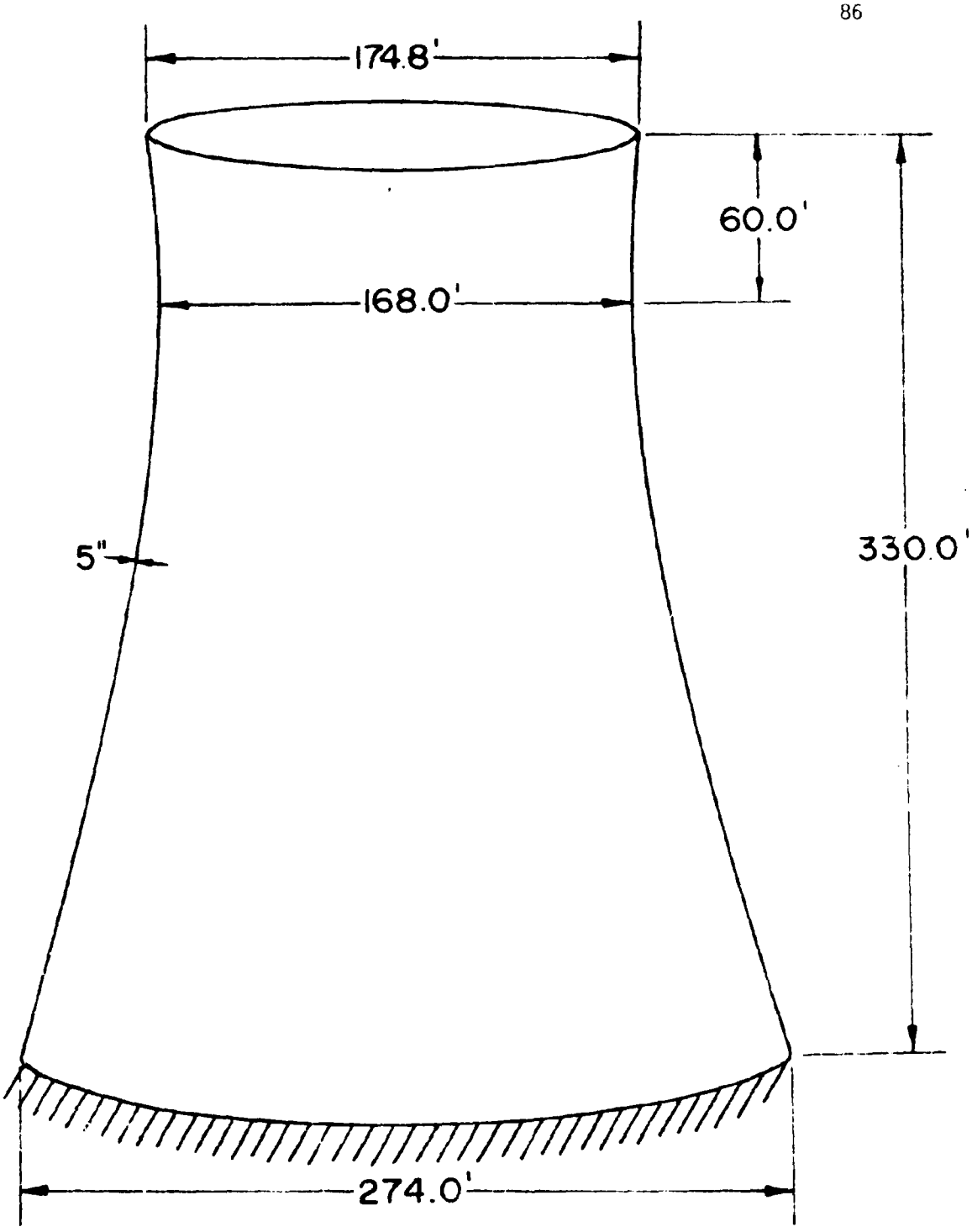

Fig. 4.3. The example of a cooling tower with base fixed.

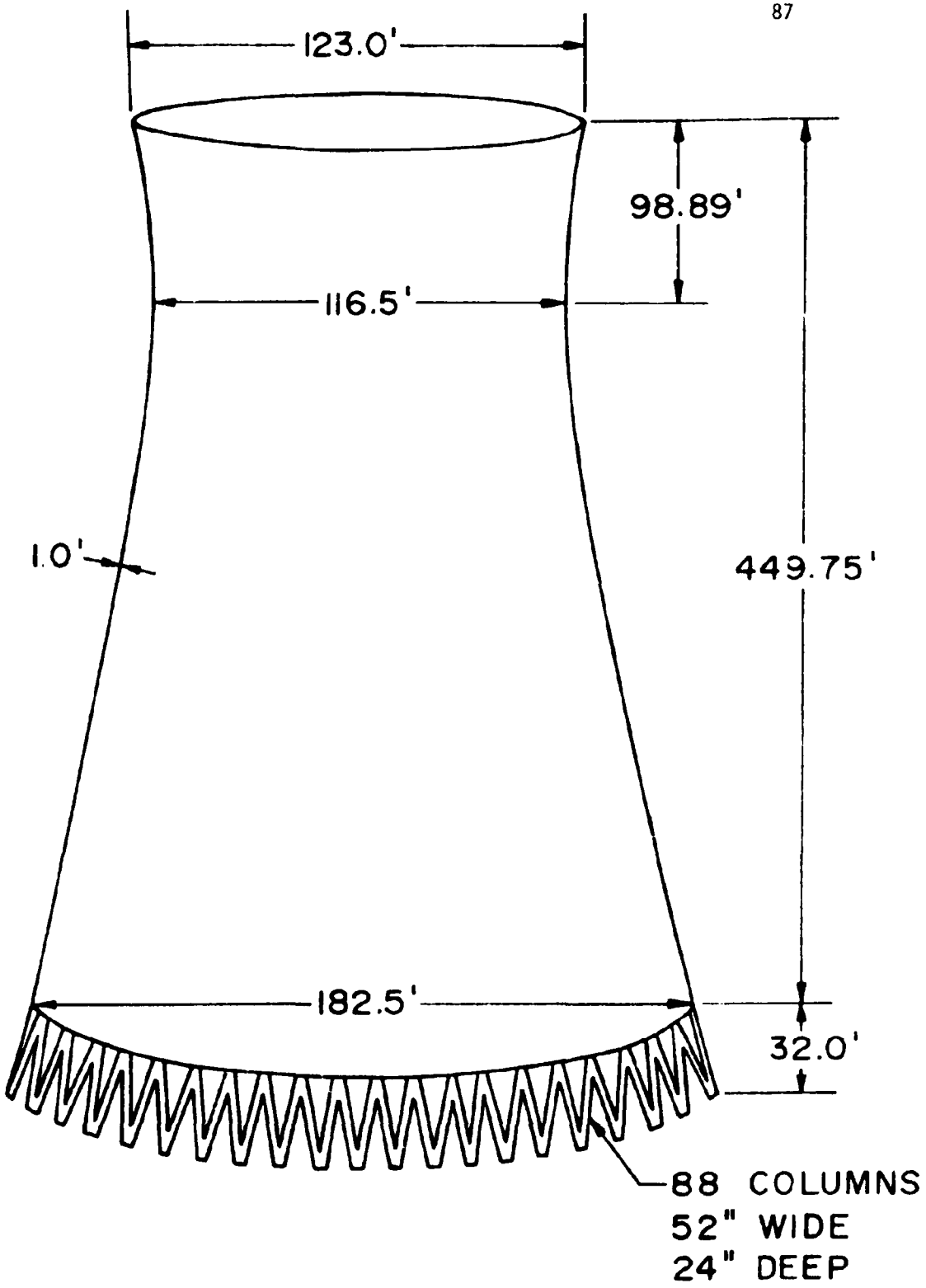

Fig. 4.4. The example of a cooling tower with discrete column supports.

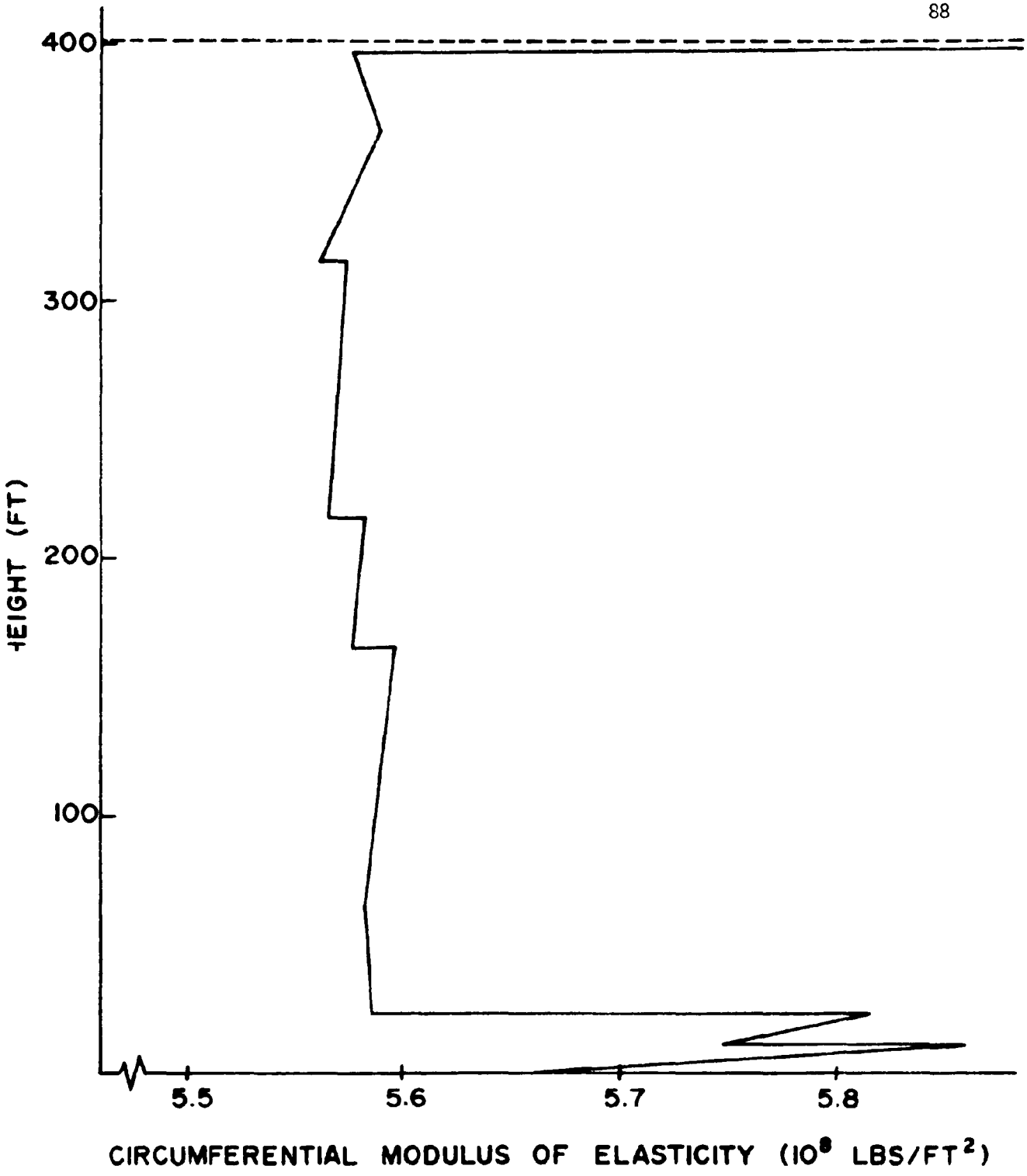

Fig. 4.5. The distribution of equivalent modulus of elasticity in the circumferential direction.

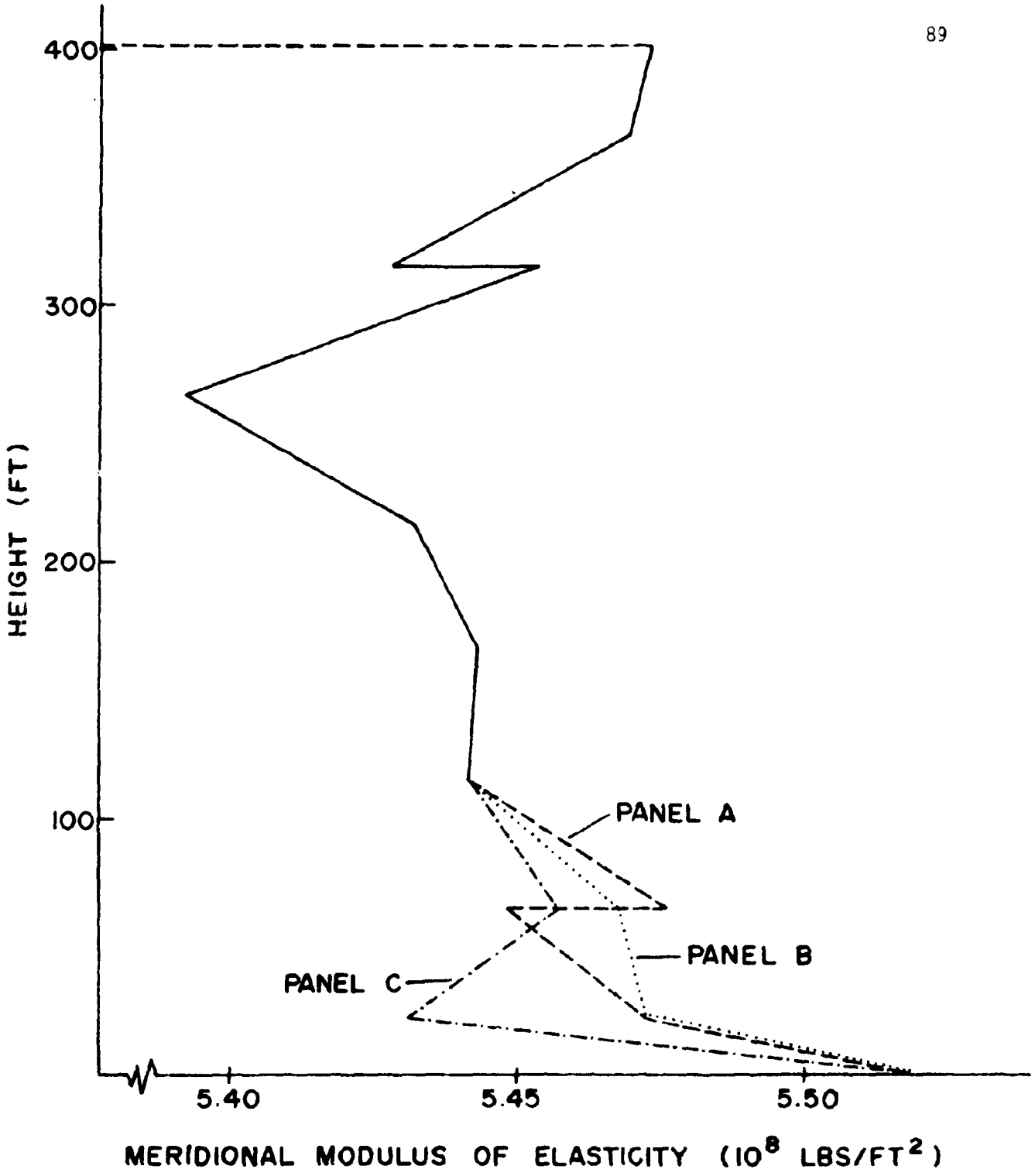

Fig. 4.6. The distribution of equivalent modulus of elasticity in the meridional direction.

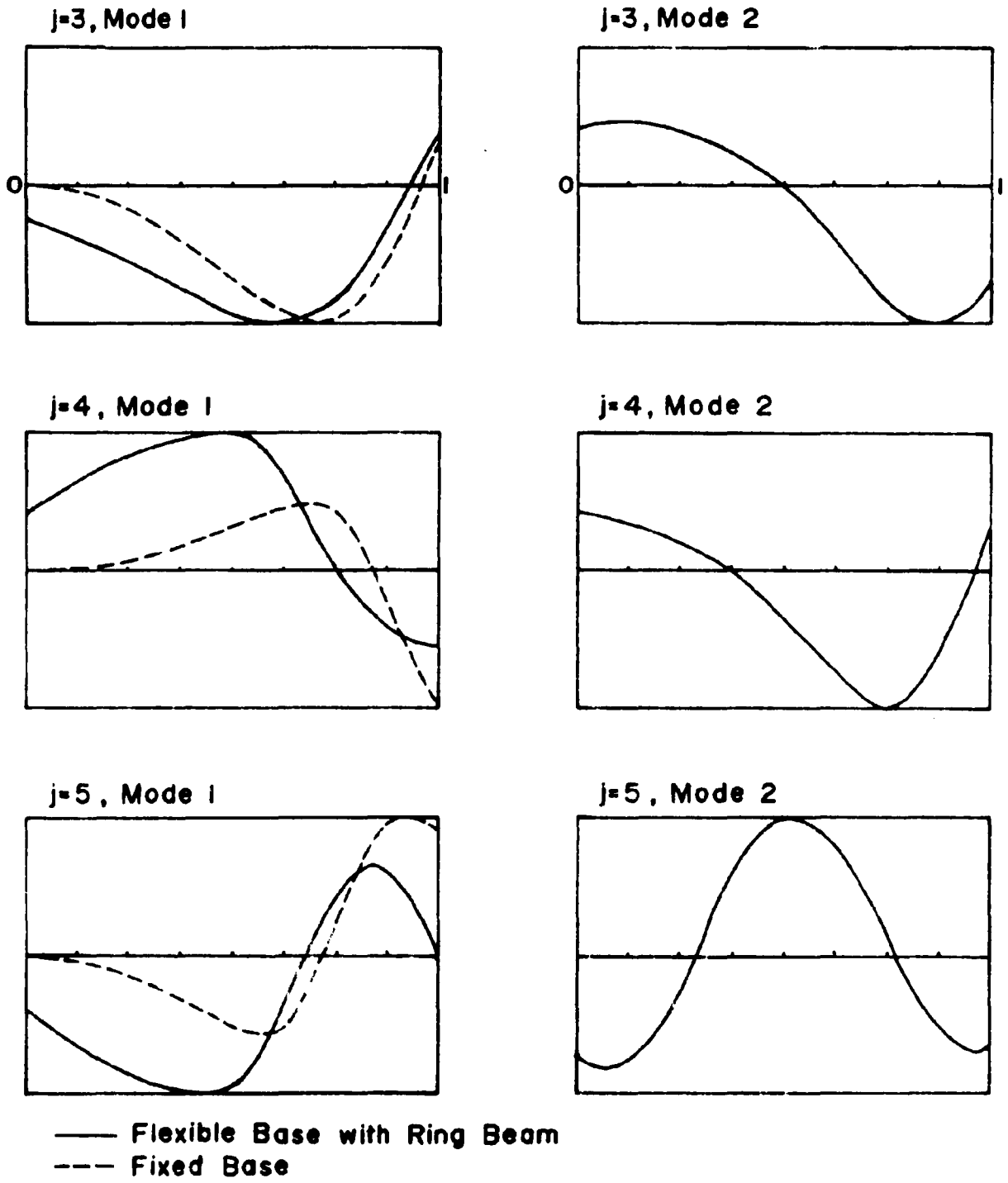

Fig. 4.7. The mode shapes for the Paradise cooling tower with discrete supports and top ring beam.

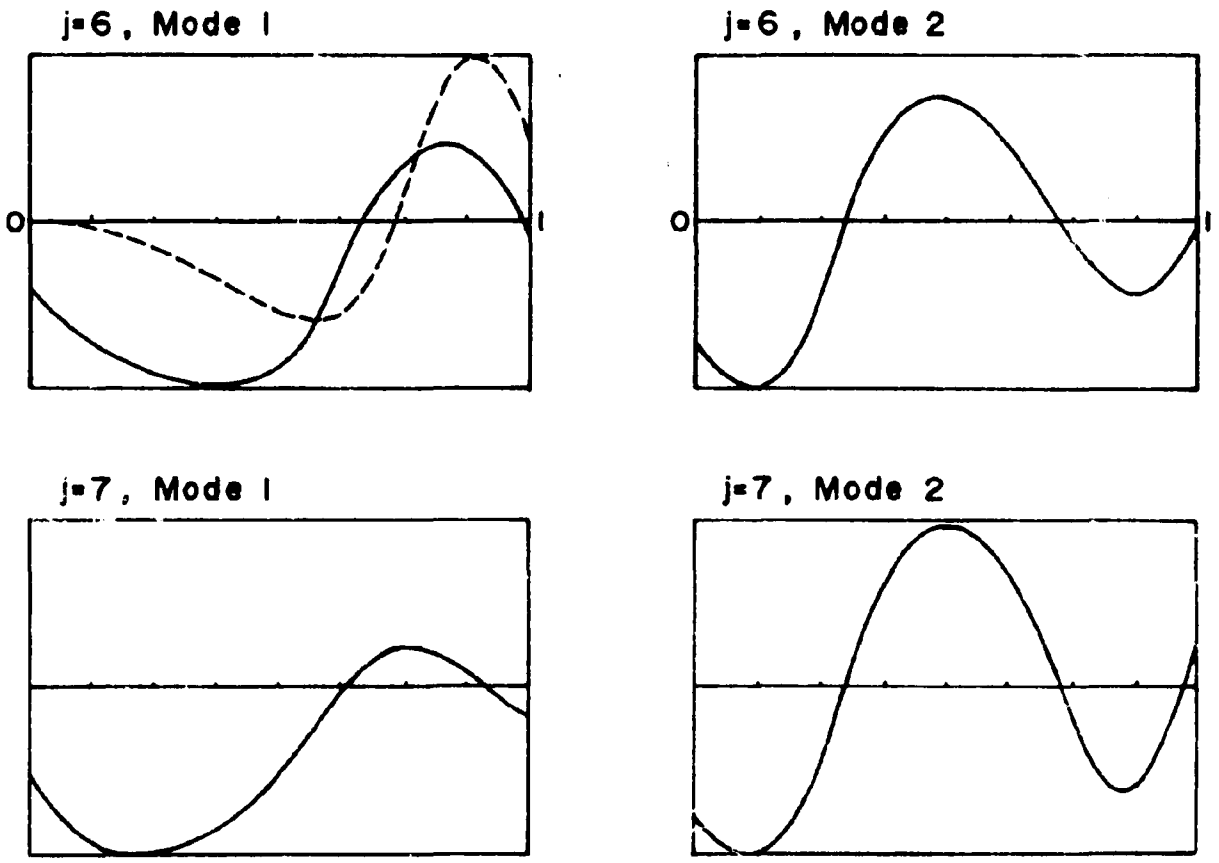

Fig. 4.8. The mode shapes for the Paradise cooling tower with discrete supports and top ring beam.

CHAPTER 5

CHIMNEY

by

HENRY T. YANG

5.1 Introduction

The 832 feet tall chimney includes two reinforced concrete shells with a 4 1/2 feet minimum air space. Each chimney has two rectangular flue openings. The chimney is analyzed with the use of eight pipe-type finite elements. The stiffness coefficients and the mass for the particular element that includes the flue openings are obtained by the use of quadrilateral shell finite elements.

Thus far, only the results for the outer shell without flue openings have been completed. Thirty seconds of time-history dynamic response of the outer shell due to the El Centro South-North earthquake have been obtained. The analysis used 1500 time points, eight modes, (for modal superposition) and 25.5 seconds on a CDC 6500 computer.

The effect of the flue openings will be included next. The inner shell will then be analyzed the same way as the outer shell.

5.2 Description of the System

The chimney is composed of two slender cylindrical reinforced concrete shells as shown in Fig. 5.1. The inner shell serves as a liner. The inner shell has a stainless steel cap at the top and two inches of fiber glass insulation on the outer surface. A 4'-6" minimum air space is maintained between the two shells.

The top surface of the chimney foundation is at elevation 390 feet. The earth fill extends to the elevation 422 feet. The height of the chimney is 832 feet above the foundation. The outer diameter for the outer shell varies from 71.8 feet at the base to 38.5' at the top. The thicknesses for the two shells also vary with their maximum values at near the flue openings.

Each of the two shells has a pair of side flue openings. They are rectangular in shape with dimensions of 28 feet by 14 feet. The base lines of the openings are 36.1 feet above the ground. Each opening at the inner shell is connected to the opening at the outer shell by steel framed flue duct. The concrete around the openings are heavily reinforced.

The compressive strength of the concrete is recommended by TVA as 6000 psi. The weight is 145 pound/feet^3. Following the ACI code, the modulus of elasticity for the concrete is computed as 4.5×10^6 psi.

5.3 Finite Elements

Two types of finite element are used for the analysis of chimney: A beam element and a plate element.

i. The finite element used in the analysis of the gross chimney behavior is a three-dimensional beam finite element with constant hollow

circular cross section. This element can only provide a step representation of the tapered chimney. This element is the same as that described in Section (b) in the chapter for the steam generator supporting frame structure. The only difference is that the input data for this element is simpler due to the axisymmetric nature of the cross section. For this element, only the inner and outer diameters need be input instead of inputing the rectangular and polar moments of inertia.

ii. For the local analysis of the chimney, the three-dimensional plate finite element described in Section (b) in the chapter for the cooling tower analysis is used. This element serves for two functions.

This element is used to model the particular chimney beam finite element that has two flue openings. With the plate element modeling, the 12 influence stiffness coefficients for an equivalent beam element (with no openings) can be obtained. The equivalent bending stiffness about the weakest axis (the diameter that parallels the axis joined the two openings) is used.

When the end displacement and force vectors for each chimney beam element are found in the dynamic response analysis, the three-dimensional plate finite element can be used to find the detail distributions of displacements and stresses within the beam element.

5.4 Assumptions

i. The chimney is rigidly fixed to the foundation at the elevation of 390 feet.

ii. The two shells are assumed as unconnected in the analysis.

iii. The Bernoulli-Euler beam theory is used. No shear deformation and rotatory inertia are considered at this stage of the study.

Table 5.1. The lowest 12 natural frequencies for the outer shell chimney with no flue openings.

Mode Number	Period (Seconds)	Frequency	
		Cycle/sec.	rad/sec.
1	3.1371	0.3188	2.0028
2	0.8789	1.1378	7.149
3	0.3746	2.6698	16.775
4	0.2153	4.6448	29.184
5	0.1973	5.0684	31.846
6	0.1445	6.9193	43.475
7	0.1082	9.241	58.063
8	0.0948	10.552	66.298
9	0.0881	11.358	71.364
10	0.0769	13.009	81.74
11	0.0571	17.506	109.99
12	0.0432	23.165	145.55

iv. Thermal effect and wind effect are neglected.

5.5 Results to Date

The analysis was first performed for the outer shell without the effect of the flue openings. To find out how many elements are appropriate for the analysis, the chimney was first subjected to free vibration analysis with different numbers of beam elements. The results are shown in Fig. 5.2 for the first four natural frequencies. It is seen that eight finite elements are sufficiently accurate for modeling the chimney. The modeling by the use of eight elements is shown in Fig. 5.3.

The results for the first twelve natural frequencies obtained by using eight finite elements are given in Table 5.1. The first, second, and third mode shapes are plotted in Fig. 5.4. The fourth and fifth mode shapes are plotted in Fig. 5.5.

The record of the El Centro earthquake occurred on May 18, 1940 was selected to analyze the time-history dynamic response of the chimney. This record is shown in Fig. 5.6. The record of the acceleration in the north direction versus time was used. The record lasted for 53.7 seconds. Since the acceleration decreases to small magnitude after 30 seconds, only the first 30 seconds were considered. The record in Fig. 5.6 shows that the acceleration oscillates at the frequencies of approximately 3 to 7 cycles per second. The results in Table 5.1 for the natural frequencies for the outer shell show that the seventh frequency is 9.24 cycles per second. Thus the first seven modes should be sufficient for the dynamic response analysis for the El Centro record by the use of modal superposition method.

The time interval for the modal analysis was set as 0.02 seconds which corresponds to 50 points for each second and 1500 points for the whole thirty

seconds period. The CDC 6500 central processing time for eight elements, seven modes and 1500 time points is 25.5 seconds.

The results for the deflection shapes of the chimney are plotted at three different time intervals in Fig. 5.7. The time history response for the deflection at the tip of the chimney (node 9) is plotted in Fig. 5.8. It is seen that the maximum deflection is about 46 inches. The results for the bending moments at the base of the chimney (node 1) is plotted in Fig. 5.9. The maximum bending moment occurs at the time of 20 seconds with a magnitude of about 34×10^6 kip-inches. Such moment produces a maximum compressive stress of 5870 psi in concrete and a maximum tensile stress of 46 ksi in reinforced bar. The maximum compressive strength for concrete recommended by TVA is 6000 psi and the yield strength for the reinforced steel is 60 ksi.

The results for the shearing force at the base of the chimney is plotted in Fig. 5.10. The maximum shearing force occurs at the time of 16 seconds with a magnitude of about 11.7×10^6 pounds. This results in a maximum shearing stress of 3100 psi in the concrete.

5.6 Results by March 1, 1976

The equivalent beam finite element that accounts for the effect of the two flue openings in the outer shell will be found. The free vibration and time-history response analysis for the outer shell with flue openings will be performed on the basis of the El Centro eqrthquake.

The inner shell will be analyzed the same way as that for the outer shell. Whether the two shells are in contact or not during the earthquake will be found.

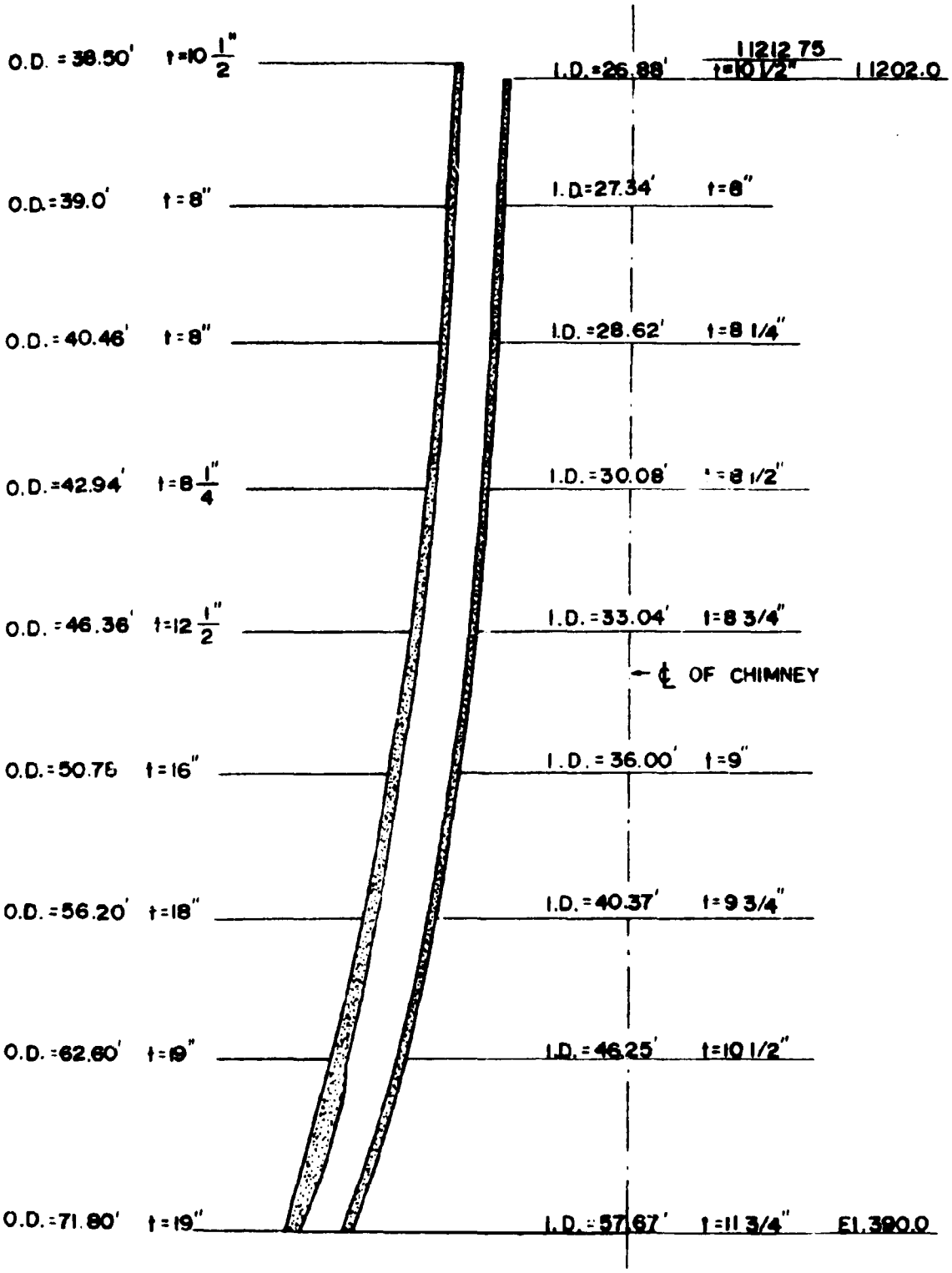

Fig. 5.1 Description of the chimney in the Paradise Steam Generating Plant

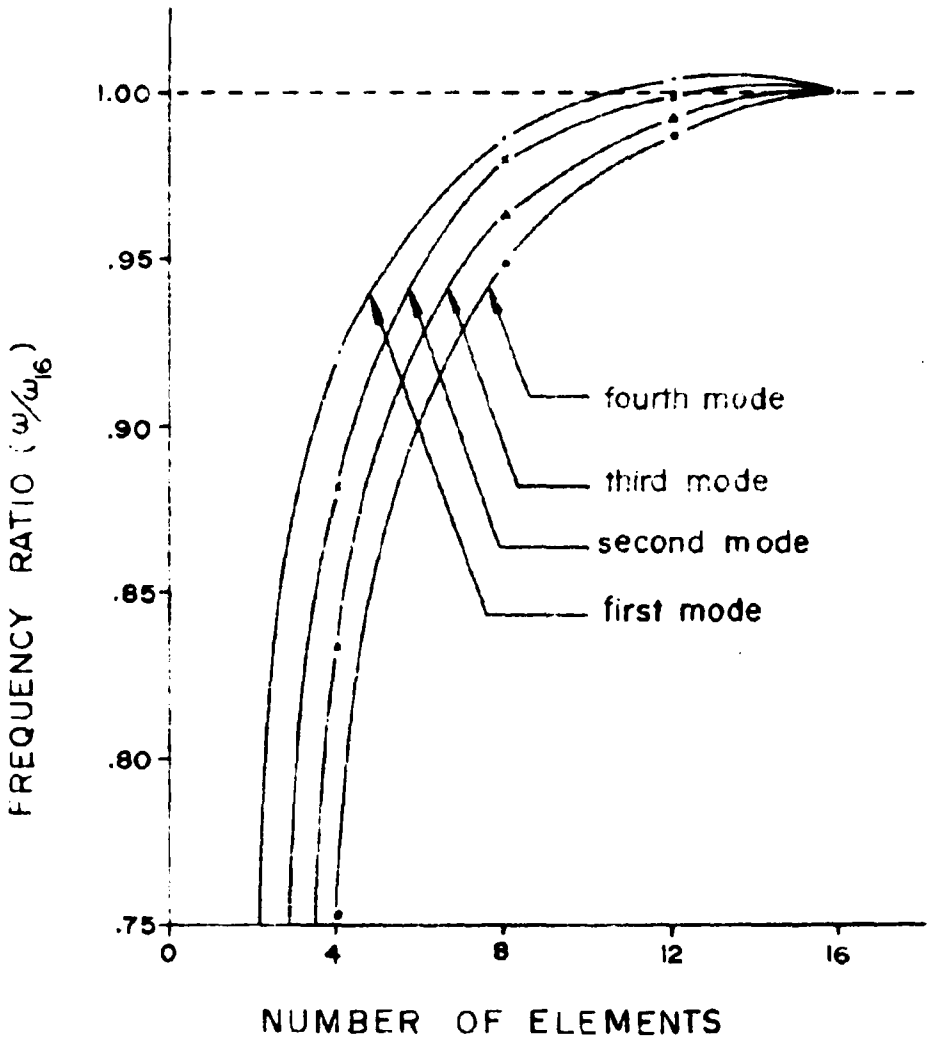

Fig. 5.2 The convergence plot for the first four frequencies for different modeling of the chimney outer shell.

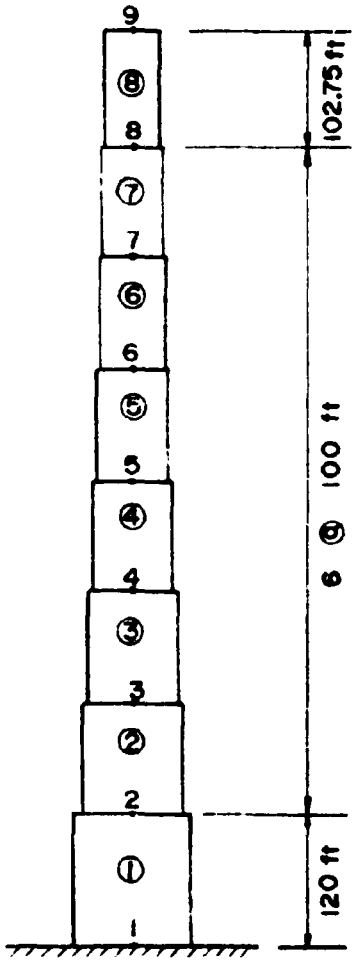

Fig. 5.3 The eight-element modeling of the chimney outer shell without openings.

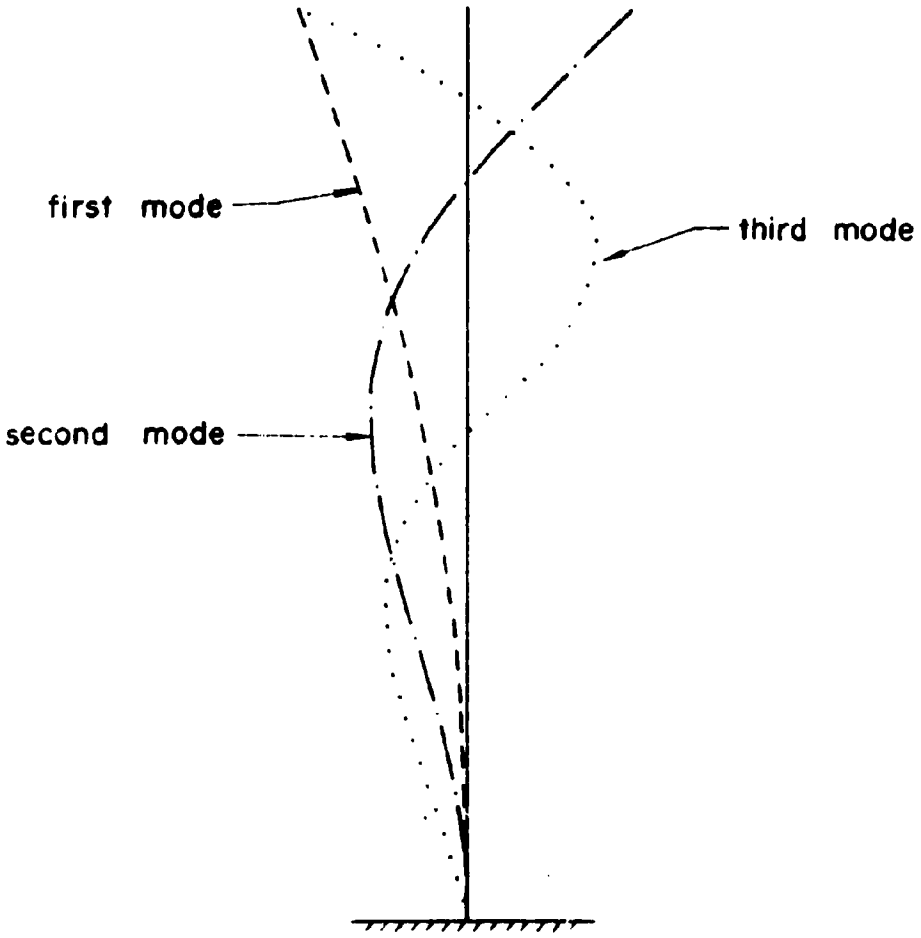

Fig. 5.4 The first, second, and third mode shapes for the chimney outer shell without openings.

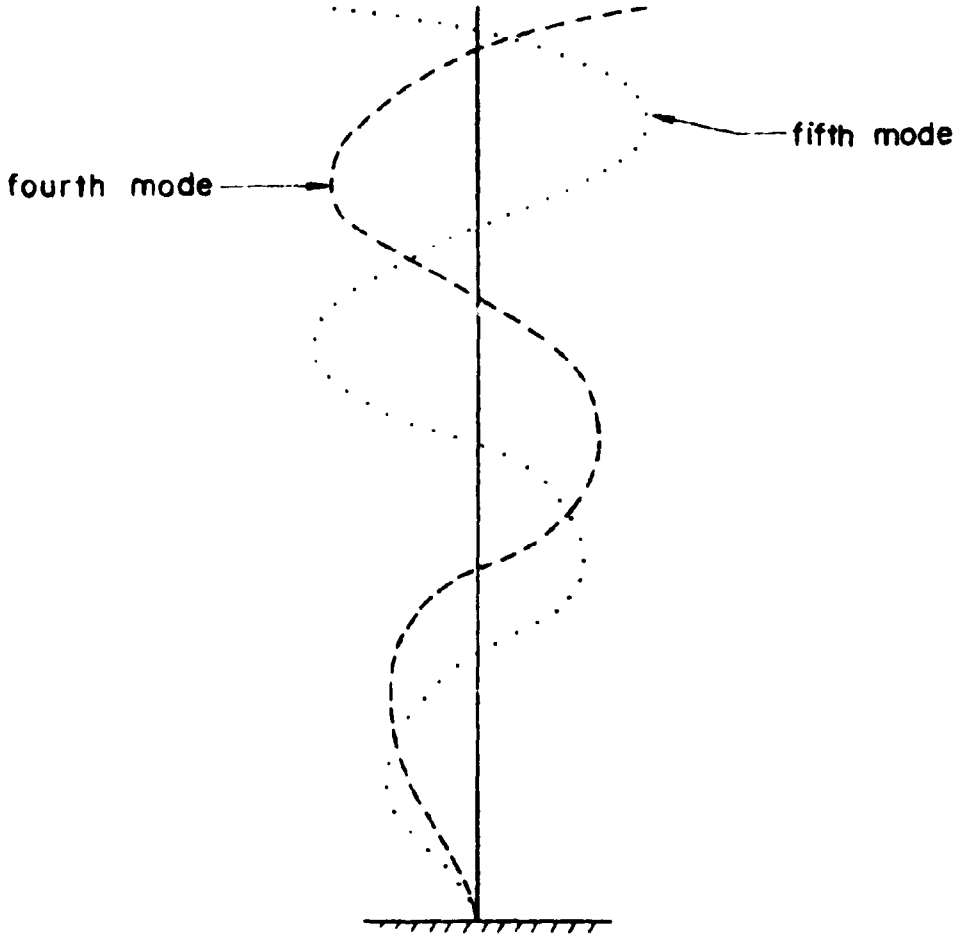

Fig. 5.5 The fourth and fifth mode shapes for the chimney outer shell without openings.

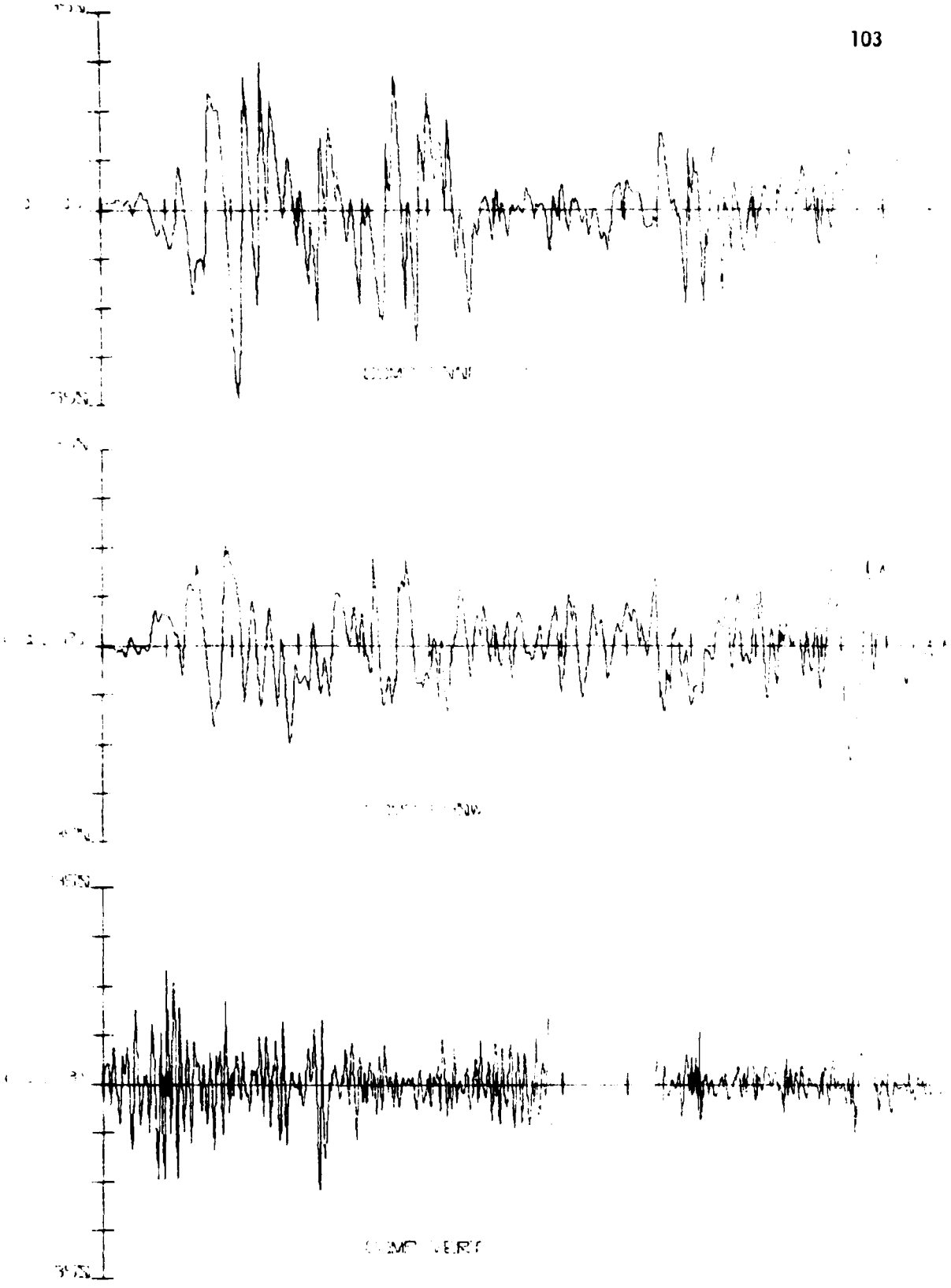

Figure 5-6

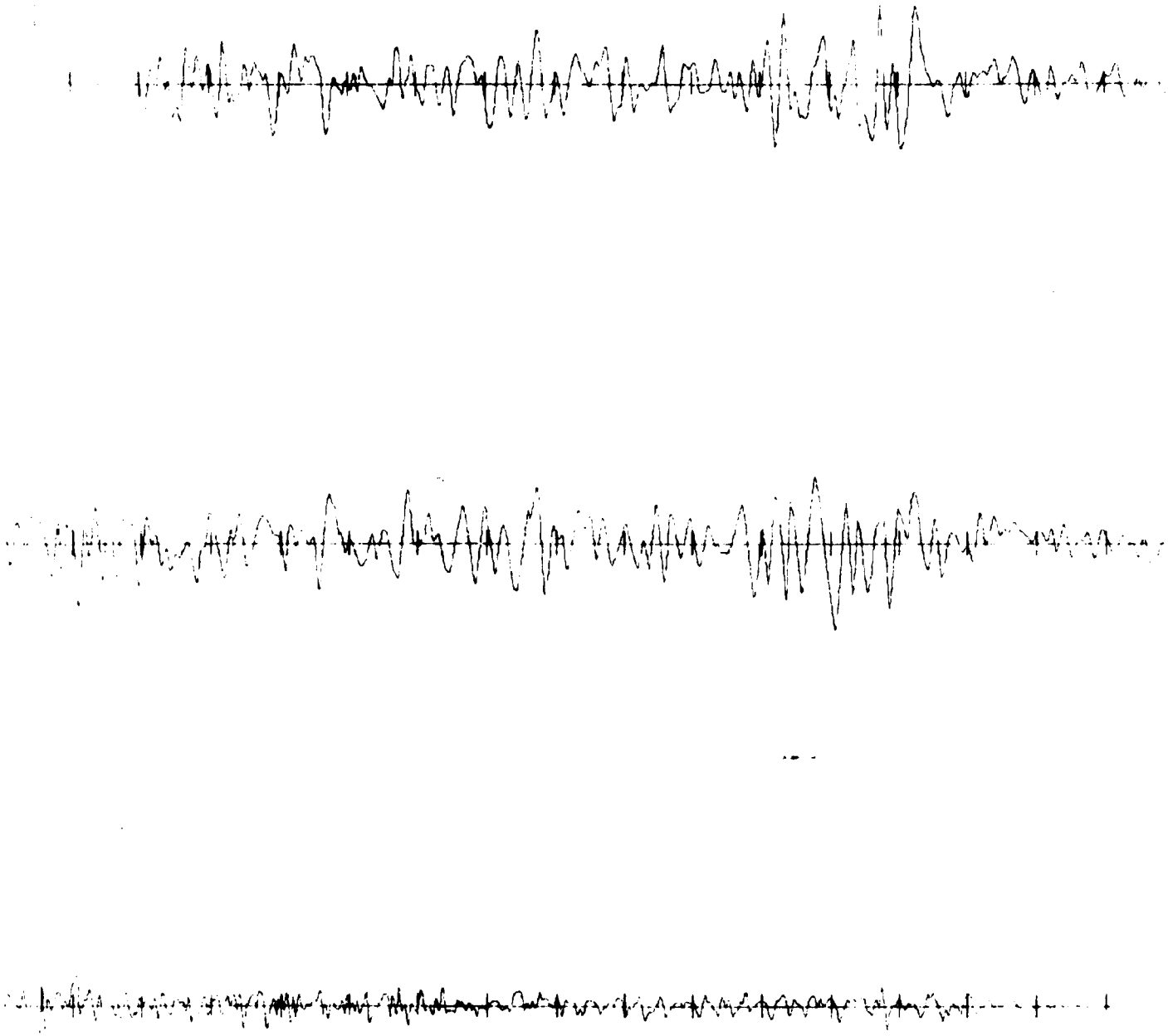

Fig. 5-6

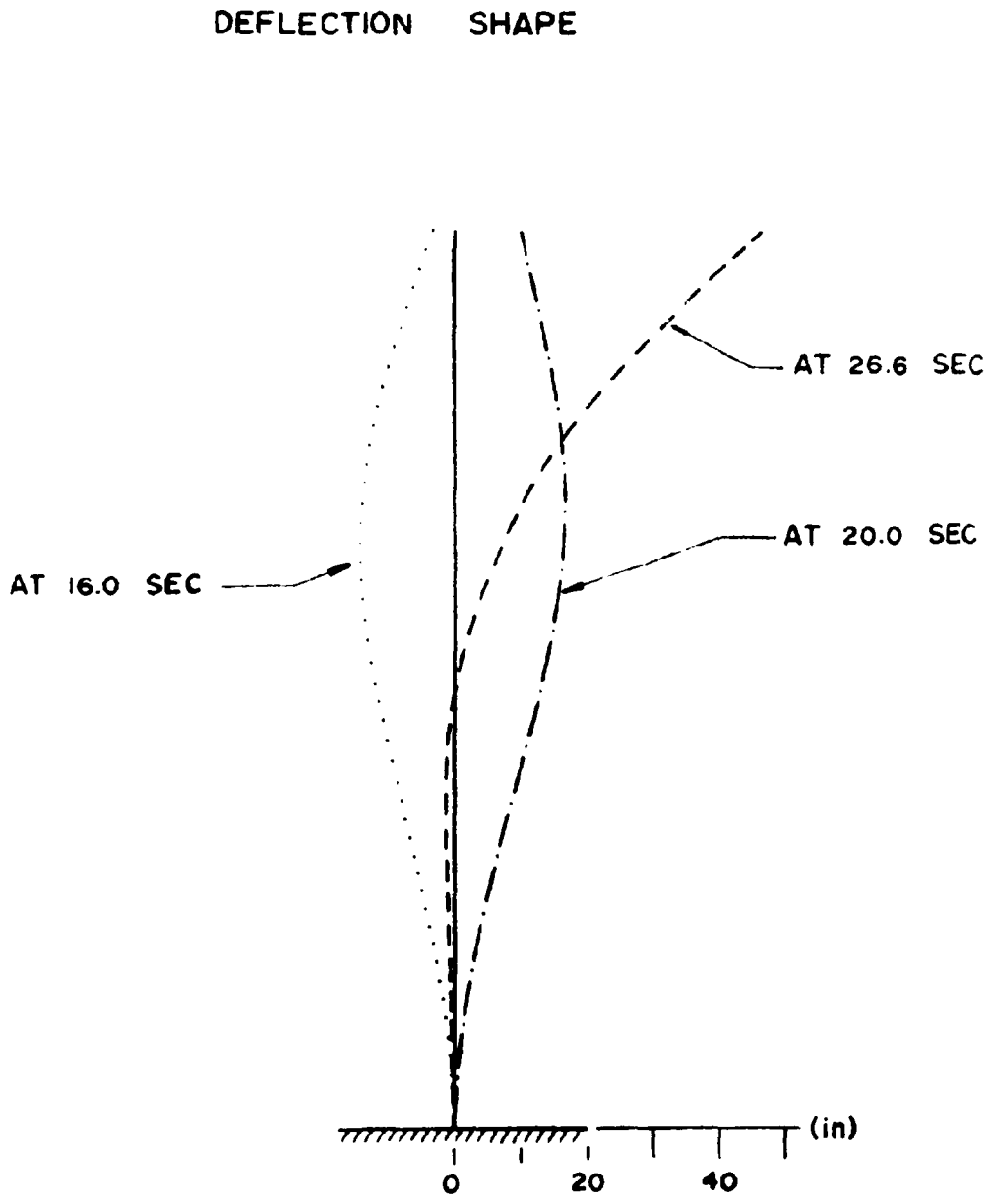

Fig. 5.7 The deflection shapes for the chimney at various time intervals during the El Centro earthquake. (South-North).

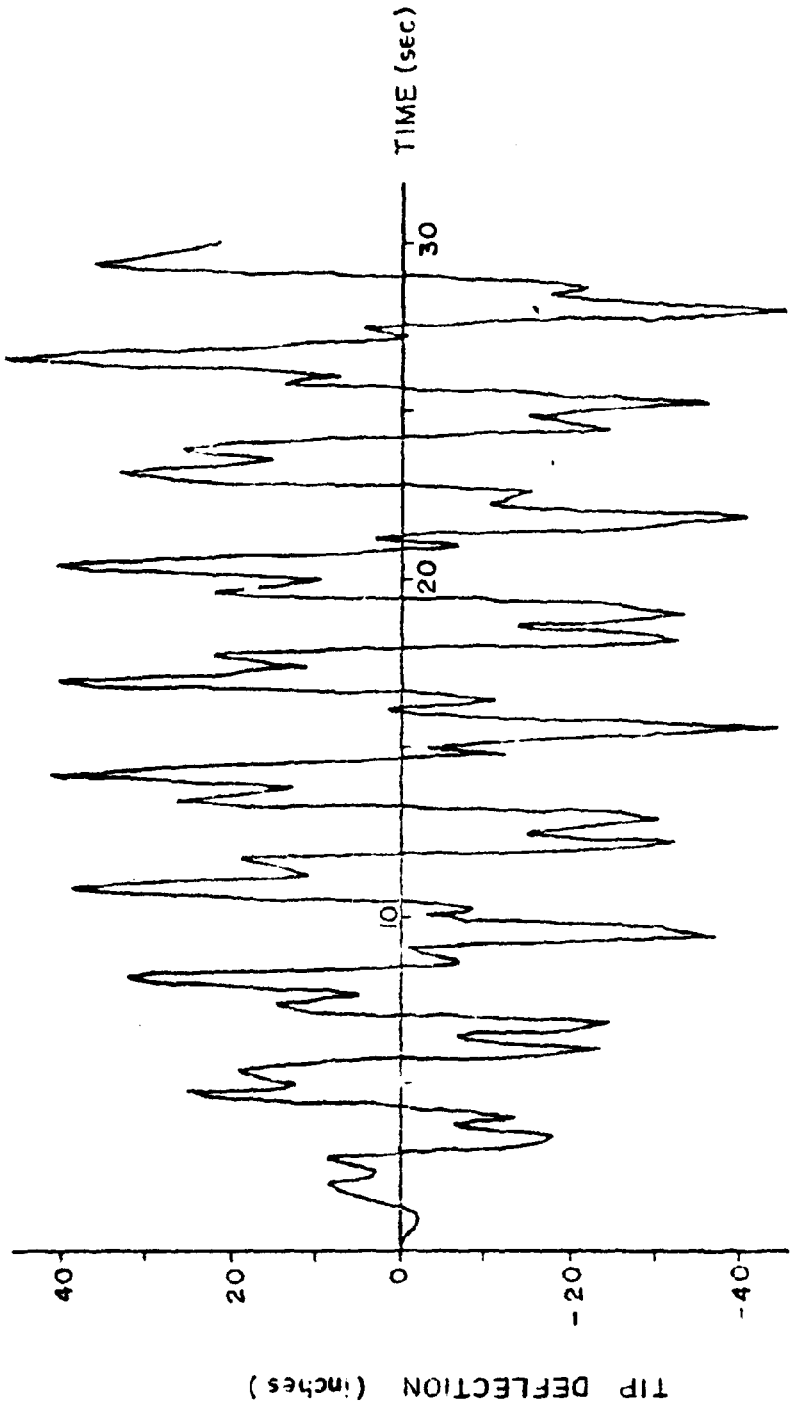

Fig. 5.8 The deflection vs. time curve at the top of the chimney.

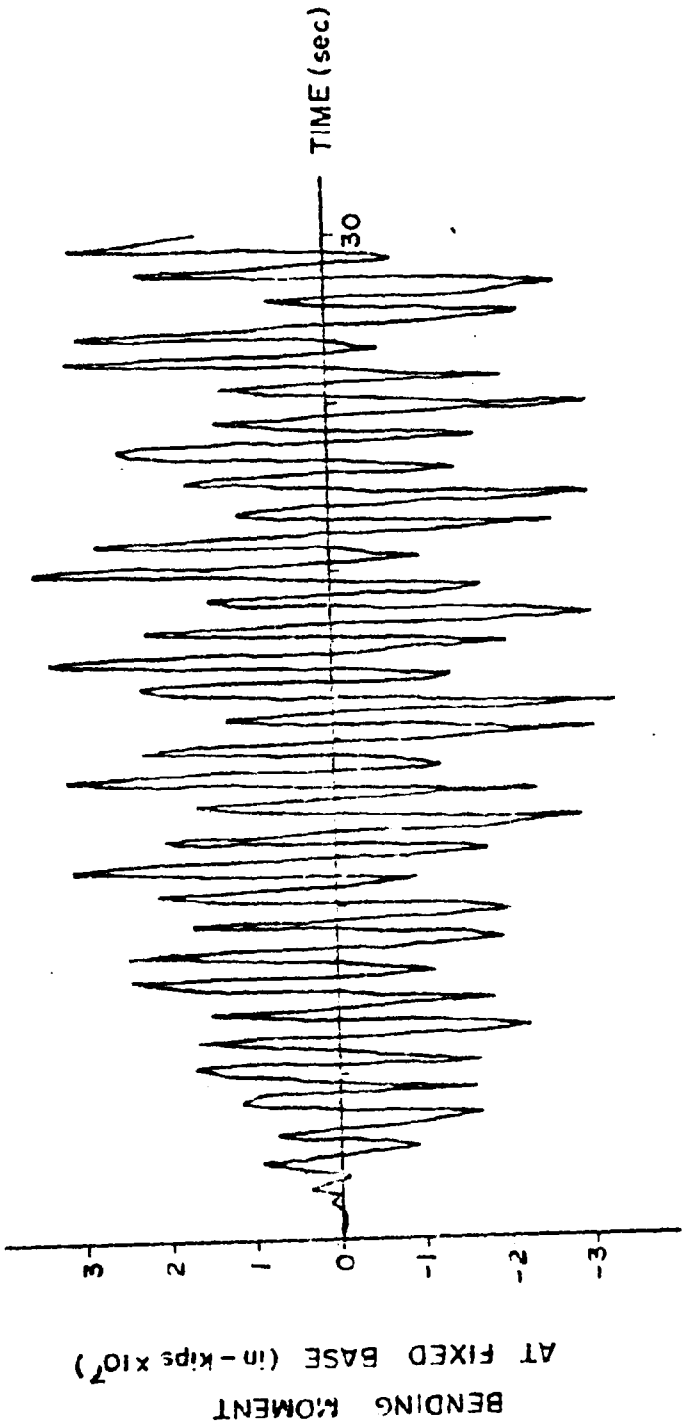

Fig. 5.9 The bending moment vs. time curves at the fixed base of the chimney.

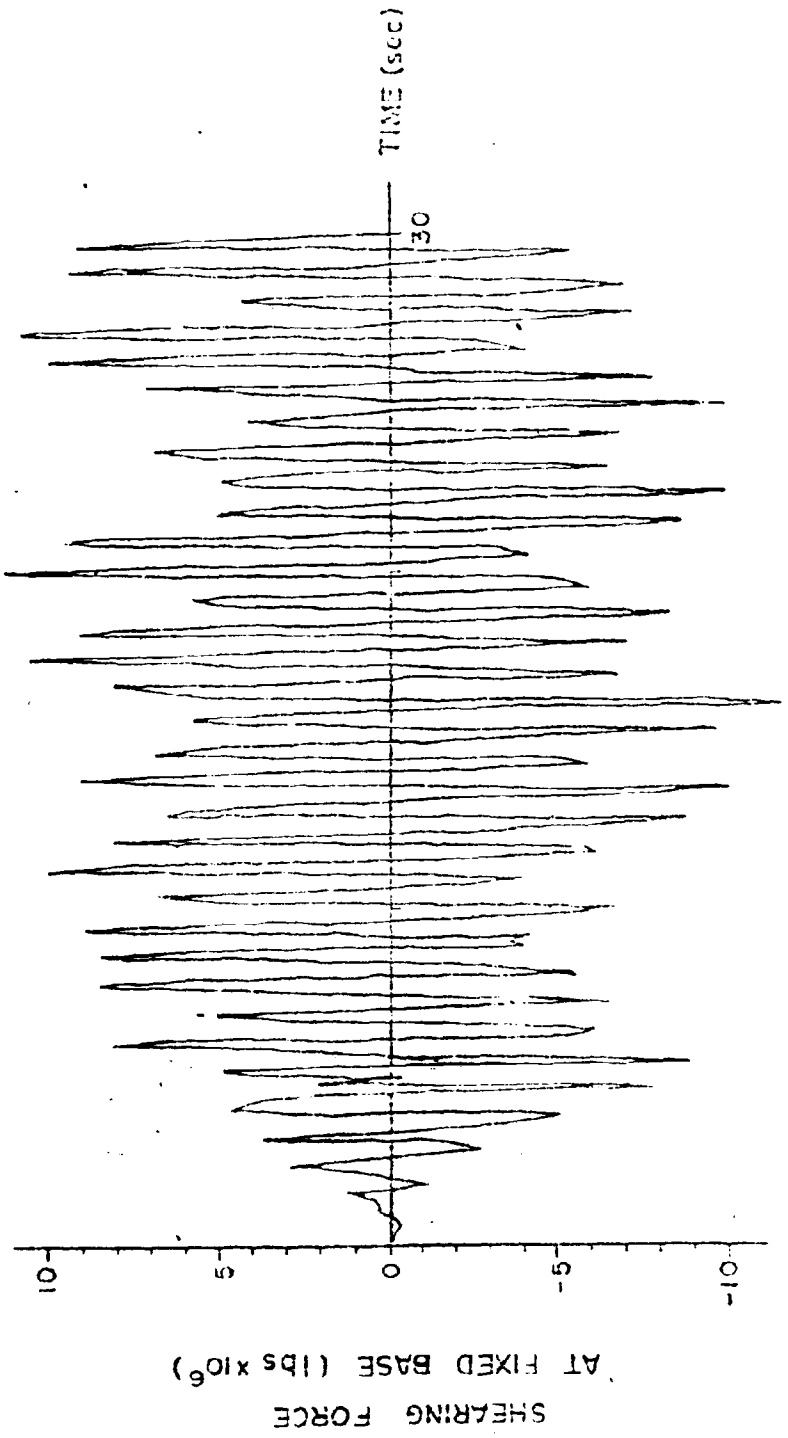

Fig. 5.10 The shearing force vs. time curves at the fixed base of the chimney.